Alma Mater Studiorum - Università di Bologna

DOTTORATO DI RICERCA IN

MONITORAGGIO E GESTIONE DELLE STRUTTURE E DELL'AMBIENTE - SEHM2

Ciclo 34

Settore Concorsuale: 08/A3 - INFRASTRUTTURE E SISTEMI DI TRASPORTO, ESTIMO E VALUTAZIONE

Settore Scientifico Disciplinare: ICAR/04 - STRADE, FERROVIE ED AEROPORTI

HIGH FRICTION AND ACOUSTIC SURFACE FOR PAVEMENTS: DEVELOPMENT OF ARTIFICIAL ENGINEERED AGGREGATES FROM RECYCLED POWDERS

Presentata da: Sergio Copetti Callai

Coordinatore Dottorato

Alessandro Marzani

Supervisore

Cesare Sangiorgi

Co-supervisore

Luca De Marchi

Esame finale anno 2022

Declaration

The content of the thesis is the result of work which has been carried out as part of the Horizon 2020 – Marie Skłodowska-Curie Actions – ITN project "SAFERUP! - Sustainable, Accessible, Safe, Resilient and Smart Urban Pavements".

SAFERUP!

Thinking Beyond the Pavement

This project has received funding from the European Union's Horizon 2020 research and innovation programme under the Marie Skłodowska-Curie grant agreement N° 765057.

Skid resistance

Pavement texture

Tire/road noise

Microsurfacing

Artificial aggregate

Geopolymer

Alkali-activation

Acknowledgments

The Ph.D. is a dream that started a long time ago and has been marked with several hurdles. However, these hurdles were surpassed with the help and support of several people, and I would like to thank them here.

First, I would like to acknowledge the importance of my supervisor Prof. Cesare Sangiorgi. I will not forget his call to tell me I got the position and the rush to make everything ready to move. Thank you for the warm welcome and for all this time we worked together.

I would like to thank all my colleagues and coworkers in the Road laboratory at UNIBO, Pier, Sajjad, Eduardo, Ettore and Sandro. A special thanks to Giulia Tarsi and Tommy for your help in navigating and conquering the Italian Bureaucracy.

Special recognition must be given to my Ph.D. colleagues, Chris and Abbas, we started as strangers from 3 corners of the world that became colleagues, and I would dare say, friends. Your company during all this period, kind words, screaming and shouting together were essential to the completion of the thesis. And, I would like to extend the recognition to all my fellow ESR's.

I would like to acknowledge several friends that contributed to different degrees, but all of importance, to this Ph.D., I will separate them geographically, from the Ijuí to Finland. Vinicius Koff, Kamilla Vasconcelos, my former advisor Liedi Bernucci, Mauro Vieira Cruz, Chicão, Douglas Morais, Rene, Pavan e Lincoln, Octavio, Navid, Aitor, Darya, Mayara, Paulo Dziobczenski, Maria Valeria and NINA.

I want to thank my family. My parents, Helena and Jaeme, who taught me the love for books and knowledge. Your words (text) saying on the day I got on the plane were quite important, as you said, "You (me and Bruna), make the opposite movement from your forefathers and foremothers. Them, from Italy to Brasil, you

from Brasil to Italy. Nevertheless, the reason is the same it is the HOPE FOR A BETTER FUTURE". Thank you both for all the support and understanding.

My siblings and their families, Andreia, Luis Fernando, Isabela, Alicia and Tomas, Vanessa, Valentina and Olivia. That supported the idea to migrate with all the love possible. To all my family and the need to celebrate Christmas, new year's, and all birthdays by video call, this made all the distance seem a bit closer.

I need to thank my dogs, Guri and Pagu. They gave me company and forced me to walk about, which gave me clarity in several moments.

And finally, Bruna, the love of my life. The support, kindness, and words of wisdom you gave me are incommensurable. We shared happiness and frustrations together but your joy, excitement at every single step were to fuel that I needed to never quit

Thank you for your patience, especially at the time I was unbearable. Thank you for being my partner, always. My eternal "companheira".

Allons-y

Abstract

As the roads and streets are an intrinsic part of our lives, we spend much time on them, either by driving or living or working close by. There is a constant need to improve the built infrastructure's quality and build new infrastructure with better designs. As users of roads, we are constantly at risk of accidents and noise exposure – either in vehicles, neighborhood houses, or offices. The risk of accidents and noise can be reduced by improving the surface properties of the pavement.

The amount of raw material used to construct all infrastructure projects, mainly roads, is worrisome, as this raw material is finite, and its exploration produces many waste materials. In order to construct environmentally-friendly roads, recycling is one of the possible steps, maybe the main one. It is possible to use these waste materials produced from the extraction of natural aggregates and treat them to replace partially or entirely the natural aggregates. New road projects must be more environmentally-friendly, safer, and quieter.

Is it possible to develop a safer, quieter and environmentally-friendly pavement surface? The hypothesis proposed if it is possible to create an Artificial Engineered Aggregate using waste materials and providing it with a specific shape that can help to reduce the noise and increase the friction?

The thesis presents the development of an Artificial Engineered Aggregate and its application as a partial replacement in microsurfacing samples. The thesis is divided into five main chapters based on papers. The first chapter introduces the topic and provides the aim and objectives of the thesis. The second chapter – is a review of the pavement solution to noise and friction. The third chapter - developing a mix design for a geopolymer mortar that used basalt powder. The fourth chapter is presented the physical-mechanical evaluation of the Artificial Engineered Aggregate. The fifth chapter evaluates the use of this aggregate in microsurfacing mixture regarding the texture parameters and indicators. In the sixth chapter, the

use of this parameter as an input to the SPERoN® model to simulate the noise behavior of these solutions.

The findings from this thesis are presented as partial conclusions in each chapter, to be closed in a final chapter. The main finding is that the Design of Experiments provided the tool to select the appropriate geopolymer mortar mix design. The Artificial Engineered Aggregate had interesting results regarding most of the physical-mechanical tests. Using this Artificial Engineered Aggregate in partial replacement of the natural aggregates in microsurfacing mixture proved feasible. The texture parameters and noise levels obtained with the sample with Artificial Engineered Aggregate demonstrate that it can serve as a High Friction and Acoustic Surface for Pavement.

Table of Contents

List of Figures

List of Tables

Chapter 1: Introduction

The primary function of highway pavement is to withstand traffic and allow mobility in a safe, comfortable, and economical way by distributing the surface loads to the existing natural subgrade[1]. As pavements are the main structural element of the road infrastructure, they must provide a durable solid structure capable of withstanding the traffic loads carried during their service life without suffering damages that can eventually reduce their safety. Along with the structure, the pavements' surface functional performance is critical due to its direct relation to safety, riding quality, noise, and appropriate visibility at night and in adverse weather conditions [2].

Among the mentioned aspects of road pavements' structure and surface, traffic noise has become one of the major environmental concerns of densely populated areas worldwide. The advent of electric cars, which are more silent as they do not possess combustion engines, will not dramatically change the noise scenario, as most of the road noise comes from the tire/road component. In fact, road vehicles are, by virtue of their numbers, traveling speeds, and strong output, a powerful sound source[3]. Indeed, population growth in urban areas has increased traffic, thus increasing noise sources and receivers, hence affecting the quality of life and, eventually, the health of people [4,5].

Designing roads with the users' safety and health as a main aspect, its paramount, at the same time as it should be aimed to target greener solutions. It is necessary to look for alternatives in pavement solutions that consider more than structural or economic parameters. The selection of proper materials that can tackle the safety, health, and environment might be achievable through alternative aggregates, such as recycled aggregate.

The depletion of natural resources is an issue that must be tackled. Traditionally road construction and projects are implemented using natural aggregates from quarries [6]. The extraction of natural materials produces large quantities of waste

materials, mostly mineral powder, which by themselves are becoming an environmental issue that requires landfilling limitations and strict legislation on their disposal [3].

The ever-increasing need for sustainable construction material is driving the research towards the reuse and recycling of waste to produce "recycled," "manufactured," and "artificial" aggregates [4]. The use of non-natural aggregates has been included in standards [9], considering them suitable for road construction and other civil engineering projects.

The present thesis aims to produce High Friction and Acoustic Surfaces for Pavements. It is proposed to use a novel Artificial Aggregate, created using geopolymerization technique [5], that produces a high-quality material that can be cast into 3d printed molds. These 3d printed molds were designed to produce a specific shape (truncated octahedron), and size (10mm), in the artificial aggregate that, according to the literature [6–8], could help to increase the friction and reduce the noise.

1.1 Aims and Objectives

The present thesis aims to develop an artificial engineered geopolymeric aggregate that can be used in specific road sections where it is needed to increase safety (skid resistance), without increasing the tire/road noise. To achieve it, the following objectives were set:

- Develop a geopolymer mortar with acceptable strength characteristics with the minimum curing time and temperature.
- Produce satisfactory Artificial Engineered Aggregates using 3d printed molds.
    - Artificial Engineered Aggregates should have suitable mechanical properties.
    - Achieve a truncated octahedron shape with a specific size (10mm).

- Produce bituminous microsurfacing solutions using the artificial aggregates in a partial replacement of natural aggregates.
    - Evaluate the surface characteristics of the microsurfacing samples using the artificial aggregates and compare them to other solutions.
    - Evaluate the noise characteristics of the microsurfacing samples using this aggregate and compare them to other solutions.

1.2 Organization of the thesis

Chapter 2 – Summarizes the current knowledge on the acoustical and skid resistance paving solutions. The literature review includes several paving solutions using different techniques and materials, including artificial aggregates. The findings in this chapter are used to define the scope of a microsurfacing solution with an artificially engineered aggregate.

Chapter 3 – Focuses on the production and mix design of a geopolymer mortar. A Design of Experiments method was proposed to define the optimum mix design, aiming to use the highest possible amount of waste material at the minimum temperature and curing time. Also, was evaluated the workability of the mortar in order to produce the artificially engineered aggregate using 3d printed molds.

Chapter 4 – Dedicates to the production and evaluation of the Artificial Engineered Aggregates using 3d printed molds. In this chapter, the aggregates were subjected to several mechanical and durability tests in order to assess their quality. This section demonstrates how promising the artificially engineered aggregate is in terms of polishing resistance.

Chapter 5 - This chapter investigates the texture parameters of microsurfacing pavement solutions using different binding agents and different aggregates. Three different aggregates were evaluated, a traditional natural basaltic aggregate, a crumb rubber aggregate and finally, the Artificial Engineered Aggregate. The study

showed that it is possible to substantially change the surface texture of the microsurfacing using alternative aggregates.

Chapter 6 – The final research chapter evaluates the microsurfacing samples regarding their noise characteristics. This chapter used the surface texture parameters from Chapter 5 and the same samples, serving as an input to a noise model software called SPERoN® . The results demonstrated that the surfaces using a substantial amount of artificial aggregate could be used to abate noise.

Chapter 7 – Summarizes the overall findings in this study and discusses the potential obstacles and limitations of Artificial Engineered Aggregates. It concludes with final considerations and suggestions for future work.

Chapter 2: A review on acoustic and skid resistance solutions for road pavements

Copetti Callai S, Sangiorgi C. A Review on Acoustic and Skid Resistance Solutions for Road Pavements. *Infrastructures*. 2021; 6(3):41. https://doi.org/10.3390/infrastructures6030041

Abstract: As cities grow in size, also traffic increases, thus making the population more exposed to road noise and traffic accidents. It is therefore important to study and understand which are the properties of the pavement that influence its acoustic impact and skid resistance performance. The pavement texture plays a major role in generating noise and friction, and it can be engineered in order to control both of them at the same time. The phenomena regulating skid resistance are today well understood. It is the same for noise generation and propagation: the literature contains methods of designing the pavement surface layer to achieve consistent results. Several types of solutions can be found for asphalt mixtures, most of them derived from decades of studies and research; they use different approaches to be effective on noise and friction, but all have in common the control of the surface macro and microtexture. Finally, some considerations are made regarding novel paving solutions with artificial aggregates instead of natural ones to address noise and skid resistance.

Keywords: Road Noise; Skid Resistance; Quiet Pavements; Polished Stone Value; Microsurfacing.

2.1. Introduction

The main function of highway pavement is to withstand traffic and allow mobility in a safe, comfortable, and economical way by distributing the surface loads to the existing natural subgrade[1]. As pavements are the main structural element of the road infrastructure, they must provide a durable solid structure capable of withstanding the traffic loads carried during their service life without suffering damages that can eventually reduce their safety. Along with the structure, the pavements' surface functional performance is a key factor due to its direct relation to safety, riding quality, noise, and appropriate visibility at night and in adverse weather conditions [2].

Among the mentioned aspects of road pavements' structure and surface, traffic noise has become one of the major environmental concerns of densely populated areas worldwide. In fact, road vehicles are, by virtue of their numbers, their traveling speeds, and their strong output, a powerful sound source[9]. Indeed, population growth in urban areas has increased traffic, thus increasing noise sources and receivers, hence affecting the quality of life and, eventually, the health of people [10,11].

With a focus on the asphalt concrete surface of roads, the pavement's texture appears to be a crucial aspect that can be controlled by the type and sizes of aggregates, type of asphalt binder, and through the laying processes. Control of these variables can increase friction, reduce water spray and splash, and abate noise. Following the surface texture description, pavement roughness can be divided into four texture wavelengths: unevenness, megatexture, macrotexture, and microtexture [12]. Each range interacts with the vehicle and its tires in a different manner. However, macro and microtexture are the most relevant ones since they have the strongest influence on noise and friction. Higher macrotexture with similar microtextures have a greater influence on friction than surfaces with similar microtextures and lower macrotextures[13]. Pavement surfaces with the same macrotexture and microtexture can also differ due to the spatial distribution of the

particles in reference to a baseline; literature shows that pavements with a positive texture (more peaks) usually have higher noise levels than those with similar macrotexture but arranged in a negative manner (more valleys) [14,15].

The term skid resistance is generally used to describe the pavement's contribution to the development of friction. It denotes a measurement of friction obtained under standardized conditions, in which the various parameters are controlled so that the effects of the road surface characteristics can be isolated[7,16]. Other studies show that skid resistance, friction, can be controlled by the pavement texture. Higher macrotexture and higher microtexture often result in higher friction, thus reducing the accident risks [17]. Adequate texture on the pavement surface is required to provide skid resistance at the tire/road interface for vehicle safety in wet conditions [6,18].

This paper aims to offer a review of the depicted topic by discussing pavement texture properties and their relation to skid resistance and noise. Besides, a pioneering asphalt pavement solution is presented, which combines noise abatement and skid resistance properties due to the adoption of innovative engineered artificial aggregates.

2.2. Road pavement surface properties

2.2.1. Texture

The pavement texture is defined as the deviation of a pavement surface from a true planar surface caused by the random arrangement of the surface elements and their superficial roughness [19]. The texture of pavement and its interaction with the tire can have desirable and undesirable outcomes, ranging from high skid resistance (desirable) to discomfort and wear in the vehicle (undesirable). These effects mainly depend on the wavelength range of the texture, as shown in Figure 1. ISO [19] identified different orders of the texture of a road pavement:

- Microtexture covers wavelengths that are of the same order as the texture of aggregates, with wavelengths below 0.5 mm.
- Macrotexture covers wavelengths of the same order of size as tire tread elements, i.e., from 0.5 mm to 50 mm.
- Wavelengths over 50 mm correspond to megatexture and unevenness.

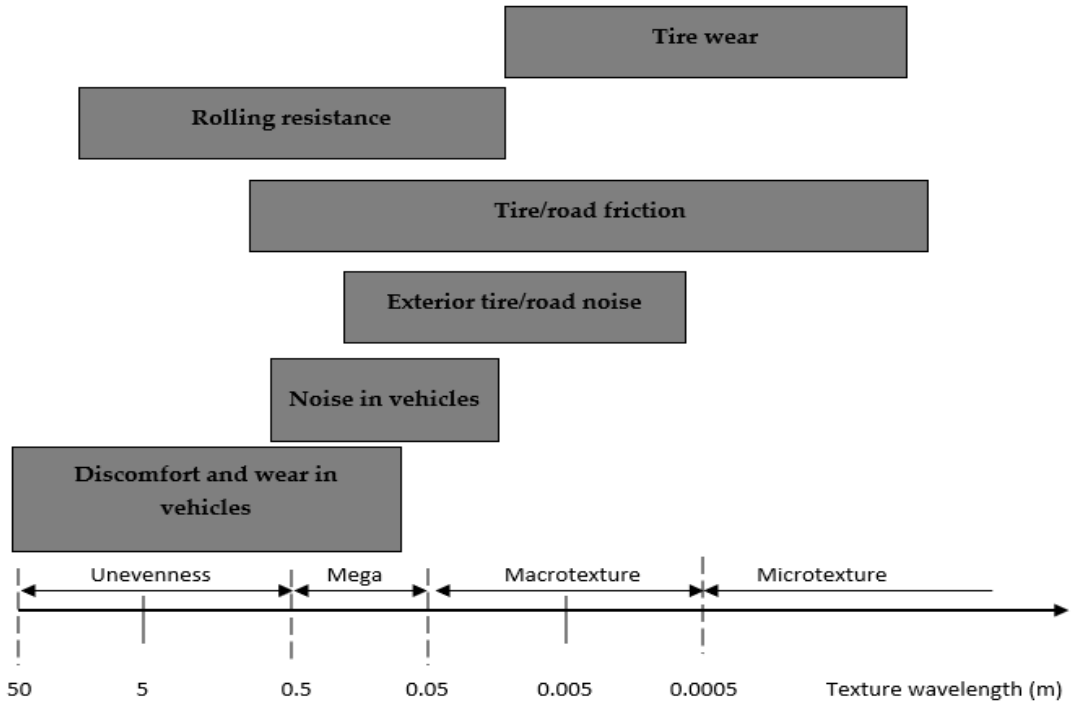

Figure 1. Tire/pavement interactions and ranges of texture wavelength and spatial frequency (adapted from[20]).

Unevenness and megatexture are usually undesirable textures, while road friction and tire/road noise can be regulated by controlling the macrotexture and microtexture. The macrotexture is primarily influenced by the size, shape, and gradation of coarse aggregates; it is mainly the nominal maximum aggregate size [21]that governs the surface 3D geometry and the other parameters affecting the volumetrics of the asphalt surface. As for microtexture, it is primarily influenced by the aggregate particle mineralogy that affects the initial texture of the aggregate and its capability to preserve texture due to the polishing action of traffic and environmental actions [21].

It has been proven that the texture of the pavement can have a given wavelength. However, it may have a different outcome when interacting with the tire due to how this wavelength is distributed on the pavement. It is considered positive when its particles are protruded above the plane of the surface. The texture can also be negative, which is when it is comprised of voids between the particles and usually have a flat rolling surface. Both situations are represented in Figure 2.

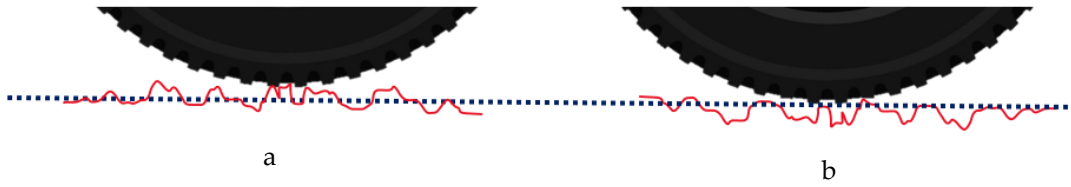

Figure 2. Schematic representation of a positive texture (a) and negative texture (b).

According to researchers depending on the size of particles, positive texturing leads to higher indentation levels in the rolling tire, thus having good results for skid resistance. In comparison, negative textures contribute to the lower noise levels due to valleys' predominance [22–24]. The surface arrangement of texture, positive or negative, is of the highest importance. It has been reported that negative texture results in a decrease of rolling noise, while the positive texture is more detrimental from an acoustical point of view [25].Research has been conducted on how to achieve better skid resistance and lower noise, as is described in the following sections.

2.2.2. Skid resistance

Concerning the Sustainable Development Goals devoted to the health and well-being of the population (SDG n°3) and the sustainability of cities and communities (SGD n°11), different research shows that when the pavement texture design has improved, the risk of accidents is significantly reduced [26–28]. According to the World Health Organization (WHO) report on traffic, road traffic injuries are among

the top leading causes of death for people of all ages [29]. The death toll was rising and reached 1.35 million in 2016. Hence, road traffic crashes constitute an important public issue with significant health and socioeconomic costs, which should be tackled by road agencies and research [29,30].

The interaction between tire and pavement that governs the vehicle driving actions depends upon pavements' surface characteristics (including its contamination) and tire mechanical and physical properties. Skid resistance is the force developed when a tire that is prevented from rolling starts to slide on the pavement [31]. This interaction is usually identified with skid resistance, which is defined as a measure of the friction phenomena that have a direct and important effect on the perceived and quantified road safety [14].

For instance, existing data plotted in Figure 3 shows that, as the coefficient of friction (given as a parameter of skid resistance) increases, the crash rate is reduced; the crash rate (every 108 vehicle-km) is here plotted against Scrim data (from the Sideway-force Coefficient Routine Investigation Machine).

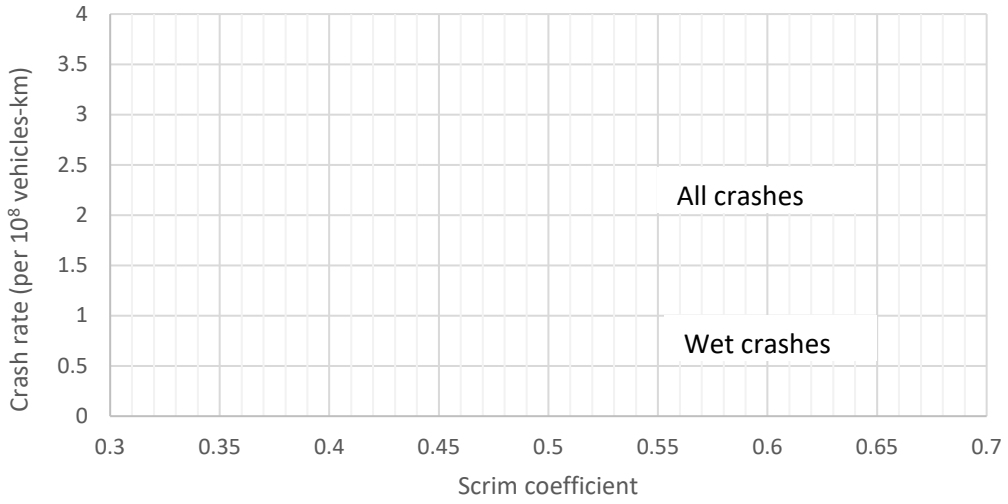

Figure 3. Scrim coefficient vs. crash rate (adapted from [26]).

The skid resistance of pavement, especially in wet conditions, is of utmost importance. In fact, a set of studies showed that approximately 20% of all road accidents occur when the surface is wet [30,32].

In theory, the available skid resistance is given by the frictional forces developed at the tire/road interface, which are partially governed by the surface properties of the pavement, i.e., texture and its level of contamination [33]. Moreover, the geometrical dimensions and the aggregates' source are relevant properties, as far as skid resistance development is concerned. This is because aggregates' mineralogy can affect the resistance to polishing, hence the aggregate's microtexture. It should be recalled that the microtexture of the surface aggregates and the overall macrotexture is directly related to the two main components of the friction, which are hysteresis and adhesion, as represented in Figure 4 [34,35].

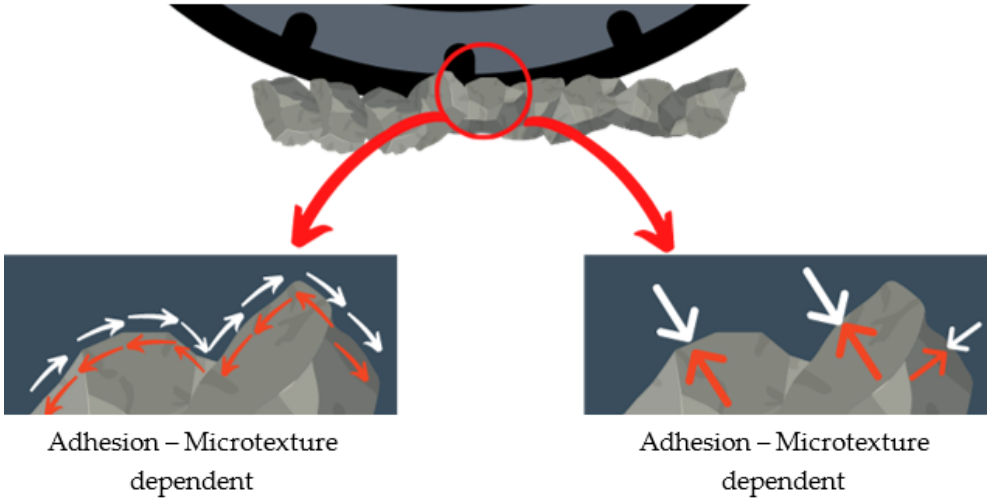

Figure 4. Key parameters of pavement-tire interaction (adapted from[34]).

Both phenomena concur to regulate friction; the adhesion is the friction that results from the small-scale bonding of the tire's rubber and the pavement surface, while the hysteresis results from the energy loss due to the bulk deformation of the tire rubber when it deforms against the pavement surface. The stress causes the deformation energy to be stored within the rubber [34]. The adhesion is often neglected because when the texture is positive, the hysteretic part is more relevant

to increase the skid resistance. However, this behavior changes once the texture becomes smoother[36], with fewer peaks and valleys. The presence of contaminants or water can influence both adhesion and hysteresis, which will decrease the number of contact points needed for the friction to occur.

2.2.3. Noise

Noise pollution from roads has major effects on people's health [37]. Studies indicate that it is directly related to several common diseases such as cardiovascular ones, myocardial infarction, deafness, and depression. Noise also has an influence on birth rate, work-related stresses, and productivity, as well as impairment of learning of children in schools [38–41].

According to the Imagine-Project [42], tire-pavement noise is the most relevant component of the overall traffic noise at speeds over 40 km/h, as represented in Figure 5. The overall noise is mainly given by the propulsion and tire-pavement noises, which both are speed-dependent, but the tire-pavement prevails at speeds over 30 km/h for car traffic and for trucks when their speed is above 75 km/h [42].

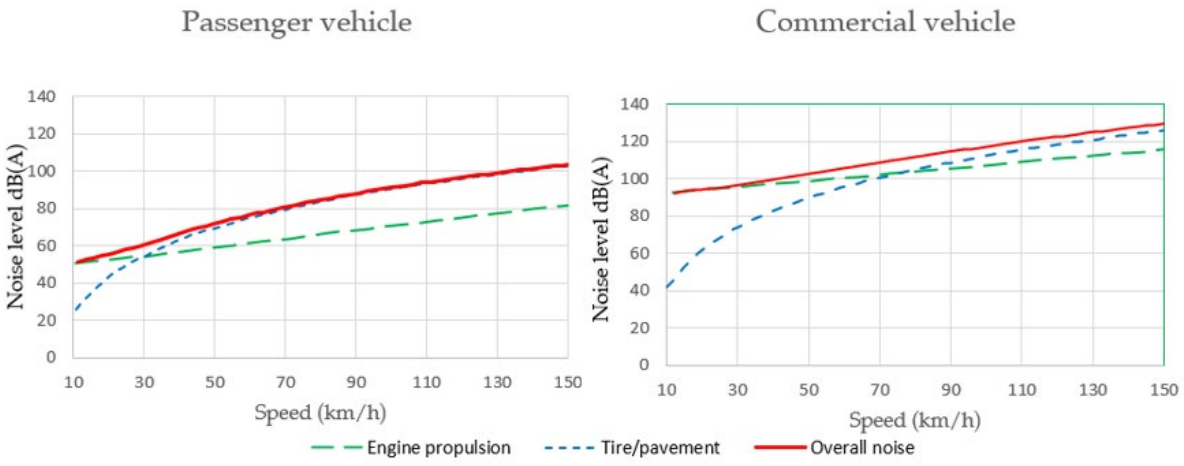

Figure 5. An estimate of passenger and commercial vehicle noise and main sources(adapted from[42]).

It is important to notice that even at higher speeds if the tire-pavement noise is reduced, it is possible to mitigate the overall noise; the noise levels are on a logarithmic scale.

The most important noise generation mechanisms and propagation have been identified [9,34], as represented in Figure 6. Road engineers can design road surfaces by focusing on these mechanisms, aiming for the most appropriate material selection to achieve specific layer characteristics.

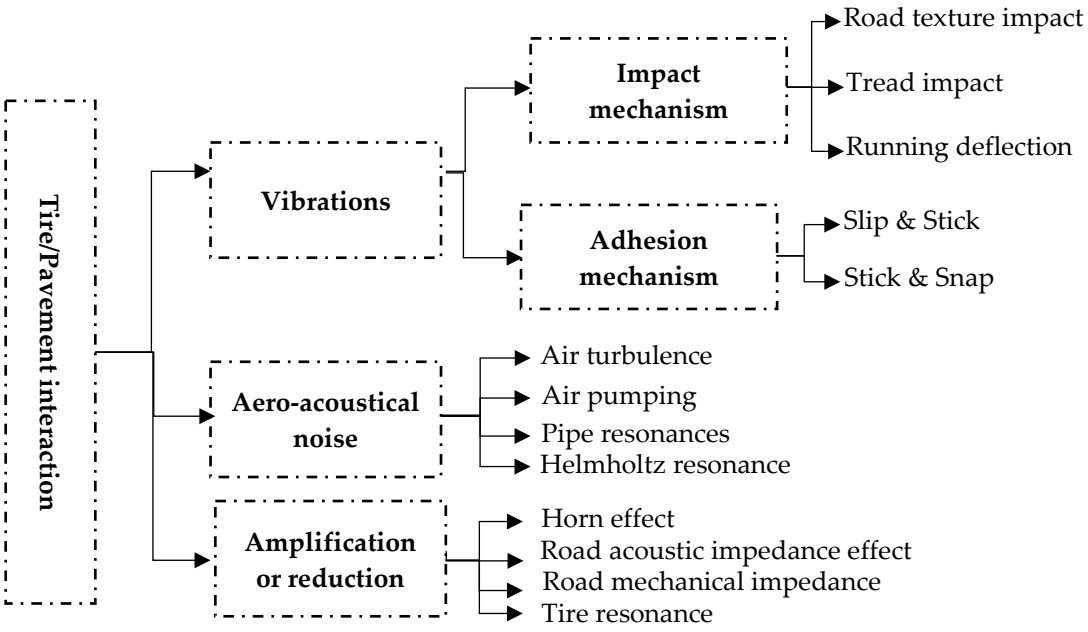

Figure 6. Road noise mechanisms due to tire/pavement interaction (adapted from [6]).

The tire/pavement interaction related to noise consists of three main generation and amplification or reduction phenomena. Vibrational mechanisms are deformations related to the impact and tire rolling, mainly on the hysteretic component, and adhesion mechanisms are mainly related to the adhesion component of the interaction. They are highly dependable on the tire characteristics, as well as the pavement material and texture. Aeroacoustics depends mainly on the geometry of the tire/pavement contact and the number of air voids. The amplification or reduction also depends on the geometry and the mechanical and acoustic absorption properties of the pavement. For instance, to reduce the tire tread impact noise generation, a lower layer stiffness can be achieved by means of asphalt rubber or rubberized asphalt. Similarly, aggregate selection can be targeted to improve

microtexture, thus addressing the noise generation mechanisms related to surface adhesion, i.e., “stick and slip” and “stick and snap

The noise generation and propagation can also be attenuated or mitigated by reducing the pavement surface layer's stiffness by increasing its porosity while reducing the size of aggregates and making its texture negative [43], or when rubber is added to the asphalt mixture [44,45]. There are studies aiming to model the texture and predict the noise [46–48].

In Figure 7, it is shown that the skid resistance increases as the noise increases; this can be due to many factors, but because the most important ones are the texture depth and whether the surface is positive or negative. It should be considered that it is quite difficult to achieve a low noise surface while recording a very high skid resistance; it is usually a tradeoff that should also consider other pavement characteristics, above all, durability.

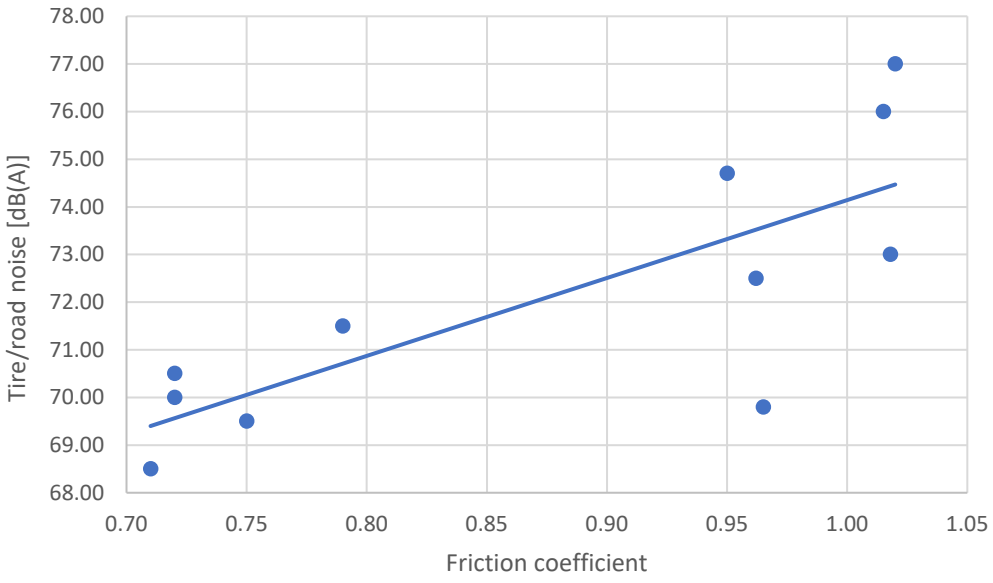

Figure 7. Noise level versus friction coefficient on a dry pavement (adapted from [49]).

2.3. Existing pavement solutions to address noise pollution and skid resistance

Several different asphalt layer alternatives vary in terms of the sieve size distribution (open-graded, dense, gap graded), type of binder, production and laying processes, pavement stratigraphy, and other connected variables. These alternative pavements might be suitable to perform as acoustic surfaces or to improve the wearing course skid resistance, or, in some cases, to target a compromise between both aspects. In the following sections, each type of pavement will be briefly described, and comments on their main characteristics will be given in terms of acoustic and/or skid resistance performance.

2.3.1. Dense-Graded Hot Mix Asphalt

Dense-graded Asphalt Concrete is the base benchmark for all comparisons because it is the most common asphalt pavement and is the commonly used pavement for comparing standardized noise measurements [50]. It has a dense aggregate gradation curve, with a low amount of air voids in the compacted mixture. Since it is not produced as acoustic pavement, it has, in principle, no noise reduction capabilities, but a proper selection of particle size distribution can lead to reduced noise impacts. The sound pressure levels are usually higher as 84 dB(A)[51,52], while initial friction values are approximately 60-65 BPN [52]. Variations in data are obviously expected according to the gradation size, aggregate type, and mixture proportions.

2.3.2. Open Graded Friction Courses

According to Alvarez et al. [53], open-graded friction courses are special gap-graded asphalt mixtures that are known for having a large proportion of interconnected air voids. This volumetric property results in large permeability values and noise reduction capabilities, with the air voids contents ranging between 15 to 35%. Due to its porosity and aggregate gradation, this asphalt concrete has a negative texture, and it can mitigate noise with sound pressure level differentials of approximately 3.5 dB(A) at standard speeds. Usual levels can range from 74 to 76

dB(A) [54].As for friction, the initially measured values can range from 50 to 70 BPN [55]. Moreover, it has a positive performance in wet conditions because its permeability reduces the water spray and splash phenomena.

2.3.3 Stone Mastic Asphalt (SMA)

Stone Mastic Asphalt (SMA) was developed in Germany in the 1960s as a solution for paving heavily trafficked roads. The asphalt layer has a high content of coarse aggregates, which forms a gap-graded skeleton-like stone structure [56],as shown in Figure 8. SMA has a low air voids content. However, it can mitigate the noise pressure levels up to 2-3 dB(A)[57,58], with typical values ranging from 76 to 80 dB(A)[59]. The selection of appropriate aggregate size is crucial to achieving consistent noise mitigation. SMA has good behavior regarding friction with values ranging from 50 up to 65 BPN [60].

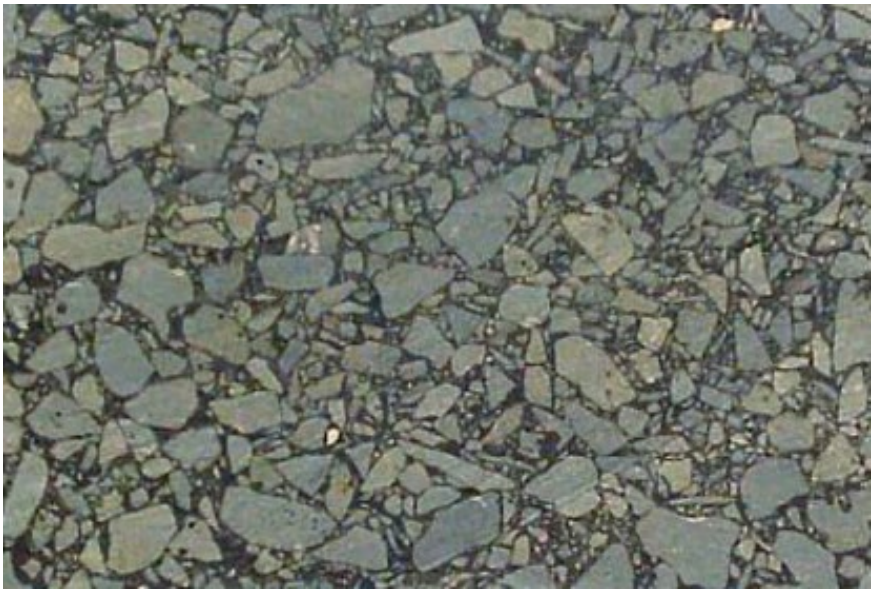

Figure 8. The inner section of a typical Stone Mastic Asphalt compacted layer [58].

2.3.4. Porous Elastic Road Surface (PERS)

Porous Elastic Road Surface (PERS), Figure 9, is made with rubber, usually from scrap tires, and it has 20 to 40% air voids content. The rubber content comprises about 20% volume of the total mix. This pavement type is still experimental and

more research is required to confirm its performance in terms of durability and safety [9,57,58]. However, as it has a low stiffness modulus and is highly porous, it can effectively mitigate noise, achieving results that can potentially reach differentials up to 10 dB(A) [61,62]. Studies conducted by Goubert [54] and Ejsmont et al. [61] state that the noise reduction can be as high as 12dB(A), and skid resistance is around 60 BPN, which is acceptable. However, more studies should be conducted to assess the skid resistance values' consistency [63].

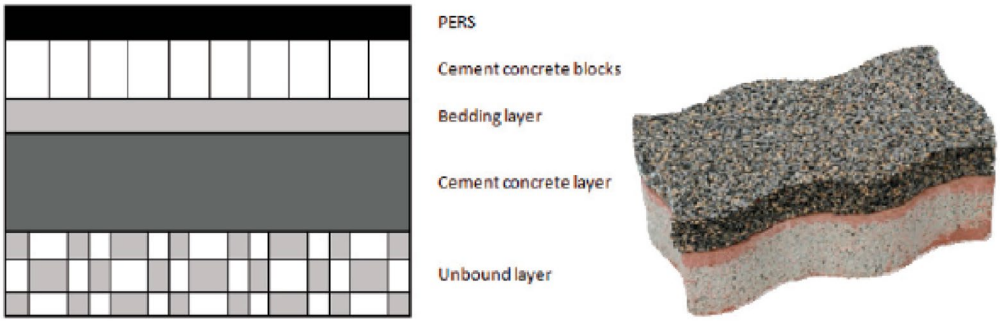

Figure 9. Porous Elastic Road Surfaces samples [62].

2.3.5 Twin layer courses

Twin layers were first developed in the Netherlands in the 1990s and were originally called “twinlay” because of the two porous layers with different gradations (Figure 10). This solution has been proven to have a good performance in mitigating noise at the source and has some of the porous asphalt course's similar pros and cons, like reducing splash and spray effects. Moreover, since it has two layers, the top one acts as a filter hindering clogging and preventing that the bottom layer from eventual clogs [64,65]. Studies have shown that the twin layer's noise reduction capabilities can reach up to 6-7 dB(A) in reference to a standard HMA[66–68].

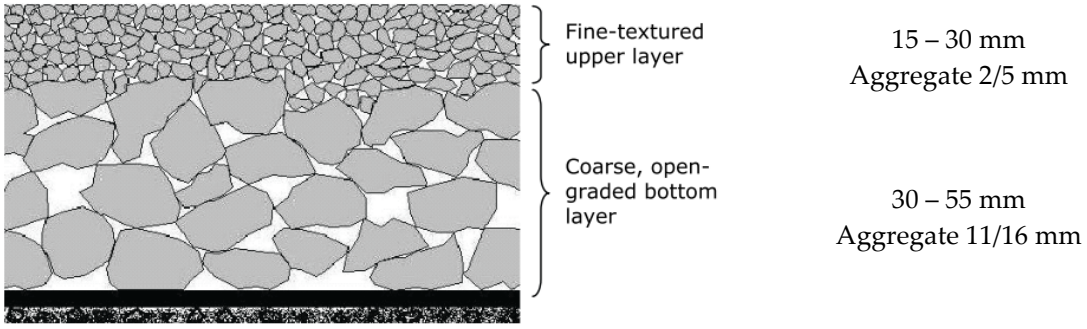

Figure 10. Twin Layer scheme (adapted from [64]).

2.3.6. High Friction Surface Dressing (non-bituminous)

According to Woodward and Friel [69], a High Friction Surfaces is a special type of road coating with very high skid resistance, mainly used in locations with a high risk of accidents (including pedestrians), and it has been used in the UK since the 1960s. It is a cold applied mixture of selected aggregates (high resistance to abrasion and polishing) mixed with a bond coat resin (epoxy, polyurethane, resin, or acrylic) an example can be seen on Figure 11. These proprietary solutions are commercially available, and typically, they have a higher economic impact and do not aim to mitigate road noise. Nevertheless, in specific design scenarios, such as intersections, it has been shown that, in optimal conditions, they can abate up to 5 dB(A) of noise [9].

Figure 11. High Friction Surface Dressing.

2.3.7 Microsurfacing

Microsurfacings are polymer-modified, binder emulsion based, dense graded, cold mixed, and quick setting asphalt surfacing materials. They are a widely used solution for pavement maintenance and to increase safety. They act as a protective wearing course that can be applied over the existing pavement, thus reducing some irregularities and filling cracks. They provide a surface with a regular and even texture, as shown in Figure 12. Microsurfacings are well-known as a construction method with economic and environmental benefits [30,70,71]. Apart from the proven positive effects in terms of skid resistance, recent studies were conducted to assess their performance in terms of noise reduction when a specific mix gradation and powdered rubber were used in combination [72].

Figure 12. Cold laid acoustic microsurfacing in an Italian experimental site [73].

Table 1, provides the typical values of skid resistance, given in traditional BPN units, and noise levels in terms of absolute sound pressure levels. It is important to recall that these values can be found in the literature. They are referred to as specific

admixtures in terms of constituents, proportions, aggregate size, and physical characteristics.

Table 1. Typical friction and noise characteristics of different paving solutions.

Paving solution	Friction (BPN)	Noise (dB(A))	Ref.
Dense-Graded Hot Mix Asphalt	60-65	> 84	[48,70]
Open Graded Friction Courses	50-80	74-76	[50,51,70]
Stone Mastic Asphalt (SMA)	50-65	76-80	[53–56]
Porous Elastic Road Surface (PERS)	60	-10 dB(A) reduction[1]	[57,59,71–73]
Twin layer courses	Like open graded courses	-6 dB(A) reduction[1]	[62,63]
High friction Surface Dressing	Up to 90	-5 dB(A) reduction[1]	[52,74,75]
Microsurfacings	54 -72	69-75	[76,77]

The reduction is in reference to a standard hot mix asphalt called the ISO surface(ISO 10844:2011).

2.4. High Friction Acoustic Surface Pavements

Surface treatments, especially those using cold binders, play a major role in the development of more sustainable and safer pavements. This paving solution (valid both for new constructions and maintenance interventions) shows promising results in terms of friction performance and can also be specifically designed to address noise; this is still under research and has been recently addressed as High Friction Acoustic Surface for road pavements, in order to distinguish it from the High Friction Surface Dressing.

The most advanced High Friction Acoustic Surface Pavement (HiFASP) makes use of engineered artificial aggregates, partially made of waste materials, which are applied in slurry seals or microsurfacings on a new or existing road, as they are not designed to bring in structural benefit to the pavement.

The HiFASP engineered artificial aggregates must be polished- and abrasion-resistant and be shaped in an Archimedean solid that enables space-filling as well as their handling, mixing, laying, and eventually repairing in a bound layer; they can be used along with other natural or recycled particles or fillers to form the so-called aggregates matrix. The engineered layer should provide a surface with

designed homogeneous micro and macro texture that can abate noise pollution and increase skid resistance if compared to a standard friction surfacing. Furthermore, as the HiFASP is an innovative solution that has the High Friction Surface Treatments basis in its conceptual background, it becomes mandatory to focus research on its durability and recyclability.

2.4.1 HiFASP with natural aggregates

Aggregates used in traditional high friction surfaces are selected to have a concentrated distribution of high contact pressures in the tire/pavement interaction surface, thus eventually providing higher skid resistance. To achieve such a surface property, it is necessary to use specific aggregates to ensure the aimed skid resistance and guarantee a sufficient life span under the common traffic wearing actions.

According to Woodward et al.[69], the aggregate particles must be extremely hard-wearing to maintain their sharp edges and must not become rounded nor wear away under the stresses of turning or braking tires. The traffic, in fact, tends to polish the aggregate, thus reducing the friction, such as shown in the schematic graph of Figure 13.

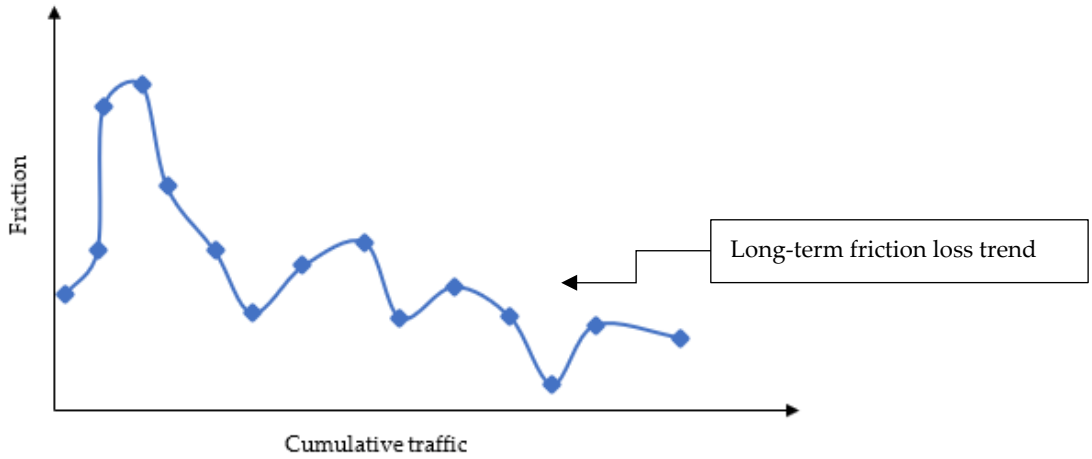

Figure 13. Possible development of friction in time for asphalt pavements (adapted from [74]).

Figure 13 shows that friction changes over time; at first, traffic causes abrasion that removes the thin binder film on the aggregates, consequently exposing their microtexture and therefore usually developing additional skid resistance. This microtexture is usually worn off over time, mainly due to polishing and reducing overall friction. Therefore, the correct selection of aggregates is important to achieve the desirable wear resistance, and thus, the sought durable skid resistance. The aggregate can be natural, artificial/industrial, recycled, or even specifically engineered, as described in the following section. Some research were conducted to evaluate the quality of aggregates [27,59,61], in which natural and artificial aggregates were compared through specific polishing tests (e.g., the well-known Polished Stone Value[70]), as well as surface texture and surface behavior. In niche literature, authors classify the aggregates through their PSV as shown in Table 2; for instance, it can be seen that the best PSV values were obtained for calcined Bauxite [67] and sandstone. According to the author's laboratory work, the aggregates were crushed to obtain cubic-shaped particles. Table 2 also presents the Texture Depth and Pendulum Test results for the tests performed on asphalt concrete specimens.

Table 2. Different types of natural aggregates used in high friction mixtures: PSVs and asphalt surface characteristics.

Rock Type	PSV (EN 1097-8:2009)	Pendulum Test (PTN) (ASTM E303:1991)	Texture Depth (mm) (ISO 13473-1:2019)
Limestone A	40	82	3.29
Limestone B	54	89	3.35
Greywacke A	65	81	3.32
Greywacke B	68	85	3.26
Granite A	55	87	3.47
Granite B	55	84	3.18
Sandstone	70	98	3.05
Quartzite	58	91	3.10
Basalt	53	95	3.74
Calcined Bauxite	70+	89	3.10

Table 2 shows that high Pendulum Tester Numbers (PTN) and a higher texture depth are not related. The difference in PTN is highly dependent on the aggregate type, which also affects the PSV and the surface texture depth, denoting the importance selecting specific aggregates to achieve high levels of friction.

Similarly, the selection of aggregates is very relevant to the pavement surface's actual noise emissions, as the origin, mineralogy, and production processes of natural aggregates, and especially their nominal size and gradation, strongly affect their contribution to the overall pavement acoustic performance. The literature states that to achieve a low road-noise impact, it is crucial to create open or gap graded gradation curves with aggregates' sizes not larger than 10 mm [[9,23]]. As shown in the example graph of Figure 14 for the same type of pavement layer, only changing the aggregate size can induce a sound level difference of about 1dB(A), even after years of traffic.

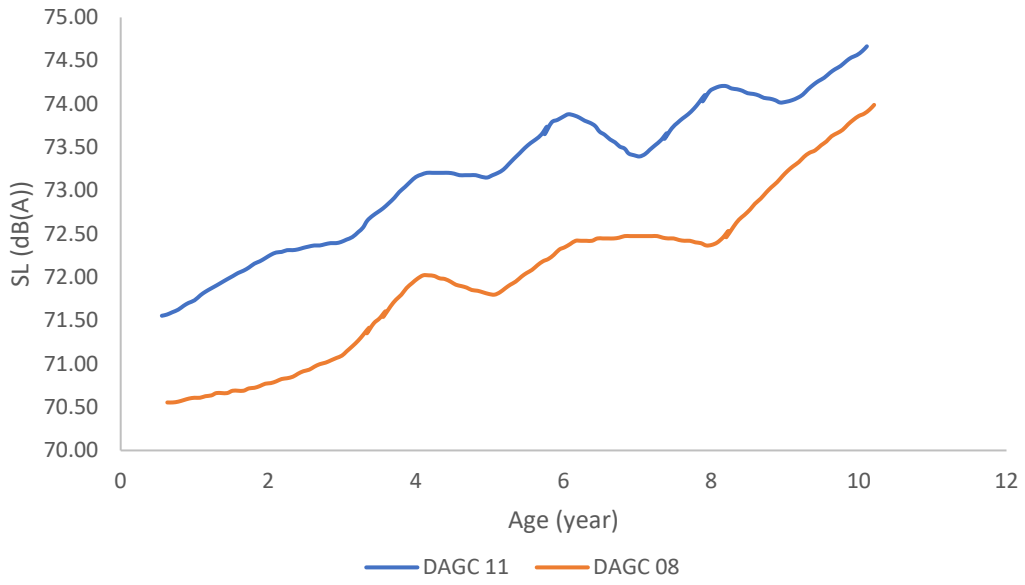

Figure 14. Noise evolution overtime for a passenger car at 60km/h for Dense Graded Asphalt Concrete with 11 and 8 mm Maximum Aggregate Size (adapted from [75]).

Aggregates with a small maximum aggregate size tend to generate a texture with fewer peaks, therefore, smoother if compared to the average size of rubber tire

treads. Their shape is also relevant, as “cubic” aggregates will allow the pavement to have a more negative texture [23,75]. However, to control noise, it is important not only to select the aggregates and their mixtures but also the compaction method during construction or even to consider the use of surface grooving techniques. Indeed, grooving/grinding techniques are more common on cement concrete pavements, with reported results ranging from 1.5 dB(A) to 3.0 dB(A) reduction when relative to traditional asphalt concretes [75].The grinding technique can also be applied to asphalt pavements with results in terms of noise levels ranging from 3 dB(A) to 5 dB(A) when compared to the previous existing surface [23,76]. This reduction is mainly due to the grinding process's effects, which eliminates the peaks, thus giving a final, more negative texture.

2.4.2 HiFASP with artificial aggregates

The use of Artificial Engineered Aggregate s for the construction of HiFASPs can appear as a challenge; from one hand, they can be considered as environmentally friendly as they can reduce the need for virgin aggregates, while on the other hand, they might have higher costs associated with the achievement of specific physical and mechanical properties. Nevertheless, the latter aspect could be overcome with the use of waste constituents and low energy production techniques, and their added value will reside in that they can be designed to a specific shape, size, and even microtexture to be used in HiFASPs.

The use of Artificial Engineered Aggregates in pavements is still under research, but interest is growing around them. One of the first successful attempts was to create artificial Light Weight Aggregates (LWA) made from clay waste minerals [77]. Recent studies have shown promising results, as surface layers containing LWAs can achieve friction levels above requirements (0.30-0.35 F60 – Friction number at 60km/h). As for the noise levels, according to the same specific literature, the reduction of 3dB (A) could be achieved even with traditional artificial LWAs[78].

The use of geopolymers or alkali-activated materials can have a predominant role in the development of Artificial Engineered Aggregates for HiFASPs or other paving solutions. In fact, those materials can be produced with specific waste powders generated from different industrial processes (e.g., mining, milling, sawing, washing, etc.) and transformed into castable construction elements, including engineered aggregates. Indeed, recent and on-going studies on the use of geopolymers and/or AAMs for the production of aggregates and mixtures are promising [3,71,79,80]. Nonetheless, with respect to their use in HiFASPs and other severe wearing surface conditions, additional research must be conducted to guarantee their durability, recyclability and to avoid any potential environmental impacts. Finally, it is straightforward that the use of Artificial Engineered Aggregates can provide opportunities in ways of smartening the pavements by embedding specific sensors and carrying different materials that can provide self-healing, self-sensing, and temperature-controlling features to the pavement layers[81,82]

2.5. Conclusions

Safety and health are of paramount importance when designing pavements, especially in the context of growing traffic; these aspects must be considered in order to find appropriate paving solutions. In the light of the proposed review, it is possible to infer the following final remarks:

- Solutions for improving skid resistance and noise exist and are currently used on many roads worldwide. They require a specific design of pavement texture to address one or both aspects.
- Aggregates are commonly natural and virgin, and for this reason, a careful selection is needed for their use in pavements providing specific skid resistance and acoustic characteristics.
- Artificial aggregates can be engineered to the desired shape, size, and microtexture so that specific characteristics can be implemented into the

pavement layers. In particular, their design can guarantee enhanced skid resistance and acoustic performance.

- HiFASPs represents a new solution that can make use of Artificial Engineered Aggregates, bringing road safety, human health, and environmental advantages. These can also be seen as highly reproducible, thus providing spatial and time homogeneity to the quality of road pavements worldwide.
- Engineered aggregates can become a tool for the implementation of different smart paving solutions. In these terms, future pavements are very likely to be a pattern of engineered surfaces having different functions and characteristics for different locations and uses.

Chapter 3: Preliminary Evaluation of Geopolymer Mix Design Applying the Design of Experiments Method

Copetti Callai S, Tataranni P, Sangiorgi C. Preliminary Evaluation of Geopolymer Mix Design Applying the Design of Experiments Method. Infrastructures. 2021; 6(3):35. https://doi.org/10.3390/infrastructures6030035

Abstract: The use of waste materials in road construction is becoming widely spread due to economic and environmental needs. Construction and demolition waste materials and mining residues have been studied for a long time. However, the use of fine materials, mainly from mine tailing and mining residue, is still complex, as they can be used as inert materials into the mix or can become a reactive agent in geopolymer mixes. In the present paper, an experimental application of basalt powder is proposed in the geopolymerization reaction to produce artificial aggregates. In order to understand the input and output variables' interactions used in the mix design, a statistical method called Design of Experiments was applied. With this design approach, it was possible to optimize the mix design of the experimental geopolymer mortars. The study evaluated several mixes with respect to their workability, compressive strength, and success rate of aggregates production. Finally, a model for predicting compressive strength is proposed and evaluated.

Keywords: design of experiments; geopolymer; artificial aggregates; mixture design; waste powder recycling

3.1. Introduction

The road construction industry is targeting greener solutions, and aggregate recycling has now become a necessary approach for many authorities and practitioners; for instance, a number of research projects and pilot trials are aiming to achieve consistent pavement performance when recycling up to 100% of reclaimed asphalt concrete. A broad set of other projects worldwide are dealing with the recycling of construction and demolition waste materials [2,83,84]. Nevertheless, aggregate quarries must still keep up with the global demand for virgin aggregates, especially required to construct the road surface layers with specific features (porous asphalt, stone mastic asphalt, microsurfacing, etc.) [85]. In this context, regarding the plant production processes for aggregates, the milling and crushing stages are usually followed by screening and washing prior to final stockpiling. Large amounts of mineral wastes are often produced, and therefore, it is important to research alternative solutions to reduce their impact on the environment. These waste materials, mostly mineral powder from plant processes, are becoming an environmental issue that requires landfilling limitations and strict legislation on their disposal [3].

Most of these fines cannot be directly used in cement concrete, cement bound layers, or bituminous layers, as they do not meet the requirements of the technical specifications, which are generally based on virgin materials' properties. Therefore, they need to be characterized according to the EN 13043, which specifies the properties of the aggregate' for road applications. [86]. In some cases, their direct use might hinder the strength and durability of the construction materials. In other cases, their recovery and recycling can be difficult and not economically feasible. However, some interesting and promising results have been obtained [87–89].

In the stream of the mentioned recycling approaches and, in order to overcome the above limitations and provide an alternative use to the scrap fine minerals, emerging solutions make use of the geopolymerization techniques. These foresee the

recycling of waste powders, known as precursors, in the alkali activation process provided by selected activators [3,90–92].

Examples of this approach exist and aim to instill additional value to the waste powders, using them as precursors to produce engineered artificial aggregates (either dense or expanded). These aggregates provide specific functionalities to the constructed layers while replacing the virgin natural materials. Artificial aggregates from the authors have shown interesting results when designed to increase friction and reduce noise in urban paving solutions [77,93,94]. Some studies were conducted to assess the use of artificial geopolymeric aggregates with interesting results regarding the physical characteristics [95,96]

The world of geopolymers is expanding, and different applications are today possible in various engineering fields, which find them suitable for their properties [11–13]. In parallel, a number of studies have assessed the environmental footprint of the geopolymers in comparison with traditional materials, e.g., cement concrete. The use of life cycle assessment (LCA) methodologies is helping to identify the actual benefits of this recycling approach towards a fully circular economy, with the obtained materials being re-recyclable.

The present research aims to characterize a geopolymer mix made of basalt powder to create artificial aggregates that have been designed into a specific shape that could tackle both noise and skid resistance issues in urban road surfaces. For this purpose, a statistical tool called Design of Experiments (DoE) was adopted to select the most suitable mix design, based on the material workability and strength and the success rate in the production of the artificial aggregates.

3.2. Materials

Geopolymers are synthesized by chemical reactions between silicates and aluminosilicate precursors under strongly alkaline conditions. These reactions lead to the creation of Si−O−Al−O polymeric bonds. Geopolymerization is an alkali-

activation process that changes vitreous structures (either partially or totally amorphous and/or in a metastable state) into a compact cementitious compound [78,97]. The inner structure of geopolymers and their properties depend mostly on the nature and proportions of the material's origin, the curing time and temperature, and the alkaline activators [97]. In fact, they are also called activators because they provide the highly alkaline medium necessary to dissolve silica and alumina. These alkaline activators are also responsible for stimulating the precursor materials' hydraulic properties in the process [78].

Geopolymer nanostructure has been the focus of many types of research, despite not being fully understood yet due to its extreme complexity [5]. The geopolymer material is composed of a mix of activators and precursors. Activators are alkaline liquids responsible for dissolving the precursors' structure and form a brand-new structure. Precursors are usually mineral powders that, when dissolved into an alkaline solution, react and, depending on their origin, will provide different characteristics in strength, finishing quality, and others.

Typically, the geopolymer design is made on a trial-and-error basis, mixing different precursors and activators' ratios. This method is used because the chemical reaction is very complex, and the materials used as precursors might not have a specific characterization. However, it is possible to use the theory from [98] to have a specific mix that, using the chemical components from the activators and precursors, allows the geopolymers' production.

3.2.1. Experimental Materials

As described above, the geopolymer mortar is an alkali-activated mix of activators and precursors. The activators are usually liquid and mixed in an alkaline solution with precursors, which are raw materials (powders) rich in alumino-silicate oxides and with selected reactivity. These components' reactions generate the geopolymer paste that, under specific curing conditions, becomes strong and durable enough to behave as a construction material for civil engineering purposes

3.2.1.1. Activators

The adopted activators are a mixture of liquid sodium silicate (SS) and sodium hydroxide (SH). Sodium silicate (SS) (Na2SiO3), also commonly known as water glass, is an aqueous solution of sodium oxide (Na2O) and silicon dioxide (SiO2) mixed according to specific proportions. A solution can be obtained with different properties by changing the ratio between SiO2 and Na2O; the solution is suitable for several applications, from the construction to the food field. The SS employed in experimentation is a commercial product, with a SiO2/Na2O ratio of 1.99 and a viscosity of 150–250 MPa·s at 20 °C.

Sodium hydroxide (SH) (NaOH) is a very basic NaOH solution, which allows the dissolution of the aluminosilicates. It increases the pH, and it compensates for the electric charge of the aluminates in the mixture. It is an inorganic compound that is a highly caustic base and highly soluble in water. A 10 M SH was used in the present work.

3.2.1.2. Precursors

Different precursors have been used in various research studies, among them fly ash [99], metakaolin [3], and blast furnace slag [100]. The type of precursor has a direct impact on many mechanical and chemical properties of geopolymers. Inert waste dust could act as a filler/aggregate in the geopolymer structure. On the other hand, a reactive amorphous waste could act as a precursor in the geopolymer matrix. Therefore, studying the precursors' mineralogy is vital to understand its constituent species and possible reactivity [3]. The materials used in this paper were metakaolin and basalt powder.

3.2.1.3. Metakaolin Powder

Calcined kaolinitic clays, otherwise known as metakaolin (MK), were one of the first precursors used in geopolymer research. MK's initial application was mainly in paper and plastic industries, where it was used as filler. The composition of metakaolin is mainly made of SiO2 and Al2O3 with a small percentage of metal oxides [98].

When used in cement concrete applications, MK increases the compressive and flexural strength of concrete, reduces its permeability, increases its resistance to chemical attack, enhances the workability, and increases the durability of the concrete [101]. Geopolymers can benefit from the MK qualities, especially as it has a high Al2O3 content, being very reactive to the activators [. In the present work, it was used a commercial metakaolin with a size passing 0.063 mm sieve.

3.2.1.4. Basalt Powder

The basalt powder is a residual from the extractions and production processes in trachyte quarries. As volcanic rocks, basalt deposits are present in almost every country. This lithotype is widely used, depending on each deposit's intrinsic characteristics, in the construction field for its mineralogical, chemical, and physical properties. The extensive use of this material for bituminous mixtures and concretes leads to the production of large quantities of sands and powders during the crushing of aggregates [3]. The basalt powder's chemical composition is presented in Table 3, based on the Reference Intensity Ratio (RIR) method for a semi-quantitative estimate with 10–20% error.

Table 3. Chemical composition of the basalt powder (Reference Intensity Ratio (RIR) method).

Name	Composition	Percentage
Leucite	$(K(AlSi_2O_6))$	44
Augite	$((Ca,Mg,Fe)_2Si2O_6)$	17
Anorthite	$(Ca(Al_2Si_2O_8))$	12
Orthoclase	$(K(AlSi_3O_8))$	5
Muscovite	$(KAl2(Si_3Al)O_{10}(OH)_2)$	15
Magnesiohornblende ferroan	$(Ca_2(Mg_4Fe^{3+})\ (Si_7Al)O_{22}(OH)_2)$	4
Magnetite	$(Fe^{2+}Fe^{3+}O_2)$	2
Ilmenite	$(Fe^{2+}Ti^{4+}O_3)$	1

The data presented here demonstrate that the basalt powder has an interesting amount of aluminum and silica. These indicate that the precursors are adequate to create a geopolymer, as these minerals are responsible for the proper geopolymer structure [5,98].

3.3. Methodology

3.3.1. Design of Experiments

For research in every field, the development of experiments is paramount to achieving a result. At any given experiment, a set of variables can or cannot be controlled, with different degrees of interactions and influences on the experiment's outcome. In such a complex scenario, the use of Design of Experiments (DoE) has been widely employed. DoE is a statistical approach used to plan an experiment so that the data can be analyzed to a valid and objective conclusion, as it helps understand the correlations between variables and their interactions [105].

In a DoE, the first step is the experiment goal. It can be the optimization of a process or responses or could be the study of the effect of individual factors or variables on the outcome. After deciding the experiment goal(s), it is necessary to define the boundaries of the experiment. The boundaries could be the temperature range of the curing, from 40 °C to 70 °C, as an example. It will define the experimental region. This must be done to each variable that can be controlled, determining the levels for each of the factors.

In this paper, it was used to plan the experiment and define the most appropriate mix design for the mixture, aiming for a specific outcome. It allows an understanding of how the input variables interact with each other and how they influence the output variables. An attractive property of the DoE is that it is possible to optimize the experiment, reducing the number of levels of each variable (factor) or even the number of variables. Thus, assessing only the relevant interactions to the desired outcome, the DoE can generally be represented as in Figure 15.

First, there is the controlled input: these inputs gather all the parameters that are measurable and controlled by the researcher. An example is the solution pH: it is a parameter that it is possible to control and measure, but it remains unchanged throughout all the experiments. Moreover, the uncontrolled input is not measured by the researcher, either because they are by definition unmeasurable, or their

control is too difficult or useless. As an example, it can be stated that the room temperature variation is an uncontrolled input, and maybe within a specific range, it is irrelevant. The input variables contain the actual parameters that the researcher will control and assess during the experiment, such as curing time and temperature and the amount of each material in the mix.

The outputs are also controlled and uncontrolled. The first one refers to the desired and measured actual results of the experiment, such as compressive strength. The former refers to the results that are either not measured or not accurately measured for any reason.

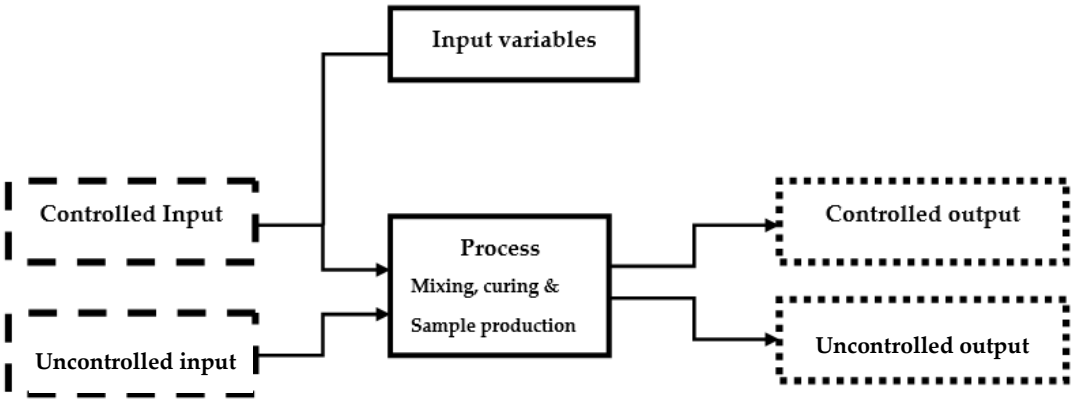

Figure 15. Flow chart of the adopted Design of Experiments (DoE).

It is relevant that when doing any experiment, the researcher is aware of each one of these parameters, especially on the DoE, as these parameters will serve to assess, by statistical analysis, their interaction.

In the present research, the inputs are:

- Controlled input—Mixing time.
- Controlled input—Mixing temperature.
- Uncontrolled input—Air humidity.
- Input variables:

- Percentage of basalt: it represents the amount of basalt in an MK-and-basalt mix.
- L/S ratio: it is the ratio between activators (liquid) and precursors (solid).
- Temperature: it is the controlled temperature used to cure the samples.
- Time: it is the controlled curing time.

As for the output variables, the controlled and uncontrolled are:

- Controlled output—Fluidity is a measurement of the mortar spread. It gives an indication of how workable the mortar is.
- Controlled output—Success rates the percentage of sound aggregates produced.
- Controlled output—Compressive strength is the resistance unconfined compressive strength of cubic samples.
- Uncontrolled output—Sample humidity.
- Uncontrolled output—Sample leaching.

3.3.2. Sample Production and Testing Procedure

The procedure adopted for the production and testing of geopolymer samples was conducted as described in the literature [5,98], and it is depicted as a flowchart in Figure 16.

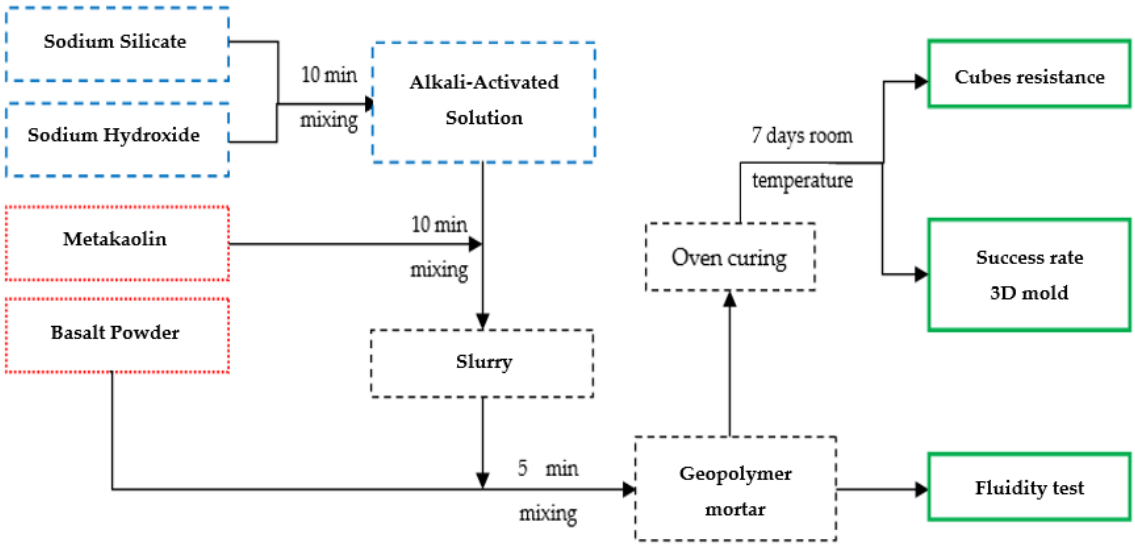

Figure 16. Flowchart of the production and testing procedure.

The activators are mechanically mixed for at least 10 min to generate the alkali-activator solution. Then they are mixed for an additional 10 min with the addition of the MK powder; the next step is to mix the obtained paste with the basalt powder for another 3 min at least or until it appears homogeneously mixed. The mortar paste is subsequently tested in terms of workability using a fluidity test; the remaining material is cast into the cubic molds and into artificial aggregates molds. The molds are then placed into the oven at the specified curing temperature and time. After curing, they are removed and unmolded. The artificial aggregates are evaluated in terms of production success rate. At the same time, the cubic samples are placed into plastic tape for an additional seven days' curing at room temperature and then tested for compressive strength.

3.3.3. Fluidity of Grout According to EN 14824-3: 2012

The fluidity can be considered as an indicator of how easy it would be to inject the mortar mix into the 3D-printed molds in the laboratory. A similar approach shall be used in the case of industrial production. The fluidity test was conducted using as reference the following standard: EN 14824-3: 2012 Grout for prestressing

tendons—Part 3: test methods. Even if the reference used is for cement-based grouts, it can give a valid indication of whether the fluidity for geopolymers as a specific standard is still unavailable.

The fluidity (flowability) is measured by the diameter of the circle created by the geopolymer mortar mix flown onto a smooth plate. The test consists of placing the mix into a cylindrical mold with a diameter of 39 mm and 60 mm in height. The cylinder is made of plastic or steel (if used it is necessary to clean it immediately), and the base plate should be smooth.

This cylinder is placed onto the plate surface, filled with the mortar, and moved upward at about 15 cm for a maximum of 30 s. The material spreading should be measured in two different perpendicular directions. The mean diameter is calculated by the average of the two measurements. In Figure 17, it is possible to see the cylinder with the mortar mix inside and ready for testing; other pictures show the spread material being measured in diameter.

Figure 17. Fluidity testing for geopolymer mortars' fluidity.

3.3.4. Success Rate of Aggregates Production

As the mortar was used to manufacture artificial aggregates with a specific geometrical design, it was necessary to evaluate the production success rate. In order to quantify it, a simple visual test was conducted after the curing process; the samples were unmolded, and each artificial aggregate was classified as "good" or "bad" on a subjective basis. Suitable aggregates were the ones that kept the desired

shape and presented no visible holes or imperfections, while bad ones were those that had any kind of visible defect. Figure 18 serves as an example of the visual test and shows some considered defects from production. Thus, the success rate is the percentage of aggregates with good quality.

The present method for classification cannot be applied to mass production for obvious reasons. Therefore, it is suggested to use the sieving technique to select the aggregates with the most appropriate shape and separate them from those with significant failures.

(**a**) (**b**)

Figure 18. Success rate example over production of 20 aggregates: (a) classification of aggregates; (b) failure examples.

3.3.5. Compressive Strength: EN 1015-11: 2019

The selected mechanical test was the unconfined compressive strength on geopolymer hardened cubes of 40 mm side length. The cubic samples were cast and cured as instructed in the DoE. The compressive strength was measured as described in the EN 1015-11 standard by means of a hydraulic press (Figure 19) at constant load speed.

As for the surface treatment in the cubic samples, it was unnecessary as the samples are completely smooth without peaks or holes (Figure 19), and a preload of 5 daN was always applied before running the tests. The compressive resistance for each type of mixture of the DoE is calculated as the average strength of four tested cubes.

(a) **(b)**

Figure 19. Compressive strength of geopolymer cubes: (a) sample in hydraulic press; (b) cubic sample before the test.

3.4. Testing Results and Analysis of the DoE Approach Outcomes

The input variable used in the DoE is shown in Table 4. The first column corresponds to the run order of the experiments, while the second lists the amount of basalt in percent (for instance, 60% basalt means a 40% MK). Other columns are the ratio between the activators and precursors (L/S), the curing temperature in °C, and the curing time in hours.

Table 4. Design of Experiments input variables.

Run Order	Basalt (%)	L/S Ratio	Oven Temperature (°C)	Curing Time (hours)
1	80	0.50	50	6
2	90	0.65	50	2
3	80	0.65	60	8
4	90	0.50	60	4
5	90	0.60	70	8
6	70	0.55	50	8
7	80	0.55	70	4
8	70	0.65	40	4
9	80	0.60	40	2
10	60	0.55	60	2
11	70	0.60	60	6
12	60	0.55	40	8
13	60	0.60	50	4
14	90	0.55	40	6
15	60	0.65	70	6
16	70	0.50	70	2

Every single mix was produced and tested for the fluidity of the geopolymer paste, for compressive strength on cubes, and for success rate on aggregates as described in Figure 16; results are listed in Table 5.

For each run order, three samples were used to calculate the average grout spread. As for the compressive strength, four samples were used to calculate the average. As for the success rate, it was assessed by the overall production for each run order.

The percentage variation is presented on the Table 5 for the grout spread method and compressive strength.

Table 5. Results obtained for the controlled output variables.

Run Order	Grout Spread Method (cm) [106]	Percentage Variation (%)—Grout Spread Method (cm) [106]	Compressive Strength (MPa) [107]	Percentage Variation (%)—Compressive Strength (MPa) [107]	Success Rate (%)
1	5.30	13	17.27	9	25
2	13.55	1	0.67	14	85
3	11.75	1	13.11	4	75
4	8.75	4	5.26	3	75
5	12.50	0	1.60	4	20
6	5.35	1	36.59	14	80
7	8.85	1	11.99	9	95
8	10.50	8	35.56	18	55
9	10.70	1	22.70	11	25
10	-	-	39.74	16	0
11	8.80	8	29.37	9	50
12	-	-	45.82	10	0
13	5.55	11	44.33	22	40
14	11.20	0	4.49	10	45
15	8.20	3	35.51	19	100
16	-	-	25.89	23	0

The analysis of results made for each output variable shows:

- Grout spread method (fluidity) [106]:
  - Samples 10, 12, and 16 did not provide any measurable results because the mixture was very viscous and did not flow through the mold in the standard specified time.
  - Samples 2 and 5 achieved the largest fluidity diameters.
  - The higher the fluidity, the easier it is to pour the mortar into the mold.
- Compressive strength [107]:
  - Samples 12 and 13 achieved the highest compressive strength.
  - Samples 2, 5, and 14 recorded the lowest results.
- Rate of success:

- Samples 10, 12, and 16 gave no results, as the material was not injectable into the aggregates molds.
- Samples 7 and 15 achieved the best results with over 95% suitable aggregates.

It is important to note that results do not allow an easy understanding of how the input variables interact and which would be the most appropriate mix design. However, due to the use of the DoE approach, it is possible to assess the input variables' behavior and their influence on the output variables. The series of graphs called Prediction Profiler from JMP® software (Version 14.0. SAS Institute Inc., Cary, NC, 1989-2019) allow to understand how each input variable influences each of the output variables.

The light red shadow scale represents the confidence interval of each input variable to the corresponding output variable. The red line indicates the relation between the variables, and its tilt means in which way it interacts. Tilted from bottom to top it shows a positive interaction, from top to bottom—negative, the horizontal line indicates that there is no interaction. The cloud of points shows the real data position in relation to the pair of the input and output variables.

From Figure 20, it can be asserted that unconfined compressive strength (UCS) has an opposite relation to the basalt content, meaning that the increase in basalt content would decrease the UCS value. The temperature has an inverse relation to the UCS.

The cured samples were taken out of the oven after the determined time, wrapped in plastic film, and left to cure at room temperature for seven days, and all of them were tested at the same age. The curing time and temperature input variables had little influence on the compressive strength. This might be due to the MK used, which was not very reactive. Therefore, further study is needed on this topic.

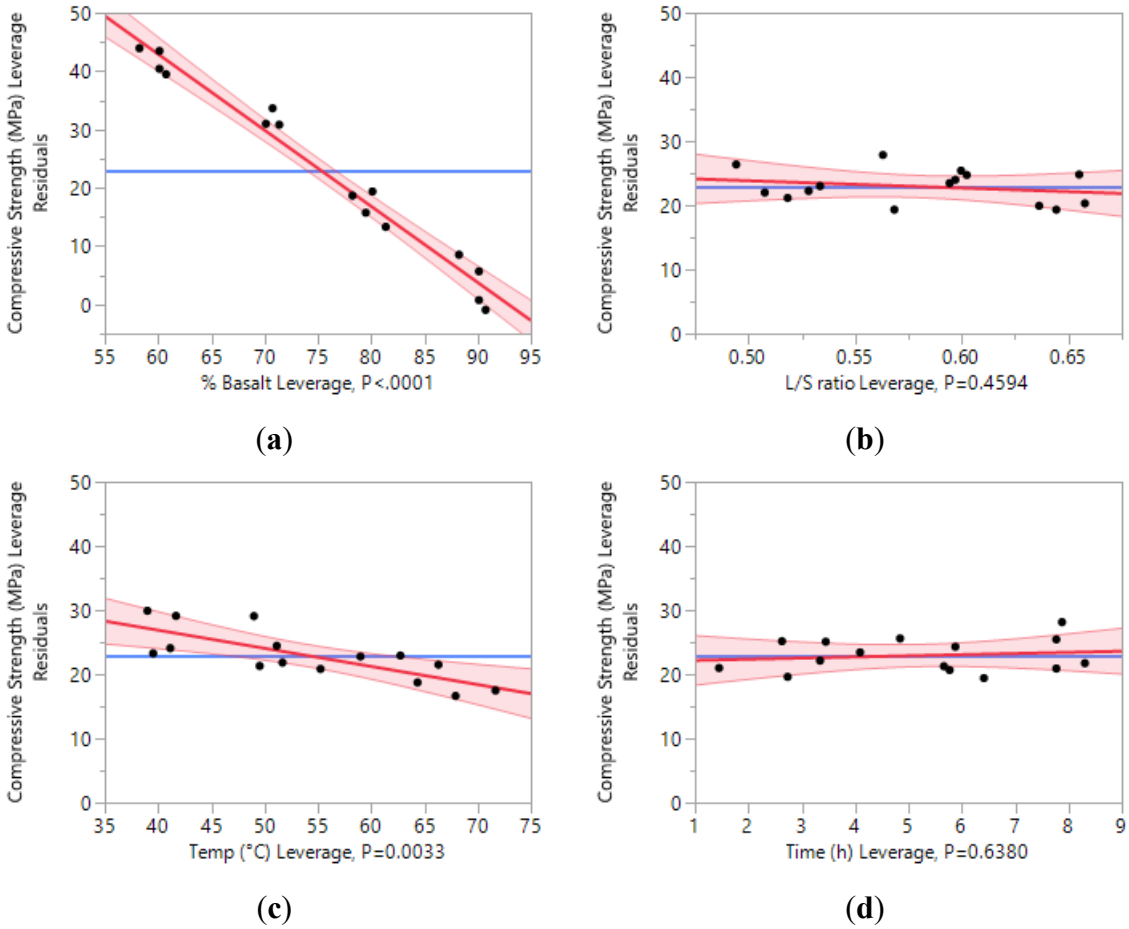

Figure 20. Input variables sensibility and influence on the Unconfined Compressive Strength (UCS): (a) basalt leverage; (b) L/S ratio leverage; (c) temp (°C) leverage; and (d) time (h) leverage (Software JMP 14).

With the parameter estimates, it is possible to evaluate their importance in a future model. Table 6 shows each term's parameter estimate, standard error, and probability for the compressive strength. The lower the probability is, the more reliable the input variable is to the model prediction, the most suitable values are identified with an asterisk. The estimate is related to how strong its importance is in the model, and standard error shows how good of a fit there is of the data in relation to the regression line. The lower the number, the better it is.

Table 6. Equation terms estimation and probability for predicting compressive strength.

Term	Estimate	Std Error	Probability > |t|
Intercept	142.14414	10.75799	<0.0001 *
% Basalt	-1.304961	0.068342	<0.0001 *
L/S ratio	-11.35938	14.76356	0.4594
Temperature (°C)	-0.282461	0.073818	0.0033 *
Time (h)	0.1791016	0.369089	0.6380

* Values with acceptable significance

In Figure 21, it is possible to note that the confidence shadow is too wide, thus meaning that the input variables have a minor relation to the output variables. Nevertheless, it is possible to note that basalt, L/S, and temperature have a minor positive influence.

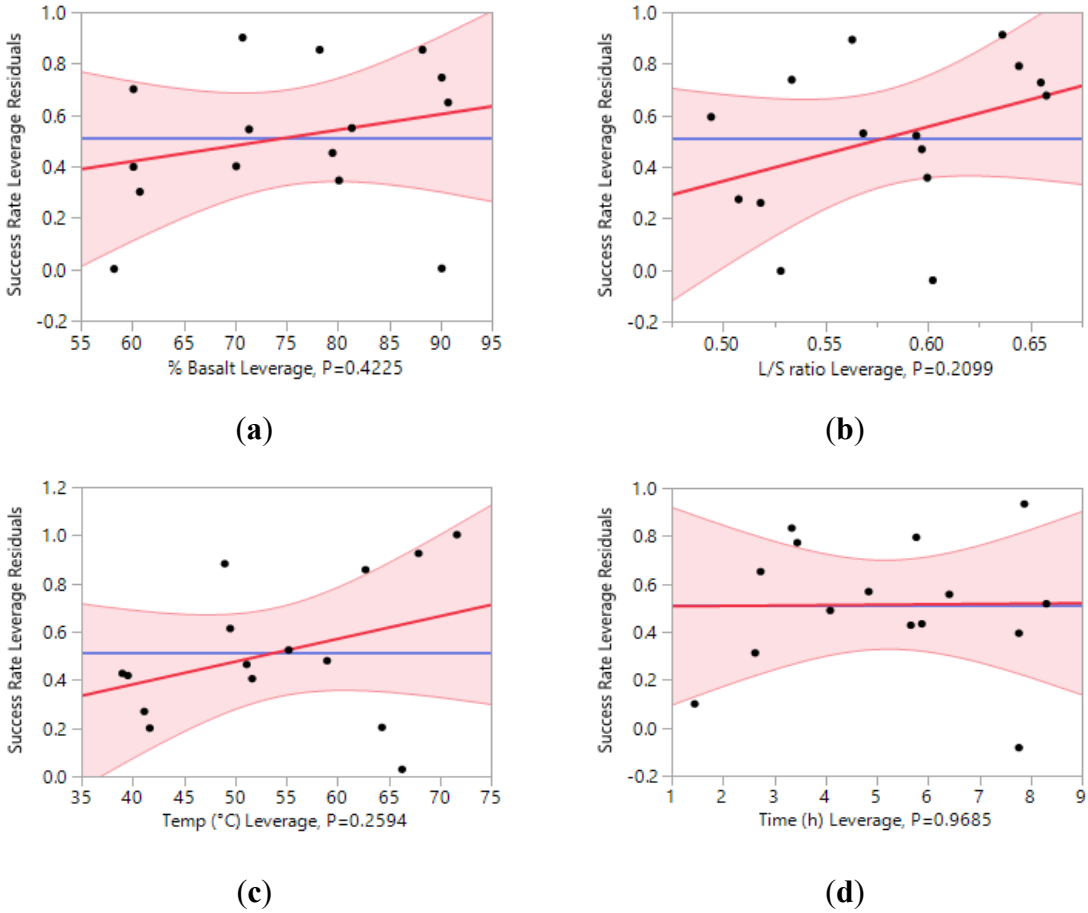

Figure 21. Input variables sensibility and influence on the success rate: (a) basalt leverage; (b) L/S ratio leverage; (c) temp (°C) leverage; and (d) time (h) leverage (Software JMP 14).

It is noted in Table 7 that the input variables have no influence on the output variables, as can be seen with the probability values. This might be due to the way the experiment was designed or a lack of sufficient data to assess its interaction.

Table 7. Equation terms estimation and probability for predicting success rate.

Term	Estimate	Std Error	Probability > |t|
Intercept	-1.690266	1.149447	0.1722
% Basalt	0.0061064	0.007302	0.4225
L/S ratio	2.1138298	1.577426	0.2099
Temperature (°C)	0.0094309	0.007887	0.2594
Time (h)	0.0015957	0.039436	0.9685

As for the grout spread method (Figure 22), it is noted that the temperature and time variables are not relevant to the test as it is performed prior to the curing. The other variables have a high interaction probability, thus making it possible to assess their interactions.

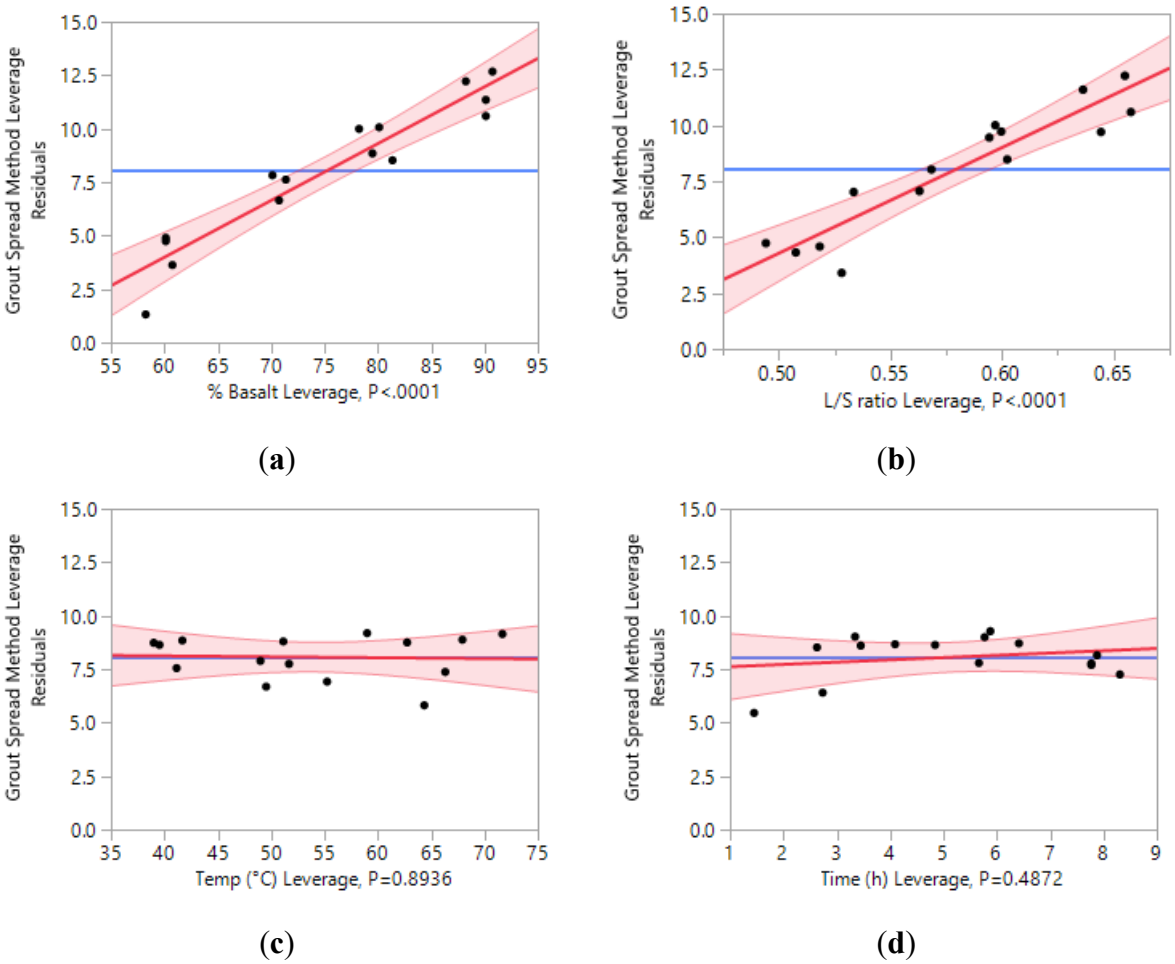

Figure 22. Input variables sensibility and influence on the grout spread method: (a) basalt leverage; (b) L/S ratio leverage; (c) temp (°C) leverage; and (d) time (h) leverage (Software JMP 14).

In Table 8, it is possible to note, as stated before, that both temperature and time do not have a reasonable probability, which is entirely correct, as these input variables have not influenced the output variable being assessed. Moreover, intercept, basalt, and L/S ratio have an appropriate probability value, meaning that these variables are intrinsically related to the measured output variable (grout spread method)

Table 8. Equation terms estimation and probability for predicting the grout spread method.

Term	Estimate	Std Error	Probability > |t|
Intercept	-39.71713	4.303934	<0.0001 *
% Basalt	0.2656011	0.027341	<0.0001 *
L/S ratio	47.310638	5.906438	<0.0001 *
Temperature (°C)	0.004053	0.029532	0.8936
Time (h)	0.106516	0.147661	0.4872

The model of compressive strength suffices to select a mix design since the grout spread method and success rate are indicators of the workability of the mortar. Avoiding the points with low grout spread results and aiming for the higher success rate values is possible to narrow the input variables suitable to be used in the model for compressive strength.

With the analysis of the input and output variables interactions in Figure 20 and Table 6, it was possible to develop a model for the compressive resistance, as given in Equation 1.

$$CR(MPa) = 142.3 - 1.30 \times Basalt - 11.36 \times Liquid - 0.28 \times Temperature(°C) + 0.18 \times Time(h) \quad (1)$$

The graph in Figure 23, plots the laboratory-measured compressive strength against the DoE-predicted one. The regression model between the two variables as a valid correlation (R2 = 0.975), thus providing results within acceptable confidence in the calculated confidence interval.

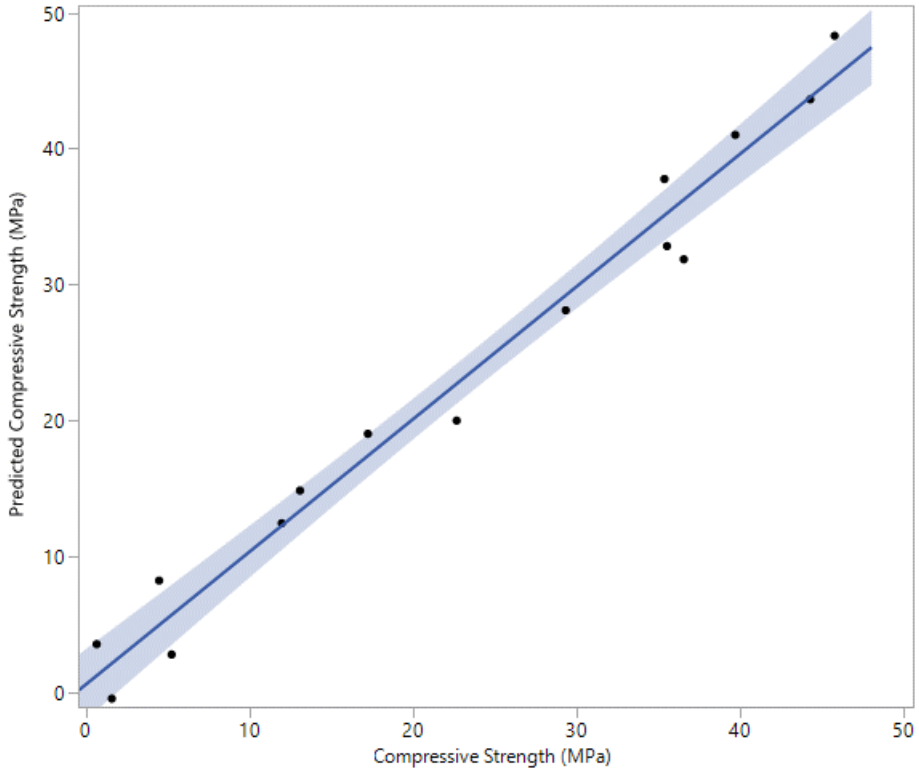

Figure 23. Predicted compressive strength vs. measured compressive strength with fitness shadow.

The shadow represents the confidence interval on how accurate the model is. Some points are out of confidence due to the estimation error of 5%.

The DoE method allows to identify the most relevant input variables: how these are interrelated among them, and which is their influence on the output variables. Therefore, it is possible to select a statistically optimized mix design and curing procedure to achieve a minimum desired compressive strength while considering a proper fluidity and success rate for the production of the artificial aggregates in the laboratory. This approach should eventually yield into sound, regularly shaped, and well-cemented aggregates.

As a concluding step for the applied DoE approach, a new set of 14 identical mixes with four cubic samples each were produced and tested to confirm the model accuracy. Each sample was submitted to the compressive strength test, and an average of them was calculated. For these samples, the mix design selected was:

70% basalt (30% MK), 0.5 L/S, 50 °C, and 2 h curing in the oven. According to Equation 1, the compressive strength should be 31.35 MPa with a confidence interval of 95%.

The results of the new samples made with this selected mix are presented in Figure 24. Out of fourteen, only for two samples the recorded compressive strength was lower than the predicted value, but only one lower than the confidence interval of 95%, represented as a dashed red square in Figure 24.

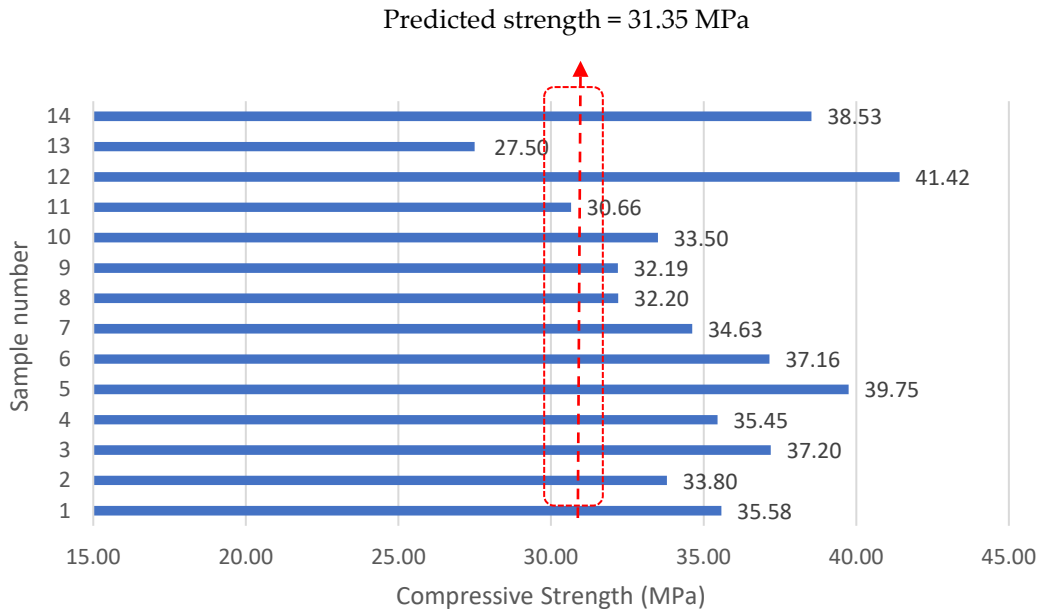

Figure 24. DoE results in confirmation by compressive strength tests on additional samples.

The success rate and grout were measured for the 14 samples, and it is noted that their values are over the expected, as presented in Table 5. It is due mainly to the uncontrolled output variables, such as an increase in room temperature, humidity, and MK quality, and the operator experience.

It is necessary to run more tests with more controlled variables to assess the significance of the input variables for grout spread and success rate.

3.5. Conclusions

The present paper proposes the preliminary use of the DoE statistical approach to optimize a geopolymer mix design with different proportions of precursors, activators, as well as selected temperatures and time for curing. This is done in order to understand how the input variables reciprocally interact and what their possible output is. The final goal is to choose a mix design and curing process that leads to a workable mixture, which is able to reach an adequate compressive strength while using as much basalt powder as possible and minimizing the curing time and temperature. The mechanical strength is considered essential for the possible production of sound and durable artificial aggregates. Furthermore, the maximization of basalt content and the minimization of curing time and temperature are essential to reduce the carbon footprint of the final material.

The following conclusions can be drawn from this preliminary study:

- The DoE used was satisfactory because it provided a reliable model to predict the compressive resistance of the proposed materials.
- According to the proposed statistical model, the temperature has little influence on the final resistance. This is debatable as the literature says otherwise. In this research, this might be due to the quality of the MK. Further studies are necessary with a different MK.
- The model helps the researcher to select the most appropriate mix design.
- The model is only relevant for this specific DoE, and it is necessary to change it if the materials used are different.
- The laboratory workability is here directly related to the success rate in the production of aggregates. A material with low workability (fluidity) was found to be difficult to inject into the aggregate's molds. These processes will more likely change at a larger production scale and so will be for the required fluidity. A new DoE will be necessary.

- Overall, the adopted DoE approach provided the authors with consistent information on how each variable behaves and interacts with the final material's characteristics.
- In light of the above, the work on the production of geopolymeric artificial aggregates from waste powders will continue. Aiming for the construction of engineered pavement surfaces that brings benefits in terms of skid resistance (road safety) and noise abatement, the large-scale production of artificial aggregates is envisaged in the near future of this research.

Chapter 4: Artificial aggregates from Alkali-Activated basalt powder: a preliminary evaluation

Copetti Callai S, Tataranni, S., De Rose, M., Natali Murri A. Vaiana, R. Sangiorgi C. Artificial aggregates from Alkali-Activated basalt powder: a preliminary evaluation. (Submitted to Materials (ISSN 1996-1944))

Abstract: : The widespread use of natural aggregates is one of the main causes of depletion of natural resources, as aggregates are constituents of several construction materials. Alternatively, it is today proven to be feasible to use the mining tailings, either natural and recycled materials, to produce artificial aggregates through specific processes. A possible way to produce artificial aggregate is through the alkali-activation of the powdered material in a process called geopolymerization. This study proposes to use a basalt powder and two different metakaolins as precursors for the production of an alkali-activated artificial aggregate, with a specific shape and size achieved by using 3D printed molds. The experimental aggregates were evaluated using traditional tests for natural aggregates, such as resistance to compression, specific density, resistance to abrasion and to fragmentation. Furthermore, the material was chemically analyzed in order to evaluate the geopolymerization process promoted by the two adopted metakaolins. The physical tests showed that artificial aggregates do not perform well in terms of resistance to wear and fragmentation, which can be improved. However, it revealed promising results in terms of skid, polishing and micro-texture.

Keywords: Artificial aggregates; Geopolymers; Basalt powder, Alkali-Activated Materials, Polished Stone Value (PSV), micro-Deval.

4.1. Introduction

Natural aggregates mainly consist of crushed rock and sand coming from crushing bedrock or possibly from unconsolidated sand and gravel [108]. The widespread use of natural aggregates is one of the main causes of depletion of natural resources, considering that aggregates are the basic constituent of several construction materials such as bituminous and cementitious concretes. According to the estimates of the year 2015, around 48 billion tons of natural aggregates were used worldwide, with a predicted growth rate of 5 % every five years [109]. Thus, finding alternatives to natural aggregates is becoming crucial in the current scenario of sustainable transition that involves the construction industry [110,111]. The increasing need for sustainable construction materials is driving the research towards the reuse and recycling of waste to produce "recycled," "manufactured," and "artificial" aggregates [4]. The latest version of the EN 13242 standard [112] lists, in fact, recycled and manufactured aggregates among the aggregates that can be used in civil engineering work and road construction.

Recycled aggregates are classified as a result of the processing of inorganic or mineral material previously used in construction, while the manufactured ones come from an industrial process involving thermal or other modifications. To date, the most common example of recycled aggregates is represented by the Construction and Demolition Wastes (CDW), which are processed to obtain recycled aggregates to partially or completely substitute the natural aggregates for the production of construction materials [113]. On the other hand, there are several examples of manufactured aggregates, such as various slags or materials produced involving thermal treatment of pumice, volcanic ashes, clays or siliceous rocks [114,115]. In the last years, in addition to these mineral-based manufactured aggregates, an increasing number of by-products or wastes have been processed and treated to produce artificial aggregates (AAs)[116]. Unlike the processing of mineral-based materials, most of the solid wastes or industrial by-products must be pre-treated in order to eliminate the presence of potential harmful substances. As an example, Incinerator Bottom Ashes (IBA) contain heavy metals, chlorides,

sulfates and other pollutants and must be pre-treated accordingly to be safely recycled and used as AAs [117]. However, despite the relatively long and expensive pre-treatment, the production of AAs contributes to the reduction in the exploitation of raw materials and represents potential economic and functional values for by-products and wastes [118,119]. Several by-products from different fields have been studied and experienced for the production of AAs, from coal bottom ash to crumb rubber, to plastic waste, to waste glass [120–125], and many others are still under investigation.

In terms of production methods, AAs generally come from a two-step procedure: granulation and hardening process [116]. The granulation process is widely adopted in different sectors (construction materials, food industry, pharmaceutical, etc.) and consists of the agglomeration of powdery substances to form grains or granules. The granulation technology for AAs production generally requires the addition of liquid (wet granulation process) to create bonds between particles strong enough to bind them together and so enlarge their sizes. The following hardening step is needed to solidify the agglomerations to achieve specific mechanical properties. Based on the type of powder and the final application of the granules produced, different hardening technologies can be adopted. According to the most widespread applications of AAs, the most common hardening procedure are: sintering, cold-bonding and alkali-activation [116]. In the first process, the AAs are produced through a thermal treatment of the fresh granules at very high temperature (up to 1000 °C). The material undergoes an expansion and vitrification process which allows the strengthen of the granule. Being the sintering a chemical and physical process, the quality of the final AA, in terms of mechanical properties, is directly related to the chemical composition of the base material [125]. As downside, this method has a significant impact in terms of emissions and energy consumption, due to the high temperature needed to run the process. On the contrary, the cold bonding hardening technology is widely adopted considering the possibility to cure the AAs in water or at constant humidity. In this case, the strength of the granule is given by a pozzolanic reaction [126]. As a consequence, not every material is suitable for

this process, being the pozzolanic reaction is directly affected by the reactivity of the base material. The chemical reaction is also the core of the third mentioned hardening method: alkali-activation. This is a chemical synthesis that occurs between silica and alumina-rich based materials and strong alkali solutions, which allows the development of ceramic materials [127]. In the production of AAs through this method, alkaline solutions such as blends of sodium hydroxide and sodium silicate are added as a binding agent as water replacement during the granulation process. Considering the relatively easy process and the absence of high temperatures for curing, the alkali-activation of AAs is gaining popularity. Moreover, several studies verified the possibility of achieving high-performance AAs in terms of mechanical properties [128,129].

Following this trend of research, in the present paper, a preliminary laboratory characterization of AAs produced through the alkali-activation of a basalt powder is presented. Even if the use of basalt for the formation of alkali-activated material has already been studied by different authors [130,131], the novelty of the present research is represented by the production process of AAs. The proposed basalt alkali-activated AAs are, in fact, cured in specific molds created with a 3D printer in order to have defined shapes and sizes, conceived to improve friction and acoustic properties when applied in the construction of road pavements wearing courses.

4.2. Materials and Methods

The geopolymer material is obtained from a mix of activators and precursors. Activators are alkaline liquids responsible for dissolving the precursors' structure and forming a brand-new structure. Precursors are usually aluminosilicate powders that, when dissolved into an alkaline solution, react and, depending on their origin, will provide different characteristics and proprieties to the final material. The geopolymer design might follow the trial-and-error method [98], mixing different precursors and activators' ratios, when the materials used as precursors constitute a

heterogeneous and complex system and the involved chemical reactions are hard to predict in advance. However, it is possible to use theoretical basis to have a specific mix that allows the geopolymers' production based on the chemical constitution of activators and precursors. In the following paragraphs, a basic characterization of the materials used in the experimental application is presented.

4.2.1. Precursors

Different precursors have been used in various research studies, among them fly ashes [99], metakaolins [3,132], and blast furnace slags [100]. The type of precursor has a direct impact on many mechanical and chemical properties of the geopolymer. Inert waste powder could act as a filler/aggregate in the geopolymer structure. On the other hand, a reactive amorphous waste could act as a precursor in the geopolymer matrix. Therefore, studying the precursors' mineralogy is vital to understand its constituent species and possible reactivity [3]. The materials used in this research as precursors were metakaolin and basalt in the shape of powder.

4.2.1.1 Basalt

Basalt powder is a by-product of the mining industry that has some commercial value. It can be used as a filler material [133] in fibers production or as a reactive part of the geopolymer mix [130,131]. In this research, the material used was a basalt powder with the following mineralogical composition, obtained by XRD analysis (Table 9).

Table 9. Chemical composition of the basalt powder (Reference Intensity Ratio (RIR) method).

Name	Composition	Percentage (%)
Leucite (L)	$(K(AlSi_2O_6))$	44
Augite (Au)	$((Ca,Mg,Fe)_2Si2O_6)$	22
Anorthite (An)	$(Ca(Al_2Si_2O_8))$	11
Orthoclase (O)	$(K(AlSi_3O_8))$	5
Muscovite (M)	$(KAl2(Si_3Al)O_{10}(OH)_2)$	5
Magnesiohornblendeferroan (Mh)	$(Ca_2(Mg_4Fe^{3+})(Si_7Al)O_{22}(OH)_2)$	4
Magnetite (Mt)	$(Fe_2+Fe_3+O_2)$	1

The XRD of the Basalt powder is shown in Figure 25, where it is possible to see the intensity of each material as described in Table 9.

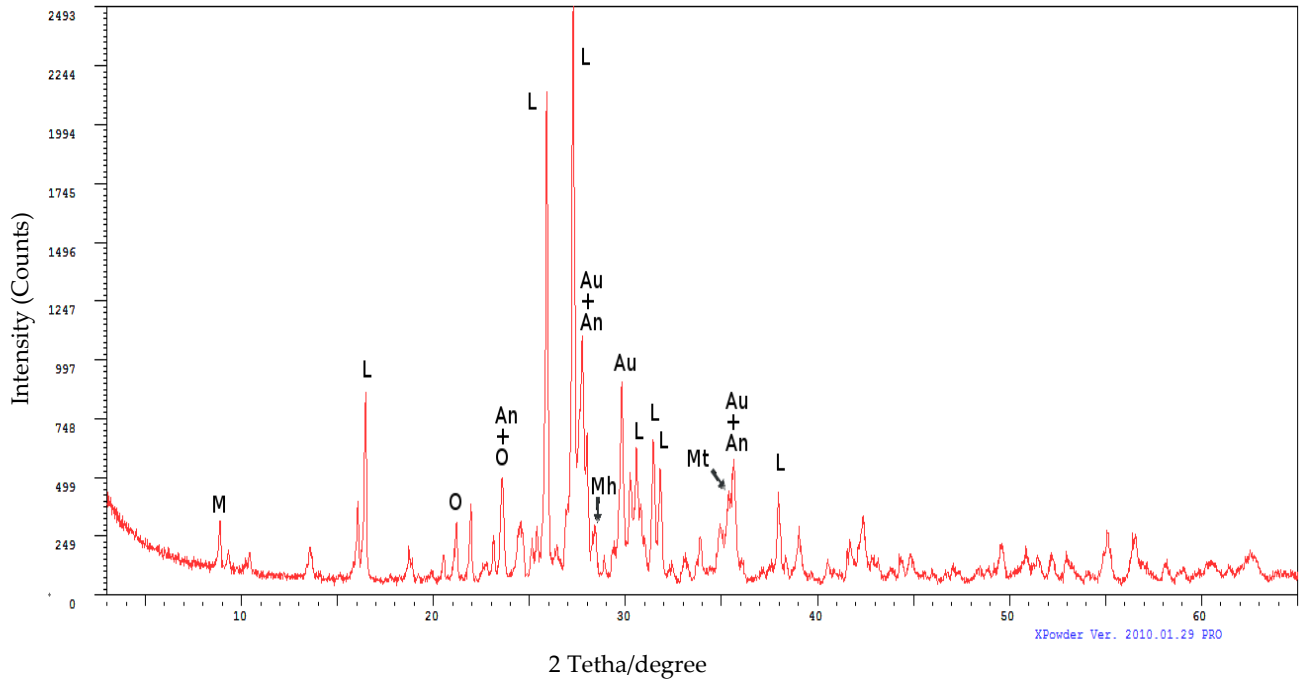

Figure 25. XRD of Basalt powder.

Several researchers used basalt as a geopolymer material [131,133,134]. The data presented here demonstrate that the basalt powder has a sufficient amount of aluminum and silica. These indicate that the precursor is adequate to generate a

geopolymer, as these minerals are responsible for the final geopolymer structure [5,98].

4.2.1.2 Metakaolin

Calcined kaolinitic clays, otherwise known as metakaolin (MK), were one of the first precursors used in geopolymer research. MK initial applications were mainly in paper and plastic industries, where it was used as filler. The composition of metakaolin is primarily made of SiO2 and Al2O3 with a small percentage of metal oxides [98]. When used in cement concrete applications, MK increases the compressive and flexural strength of the concrete, reduces its permeability, increases its resistance to chemical attack, enhances the workability, and increases the durability of the concrete [101]. Geopolymers can benefit from the MK qualities, especially as it has a high Al2O3 content, being very reactive with the activators [102–104]. In the present work, two distinct commercial metakaolin powders were used.

As for the MK2, its XRD shows (Figure 26) that it is more reactive thank MK1, given the wide hump at 15-30 2-Theta, which denotes the presence of amorphous reactive phases, [132] and thus suitable to be used.

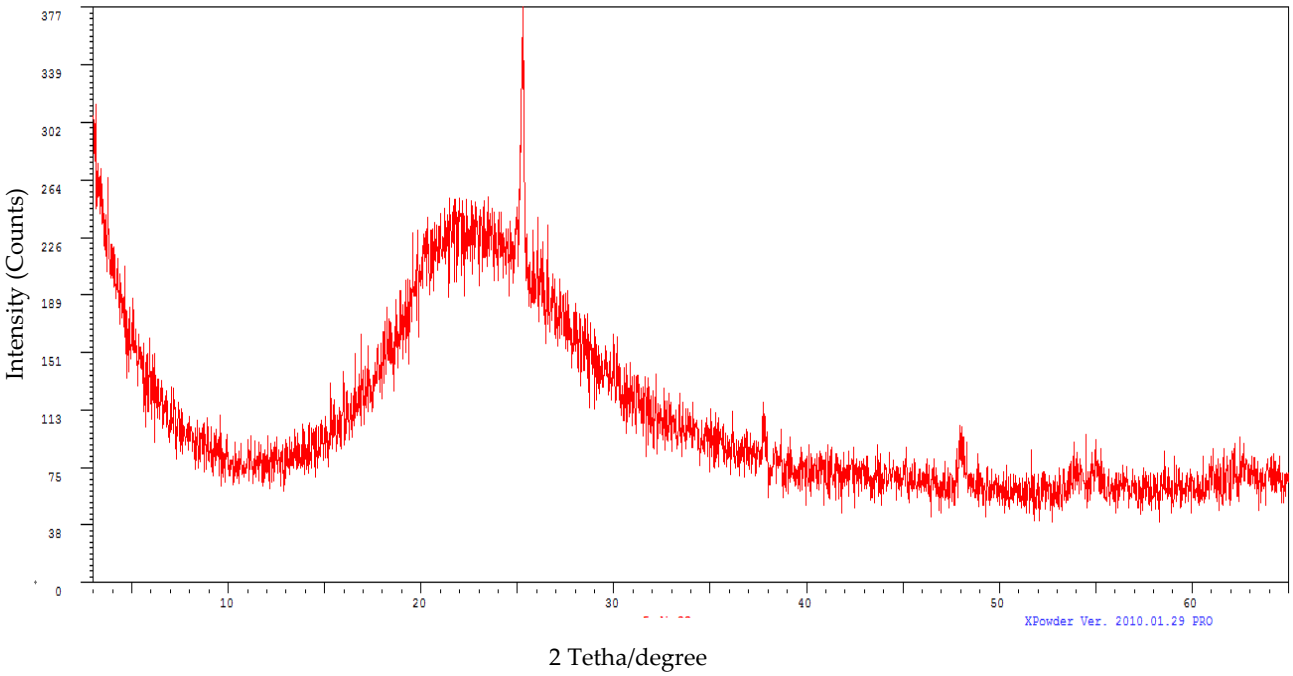

Figure 26. XRD of the MK2 metakaolin.

4.2.2 Activators

The mixture of Sodium Silicate (SS) and Sodium hydroxide (SH) create a very basic NaOH solution, which is called activating fluid, that allows the dissolution of the aluminosilicates. It increases the pH, and it compensates for the electric charge of the aluminates in the mixture. A 10M SH was used in the present work.

4.2.3 Research Plan

The characterization of artificial alkali-activated material is generally based on the characterizations of the alkali-activated paste and the characterization of the physical and mechanical properties of the produced aggregates. Due to the lack of specific tests for artificial alkali-activated aggregates, it was necessary to use the same methodologies adopted for aggregates of natural origin.

The characterization for the MK1/basalt mixture (Aggregate B-MK1) was reported in a previous study by the authors [131]. In that study the authors proposed a regression equation that had as input the variables in the mixture (e.g. MK/Basalt ration, Liquid to Solid ratio), and as a result the predicted Unified Compression Resistance. This regression equation was applied for MK2/basalt mixture (Aggregate A- MK2). Results of compressive strength tests on cubic samples prepared with the alkali-activated paste, according to the EN10151-1 standard, are 35 MPa for the MK1 mix and 47 MPa for the MK2 one.

After the selection of the appropriate mixture design for both metakaolins, artificial-aggregates' samples were prepared through casting into the molds and curing as shown in Figure 27. The A-MK2 Aggregate passed through a second curing process to evaluate if it was possible to improve some properties. The micro-Deval test after the second curing process was only performed on A- MK2 aggregates.

The molds were designed and printed with a 3D SLA printer to cast aggregates with a specific shape and size, aiming to reduce noise and increase friction in surface asphalt courses.

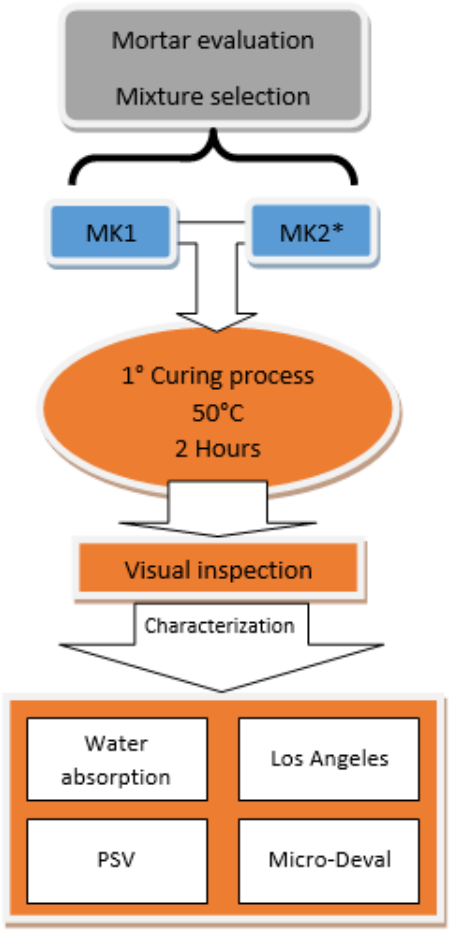

*The MK2 aggregates underwent a second curing process of 24h at 80°C

Figure 27. Flow chart of the production and testing process.

The aggregates were produced as described on a previous study [131], using the same mix proportions being the used metakaolin the only variable. Aggregate A were made with MK2, and Aggregate B with MK1.

4.2.4 Artificial aggregate production

The artificial aggregate was produced using 3D printed molds, that guarantee a specific shape and size that, according to [94,131], could have an interesting behavior in friction and acoustic prospects. The mixtures were prepared as described in Figure 28.

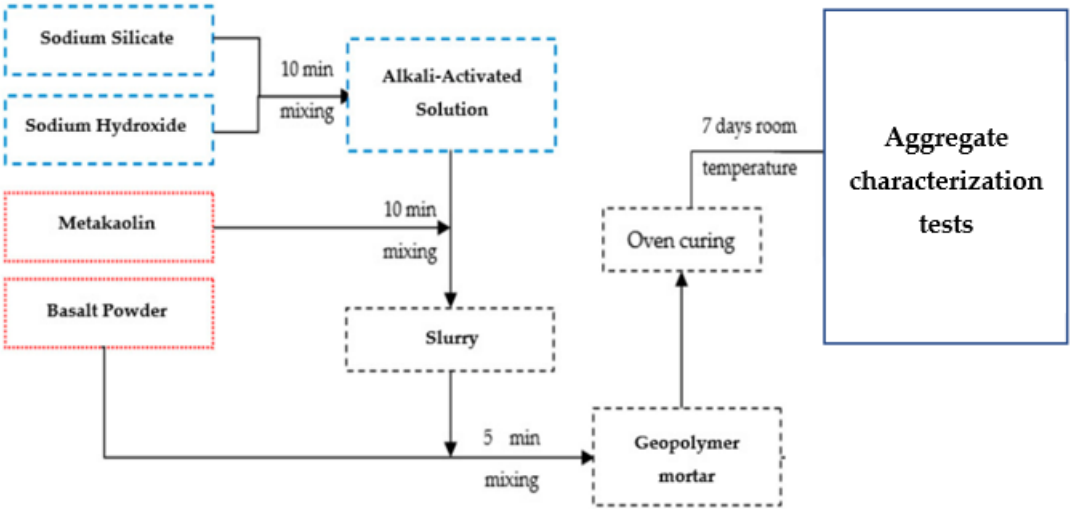

Figure 28. Flowchart of the artificial aggregates production.

The casting of the geopolymer mortar in the molds and the resulting aggregate are shown in Figure 29.

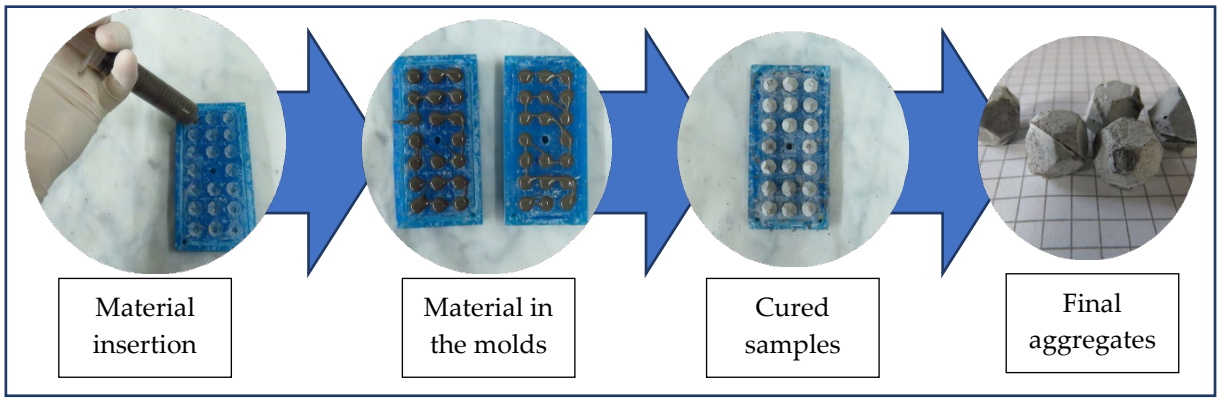

Figure 29. Process of Artificial Aggregate production using 3D printed moulds.

4.2.5 Artificial Aggregates evaluation methods

Both mixes were evaluated in terms of compressive strength in a preliminary research [131] and subjected to X-Ray Diffraction (XRD) and Scanning Electron Microscopy (SEM). The produced aggregates were evaluated in terms of specific mass and water absorption following the EN 1097-6 Standard; Aggregate B- MK1 was submitted to EN 1097-2 for Los Angeles and EN1097-8 for Polished Stone

Value (PSV), and both aggregates underwent EN-1097-1 for the micro-Deval. Water absorption was determined according to the EN 1097-6 standard.

The Los Angeles (LA) test is an empirical measure of the resistance to fragmentation of mineral coarse aggregates used for pavement courses. A sample with a certain mass, depending on the particles size, is placed in a horizontal drum together with an appropriate number of steel balls. The drum is rotated for a total of 500 revolutions, during which the ball load impact on the aggregates determining a fragmentation action, causing the formation of fine particles. The LA coefficient is obtained by the proportion of the fine particles mass created during the test and passing through a 1.6 mm sieve over the total mass of the sample [135].

The Polished Stone Value (PSV) test consists in evaluating the resistance of the aggregates against polishing action by a well-coded procedure. This test is carried out only for aggregates of specific dimension (7.2-10 mm) which are used only for asphalt wearing courses (EN 1097-8:2020). The polishing cycle has a duration of six hours, during which the polishing action is enhanced by using coarse abrasive sand and water for the first three hours and fine abrasive sand and water for the last hours. The specimens for PSV test consist in placing manually and randomly the aggregates into the mold, making sure that the flat surface of each aggregate is properly matched with the mold surface, obtaining a single layer (Figure 30a).

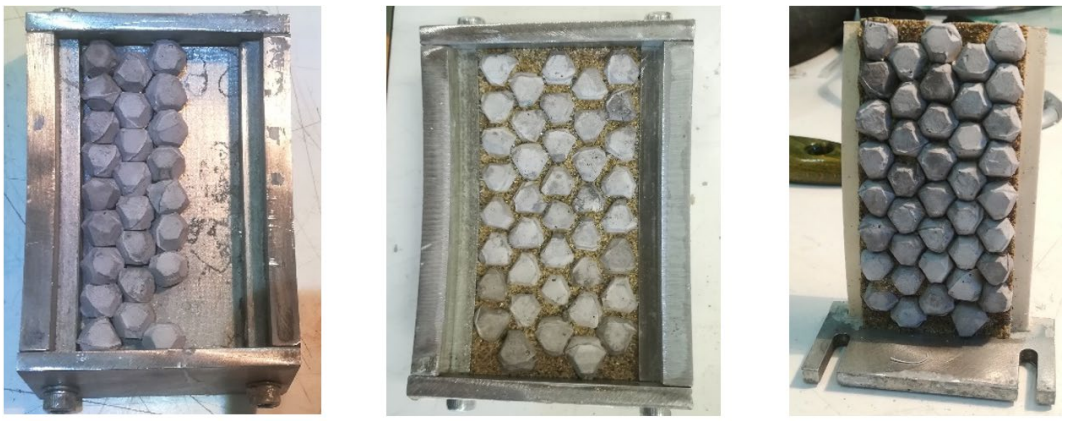

(a) (b) (c)

Figure 30. Sample preparation for the PSV test – placement of aggregates into the mould.

Interstices between particles are filled with fine sand (Figure 30b), and then a bicomponent fiberglass is poured into the mold, in order to obtain a rigid sample once the resin hardens so that it preserves the mold curvature. (Figure 30c).

For the case study, only the Aggregate B- MK1 (ID: B) was used for this test and as prescribed by the standard, it was compared with basalt aggregate (ID: C). It is worth noting that, given the lack of a control stone recognized by the standard, a suitable alternative control stone of established PSV value was used [136]. The PSV was calculated according to the following standard Equation 2.

$$PSV = \mathrm{S} + \mathrm{X} - \mathrm{C} \qquad (2)$$

where:

- S is the mean value for the aggregate test specimens (Aggregate B- MK1);
- X is the mean PSV for the source of the control stone (in this case, 49);
- C is the mean value for the control stone specimens (Basalt).

Furthermore, a roughness analysis was conducted on PSV specimens by means of a laser profilometer based on conoscopic holography methodology ISO 13473-3:2002. For each sample, five profiles were analyzed, two longitudinal profiles in the direction of the PSV wheel (a and b) and three in the crosswise direction (c, d and e), identified through the use of a mask (Figure 31). The alignments marked on

the mask and a reference system defined for each sample help to carry out the profilometric analysis of aggregate surface texture before and after the PSV test. This ensures that the same profile is detected so that can be completely superimposable with a reasonable approximation. Profiles were captured by means of a lens with an objective focal length of 50 mm and a sampling resolution of 5 μm.

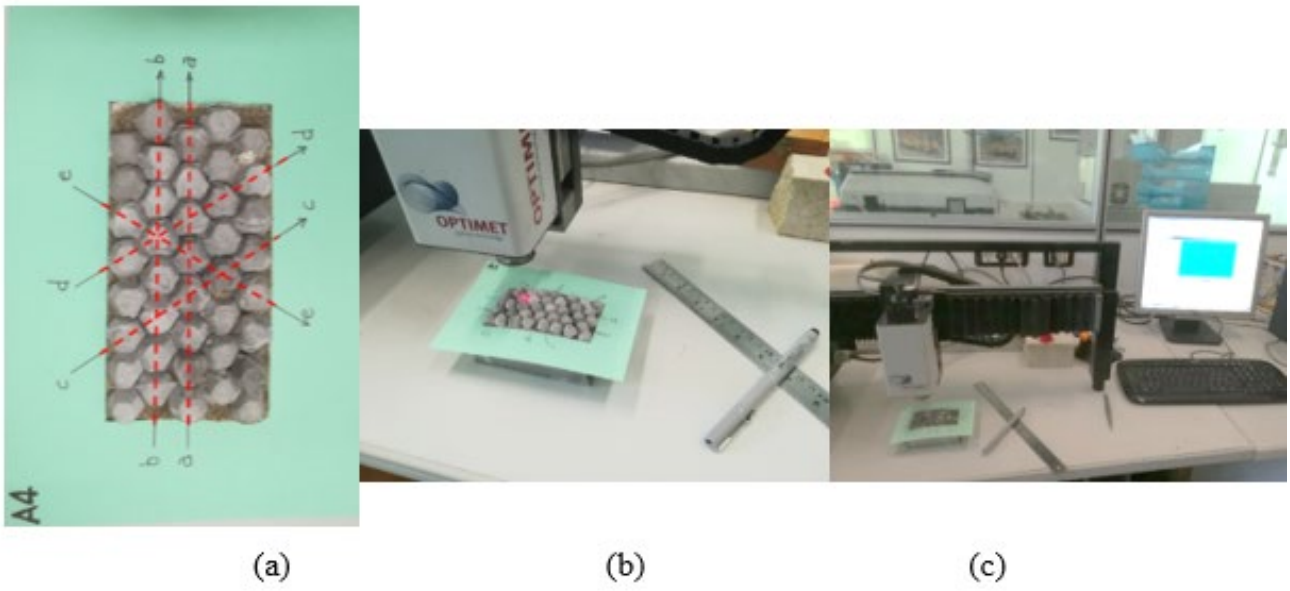

Figure 31. Roughness analysis by laser profilometer: Alignment's identification mask (a); in action for the micro-texture measurement (b) and (c).

The estimated micro-texture indexes (Table 10) are defined as follows:

I. Ra: arithmetical mean deviation roughness of the profile, which represent an average of the profile deviations from a center line;
II. Rq: root mean squared roughness;
III. Rz: average peak-to-valley height, which is based on the five highest peaks and the lowest valleys over the entire length of the evaluation segment [137,138].

Table 10. Formulas and graphical explanation of the investigated roughness indicators

Roughness Indicator	**R_a**	**R_q**	**R_z**
Formula	$R_a = \frac{1}{n} \cdot \sum_{i=1}^{n} \lvert y_i \rvert$	$R_q = \sqrt{\frac{1}{n} \cdot \sum_{i=1}^{n} y_i^2}$	$R_z = \frac{1}{5} \cdot \sum_{i=1}^{5} R_{pi} - R_{vi}$
Graphical Explanation	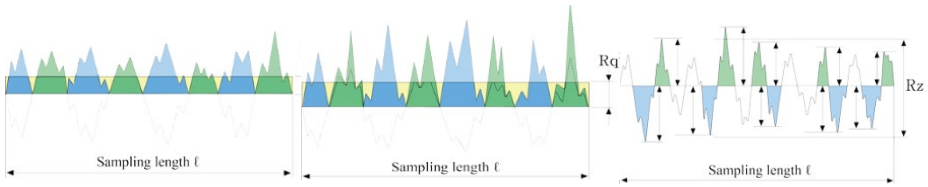		

The last test carried out was the micro-Deval (EN 1097-1), which evaluates the resistance to wear of coarse aggregates. The test provides a measure of the aggregates abrasion resistance by means of an abrasive action that occurs between the aggregates themselves and the aggregates and small steel balls in presence of water. A 500 g sample is placed together with 2.5 liters of water and an abrasive charge, consisting of a set number of steel balls, inside a specific apparatus that is rotated for 12000 revolutions. After the test, the sample is removed from the drum, washed and the oversize fraction retained on a 1.6 mm sieve is dried. The micro-Deval coefficient (MDE) is calculated by the difference between the initial mass and the oversize fraction mass compared to the total mass of the sample.

4.3. Results

4.3.1 Alkali -Activated materials' chemical characterization

The characterization of the alkali-activated materials was conducted using XRD and SEM, for both mixes. The analysis of SEM images allows the identification of the formation of geopolymer gel. Furthermore, with the XRD it is possible to identify the geopolymerization region and some of the crystals that did not react.

From the XRD image in Figure 32 it is possible to notice that a reaction occurred due to the alkaline activation of the precursors, given the hump between 20 and 30 2θ recorded on the spectra, compared to that of the constituent materials. This suggests the formation of geopolymeric structures, as observable in the SEM images. The crystalline phases detected in both samples derive from unreacted basalt and metakaolin. As expected, no new crystalline phases were formed.

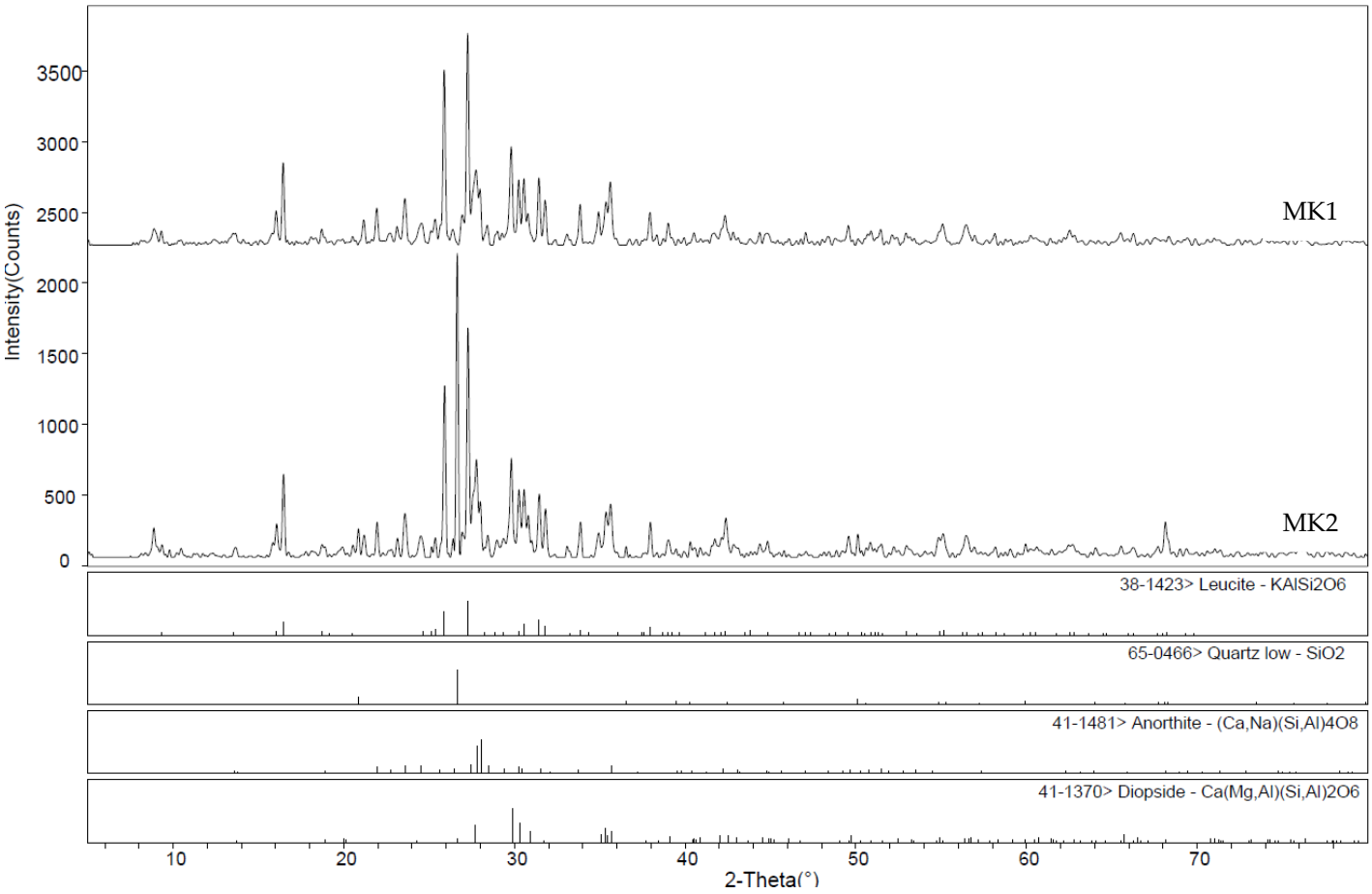

Figure 32: XRD for geopolymer mixes containing different metakaolins (MK, MK2).

Figure 33 shows at a 10000 magnification the internal part of Aggregate A and Aggregate B, being the mixes made with MK2 and MK1 metakaolin respectively.

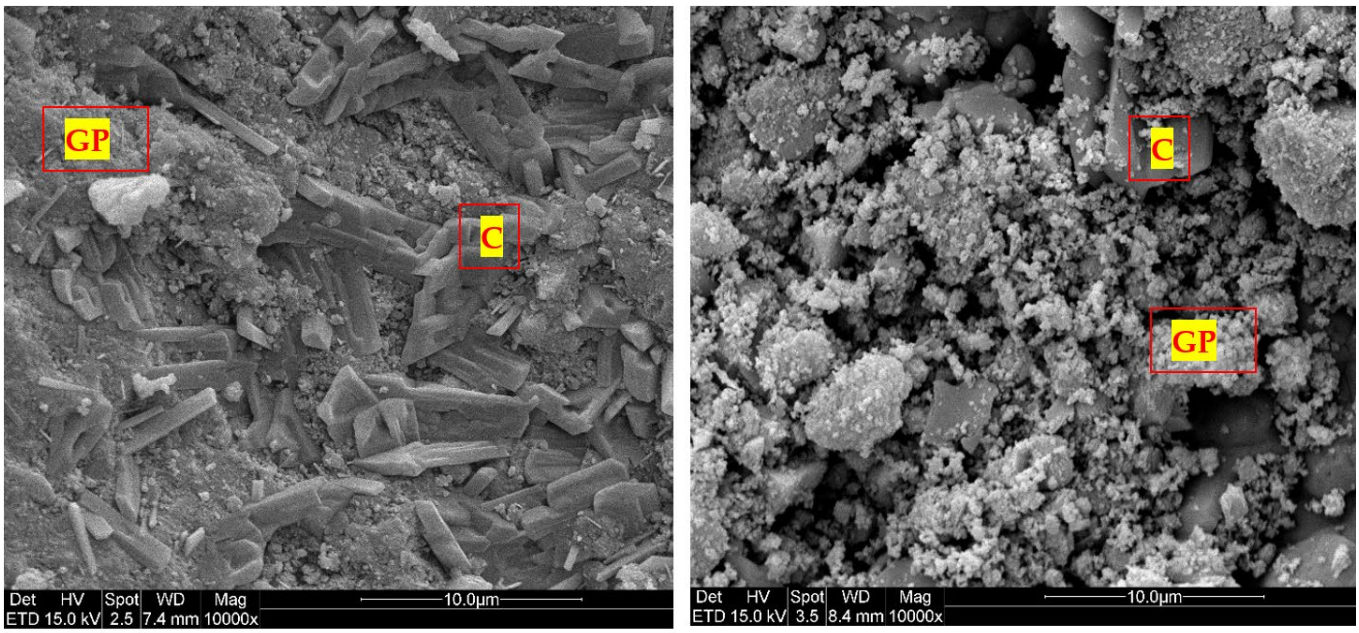

Aggregate A Aggregate B

Figure 33: SEM images of the geopolymer Aggregate A and Aggregate B.

In both materials it is possible to see the formation of a geopolymer gel (GP) and the presence of crystals of different mineral phases from unreacted precursors (C). The most notable difference is that in the MK2-mix the geopolymer gel is more homogeneous and compact, and the unreacted crystalline phases from basalt are well incorporated into the geopolymer matrix. In the other mix, the geopolymer formation resulted in a less cohesive material, with typical nanoprecipitates formed by alkali-activation unevenly disposed around the unreactive phases of both precursors. The scarce reactivity of MK1, deriving from the presence of fewer readily reactive amorphous phases and its coarser particle size, resulted in a highly porous and less compacted material, likely having lower physical and mechanical properties.

4.3.2 Artificial aggregates characterization

Aggregate A and Aggregate B were characterized in terms of water content, specific mass, Los Angeles abrasion, Polished Stone Value (PSV) and micro-Deval abrasion. Table 11 shows the results for both artificial aggregate types and their direct comparison with a natural aggregate (basalt), two artificial aggregates that

follow a different production method, (i.e. calcined Bauxite and steel slag), and an AA produced through the alkali-activation of fly ashes.

Table 11. Materials' characteristics and comparison with other aggregates

Aggregate	Water Content (%)	Specific mass (g/cm^3)	Los Angeles (%)	PSV	micro-Deval (%)	Reference
Aggregate A	19.1	2.120	-	-	35* (27)	-
Aggregate B	21.0	2.017	37	59	70	-
Basalt	< 2.5	2.700	14-20	53	14	[69,139,140]
Calcined Bauxite	6.8	2.629	10-17	50-70	5	[69,141,142]
Fly ash AA	5.5	2.140	27	-	-	[95]
Steel slag	1.1-9.0	2.96 - 3.59	14-15	25-55	6-10	[91,138,143]

*Results after treating the material into the oven for 24 hours at 80 °C, after previous curing.

It is important to note that both artificial aggregates produced in this research have a higher water content than the aggregates used as a reference. It is important to note that natural aggregate, such as Basalt, have traditionally less water absorption. Regarding the calcined bauxite and steel slag which are not geopolymer materials, the internal structure is different thus can contribute to a different water absorption. As for the Fly ash AA, even though it is a geopolymer artificial aggregate the production process is quite different. The different production process and use of fly ash can be contributor to the difference in the water absorption. The specific mass is comparable to the Fly ash AA one.

The artificial aggregate B had high results in terms of Los Angeles and micro-Deval abrasion tests, however promising results were obtained from PSV. Aggregate A was not tested in terms of Los Angeles and PSV. However, its micro-Deval was considerably better than the one for aggregate B, especially if the material was heat-treated in the oven after the initial curing.

4.3.3 Artificial aggregates micro-texture analysis

As for the micro-texture characterization, the analysis was carried out for the Aggregate B- MK1 and the control basalt. Data were obtained by analyzing micro-profiles of an average length of 0.7-1.05 mm, graphically identified on each single grain that composes a profile. For Aggregate B- MK1, a total of 119 micro-profiles with an average length of 909 μm were analyzed, whereas for the control basalt 120 micro-profiles with an average length of 834 μm were recorded.

Table 12 shows the results of the micro-texture analysis, where the collected data for each aggregate were averaged for longitudinal and crosswise profiles, for both polished and unpolished samples. The percentage variation in roughness data Ri (with i = a, q, z) registered before (Ri,bp) and after (Ri,ap) polishing is given by Equation 3:

$$\Delta R_i = \frac{R_{i,ap} - R_{i,bp}}{R_{i,bp}} \cdot 100 \quad (3)$$

Table 12. Post-processing analysis of roughness data collected by laser profilometer: mean values before and after polishing and variation (%).

ID Sample: Aggregate B- MK1 (B)	**Before Polishing (μm)**			**After Polishing (μm)**			**Variation (%)**		
	$R_{a,bp}$	$R_{q,bp}$	$R_{z,bp}$	$R_{a,ap}$	$R_{q,ap}$	$R_{z,ap}$	ΔR_a	ΔR_q	ΔR_z
Longitudinal sections (average)	12.6	16.8	50.9	19.6	24.4	69.1	+88.9	+78.0	+60.1
Crosswise sections (mean)	9.5	12.6	40.9	25.4	30.9	79.1	+173.4	+151.6	+94.5
Mean	10.7	14.3	45.0	23.1	28.3	75.1	+127.7	+111.1	+75.4
ID Sample: Control Basalt (C)	**Before Polishing (μm)**			**After Polishing (μm)**			**Variation (%)**		
	$R_{a,ap}$	$R_{q,bp}$	$R_{z,bp}$	$R_{a,ap}$	$R_{q,ap}$	$R_{z,ap}$	ΔR_a	ΔR_q	ΔR_z
Longitudinal sections (mean)	24.8	30.6	75.7	26.3	32.5	84.7	+6.1	+6.5	+14.3
Crosswise sections (mean)	22.3	27.5	67.9	27.0	32.9	80.0	+21.2	+20.0	+17.9
Mean	23.3	28.7	71.0	26.7	32.8	81.9	+14.7	+14.0	+15.8

As it can be clearly seen from Table 12 Aggregate B- MK1 shows an important increase of the micro-texture indexes, almost doubling in value, whereas the basalt

exhibits a lower variation, 15% on average, which can be considered not significant. This is in line with other studies carried out by means of a similar methodology, which recorded the low variation of the basalt aggregates in terms of roughness [137,138]

Besides, the profile tracking with the laser profilometer has provided the basis to conduct further analysis on the samples in order to obtain more information about the wearing characteristics of the materials. Thus, the percentage of loss material was estimated starting by the calculation of the area underneath the profiles (Aap: Area after polishing; Abp: Area before polishing) by means of the trapezoid method, with a step of 5 μm, and which is given by the following formula:

$$\Delta A = \frac{A_{ap} - A_{bp}}{A_{bp}} \cdot 100 \quad (3)$$

Table 13. Percentage estimation of the material loss occurs after the polishing action.

ID Sample: Aggregate B- MK1 (B)	**ΔA Variation (%)**	**St. Dev (%)**
Longitudinal sections (mean)	-16.9	±4.5
Crosswise sections (mean)	-17.4	±2.1
ID Sample: Control Basalt (C)	**ΔA Variation (%)**	**St. Dev (%)**
Longitudinal sections (mean)	-3.7	±1.4
Crosswise sections (mean)	-4.1	±1.0

Table 13 summarizes the percentage of loss material estimated for the longitudinal and the crosswise sections after submitting the samples to the PSV abrasion. Figure 34 and Figure 35 shows an example of the profile's superposition for both the Aggregate B- MK1 (A6 sample) and the Control Basalt (C2 sample), respectively. It can be clearly seen that the artificial aggregates have undergone a significant loss of material due to the polishing, whereas the basalt profiles appear to be almost unaltered.

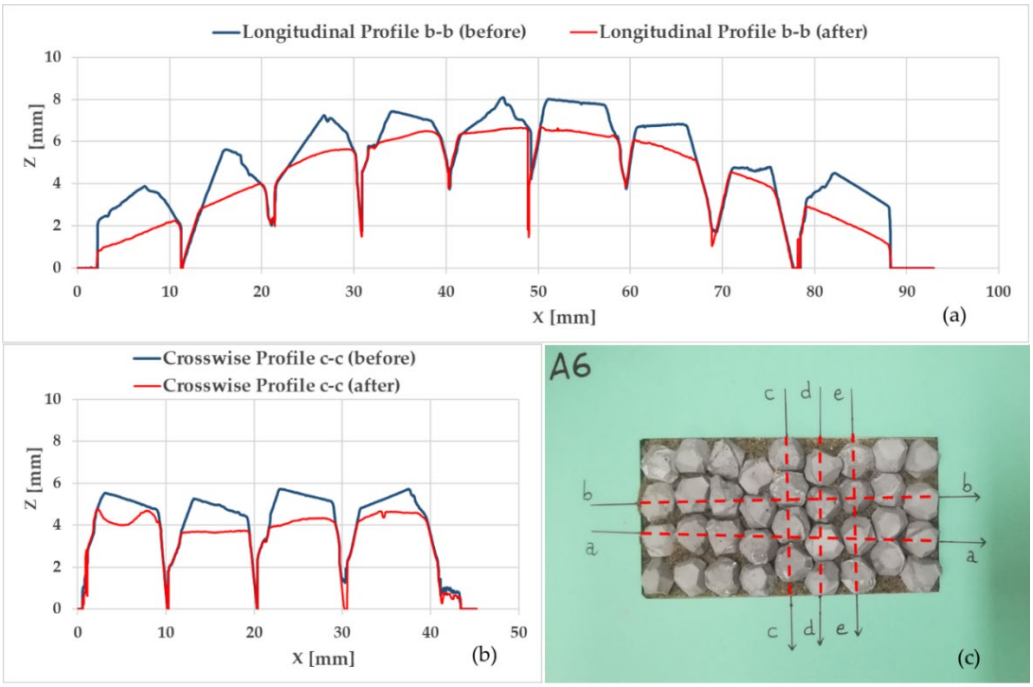

Figure 34: Example of the profile's superposition for Aggregate B-MK: longitudinal profile (a) and crosswise profile (b); Alignment's identification mask for A6 sample (c).

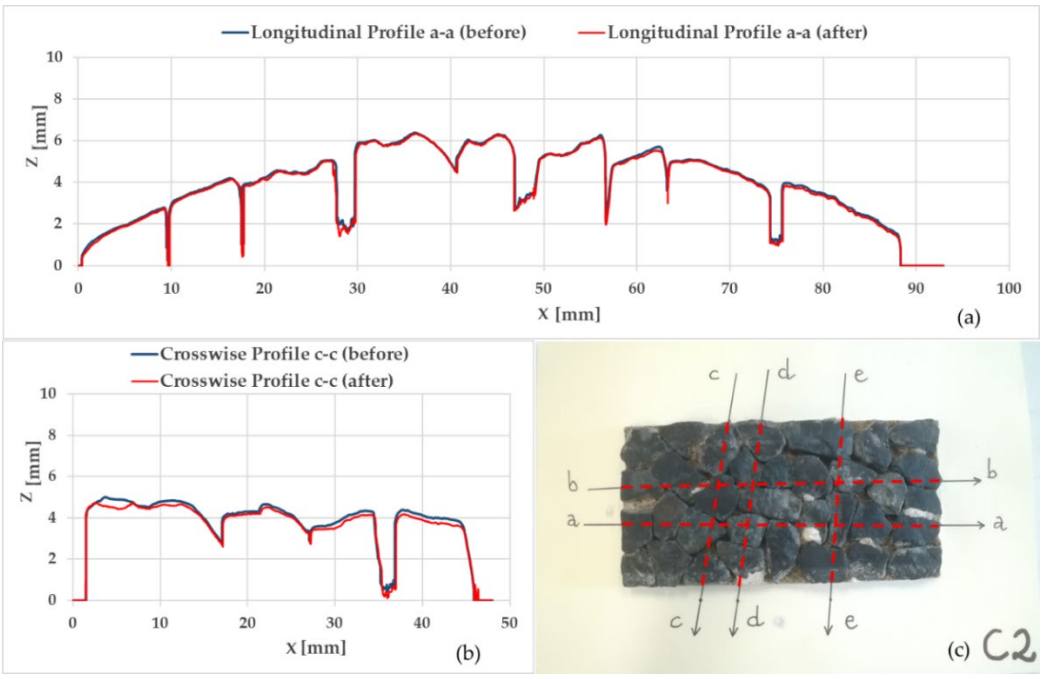

Figure 35: Example of the profile's superposition for control Basalt: longitudinal profile (a) and crosswise profile (b); Alignment's identification mask for C2 sample (c).

The Skid results obtained by means of the British Pendulum Test are shown in Table 14, where BPNb is the British Pendulum value measured on unpolished samples, whereas BPNa is the measurement after the polishing action. Aggregate B-MK1 kept high values of BPN, showing a variation of about -10% on average after the polishing, whereas the control basalt samples showed almost a doubled percentage variation (-18.3%).

Table 14. Results of the PSV test: Pendulum Test Value (PTV) before and after polishing, percentage variation and PSV values.

ID Sample	PTV_b	PTV_a	Variation (%)	PSV
Aggregate B- MK1 (B)	62	56	-9.9	59.0
Control Basalt (C)	56	46	-18.3	49.0

Based on the results, it is possible to state that the basalt kept similar value between pre and post-polishing (Table 11 and Table 12) on average and did not suffer the effects due to the polishing also in terms of loss of material. Instead, the Aggregate B-MK1 showed a significant increase of all the micro-texture indexes after the polishing. This might also be due to the initially smooth surface finishing, being the aggregates cast and cured in a mold, whereas the polishing action let the crystals (Figure 33) arise to the surface. Despite maintaining a high value of BPN after conditioning, the artificial aggregates exhibited a great loss in terms of material, which corresponded to a remodeling of the macro-texture of the samples, obtaining a quite different contact area between the surface of the sample and the pad of the British Pendulum.

4.4. Conclusions

This research aimed at the characterization of engineered artificial aggregates produced through the alkali-activation of basalt and metakaolin powders. During the research, it was noted that the selected metakaolin played a very important role, as the MK2 one had better geopolymerization results.

As for the basalt action as constituent, it is clear that it did not fully react. Part of it contributed to the geopolymerization and partly acted as a non-reactive material, as evidenced by the crystals in Figure 33. However, more research is necessary to better understand its contribution to the geopolymerization process in a multi-material system along with metakaolin.

Regarding the physical characterization, the aggregate B-MK1 showed lower results in most tests compared to the reference materials (i.e. basalt, calcined Bauxite, fly ash AA, steel slags), except for the PSV. However, despite the fact that the artificial aggregate does not perform well in those tests, it revealed high BPN values and optimal micro-texture indexes.

By changing the metakaolin in aggregate A-MK2, the resistance to wear increased, halving the loss of material due to the abrasive action. It appears that the results improved even further in terms of micro-Deval coefficient when the artificial aggregates were heat-treated.

Therefore, although the mixture requires improvements in order to achieve a better behavior in terms of resistance to wear and fragmentation, the high BPN and PSV values, as well as the quality of micro-texture indexes, are proof of potential good performance, making the artificial aggregates suitable as a replacement of natural aggregates for wearing courses in road pavements.

All in all, the research shows that producing artificial geopolymer aggregates using 3D printed molds to control their shape and size is a promising approach that could be scaled to larger industrial productions.

Future developments will foresee a complete characterization of the aggregate A that will be used for the production of microsurfacing mixes to evaluate its behavior in friction and acoustic terms.

Chapter 5: Microsurfacing pavement solutions with alternative aggregates and binders: A full texture characterization

Copetti Callai S, De Rose, M., Makoundou, C., Vaiana, R. Sangiorgi C. Microsurfacing pavement solutions with alternative aggregates and binders: A full texture characterization (Submitted to International Journal of Pavement Engineering (ISSN 1477-268X)).

Abstract: Road surface texture is responsible for controlling several quality/safety road indicators, such as friction, noise and fuel consumption. The pavement texture can be classified in different wavelengths, and it is dependent on the material used as wearing course. Aiming to assess their pavement texture, six microsurfacing samples were constructed and tested using a laser profilometer. The profiles were studied using traditional texture pavement techniques as well as statistical methods. These techniques were adopted in order to better stratify and classify the pavement texture. It was possible to confirm that the aggregate type plays a very important role in the pavement texture. The binder agent seems to be also highly important, but more studies are necessary. The use of crumb rubber as an aggregate proved to be feasible, and the texture parameters obtained were in accordance with the benchmark; therefore, it was noted that it could be a replacement in some cases. The study showed that the use of Artificial Engineered Aggregates does not impair the surface texture; in fact, it changed the surface texture substantially.

Keywords: Microsurfacing, pavement texture, MPD, artificial aggregate, Geopolymer

5.1.Introduction

The texture of the road pavement is directly responsible for several indicators from internal and external noise [1,2], safety [3,4], heat island mitigation [5–7], fuel consumption [3], tire wear and overall costs of road operation. All these aspects are regulated in one or another fashion by the texture of the surface layer also known as wearing course.

The pavement can be classified according to the texture wavelength [8], from the unevenness of the road to the microtexture of the aggregate itself. Each texture wavelength impacts differently on the vehicle and tire interaction with the road. In some cases, it can improve safety while increasing the fuel consumption, or decrease noise while increasing the risk of accident: in general, it is a trade-off among a number of characteristics [9–11].

The pavement texture is a product of the mix of one or more binders (bitumen, resin, Portland cement, asphalt emulsion), fillers and aggregates. The mix design and aggregate origin play a major role in the pavement texture [10,12–16], and consequently in noise and friction performances. The surface texture of pavement can be measured using different techniques, both in the laboratory and in the field. The main methods are volumetric, laser and permeability [17–20]. Photogrammetric techniques have been also implemented and are showing promising results [17,21–23]. The texture can be, also evaluated using tribological parameters, such as Average roughness, skewness and kurtosis [24–27].

One of the possible solutions to improve surface texture and restore skid-resistance is microsurfacing, sometimes called slurry sealing [28]. Microsurfacing is a preventive maintenance technology that involves the application of a mixture consisting of polymer-modified emulsion, dense-graded mineral aggregate, mineral filler, water and additives (if any) at ambient temperature. Several studies have been conducted to assess the properties of microsurfacing regarding noise and friction [29–32]. Recently some studies are aiming to substitute either the asphalt binder

[16,33,34] or replacing the natural aggregate with alternative aggregates, such as steel slag, recycled materials, rubber and alkali-activated or geopolymer materials [16,35–39].

The present study aimed to evaluate the texture parameters using a laser profilometer on six different microsurfacing solutions. The experiment was designed to assess the use of two different binders (asphalt emulsion and resin) and three different aggregates (natural aggregate, 3D printed artificial geopolymeric aggregate, crumb rubber) by evaluating the pavement surface texture features of the mixtures. The texture analysis was carried out not only through the use of traditional parameters, but also using more robust-statistical/tribological parameters.

5.2. Materials and Methods

5.2.1. Materials

Three types of aggregates were used in this study:

- Natural Aggregate (NA) – Basaltic quarry origin – 0/6 or 0/8 mm gradation.
- Crumb Rubber (CR) – 0.8 ÷ 4 mm gradation [40,41];
- Artificial Engineered Aggregate (AEA) – 10 mm nominal single size [38].

In particular, the Artificial Engineered Aggregate is produced using an alkali-activation technique. It consists of mixing the basalt powder and metakaolin with an activator (alkali solution). This mixture produces a mortar that is cast into 3D printed molds and cured in the oven. The final aggregate has a nominal 10 mm diameter in a truncated octahedron shape, as shown in Figure 36.

Figure 36. Artificial Engineered Geopolymer Aggregate.

For the scope of this research, six different microsurfacing mixtures (Figure 37) were prepared, as summarized in Table 15. In order to make a comparison between the different mixture combinations, two benchmark samples were identified, called Natural Aggregate Sample, "NAS1" and "NAS2", which used identical materials, in particular a 0/8 mm basaltic aggregate and modified asphalt emulsion, and represent a standard microsurfacing mixture. Basalt aggregate with 0/6 mm granulometric curve was used in sample "Yellow", replacing the modified asphalt emulsion with a commercial non-asphaltic resin binder, which color gives the name to the sample. Sample "Rubber" used asphalt emulsion, whereas the granulometric curve was designed by using 40% NA and 60% CR [40]. The last two samples used a combination of both NA and AEA, blended with asphalt emulsion. Sample "AA" used an Australian gradation curve (0/10) [42], replacing the maximum aggregate size (retained at sieve 9.5 mm) with the AEA. Mixture "AA5050" is a discontinuous mix made with 50% of 0/6 mm NA (<sieve #2) and 50% AEA (10 mm).

Table 15. Description of the analysed samples.

Name	Type of Binder	Type of Aggregate	Granulometry
AA5050	Asphalt emulsion modified with latex	NA AEA	50% < sieve #2 of 0/6 mm NA 50% 10 mm single size AEA
AA	Asphalt emulsion modified with latex	NA AEA	Australian gradation curve (0/10) replacing 10 mm NA by 10 mm AEA
Rubber	Asphalt emulsion modified with latex	NA CR	40% NA (0/14 mm) 60% 0/4 mm CR
NAS2	Asphalt emulsion modified with latex	NA	0/8 mm granulometric curve
Yellow	Non-asphaltic resin	NA	0/6 mm granulometric curve
NAS1	Asphalt emulsion modified with latex	NA	0/8 mm granulometric curve

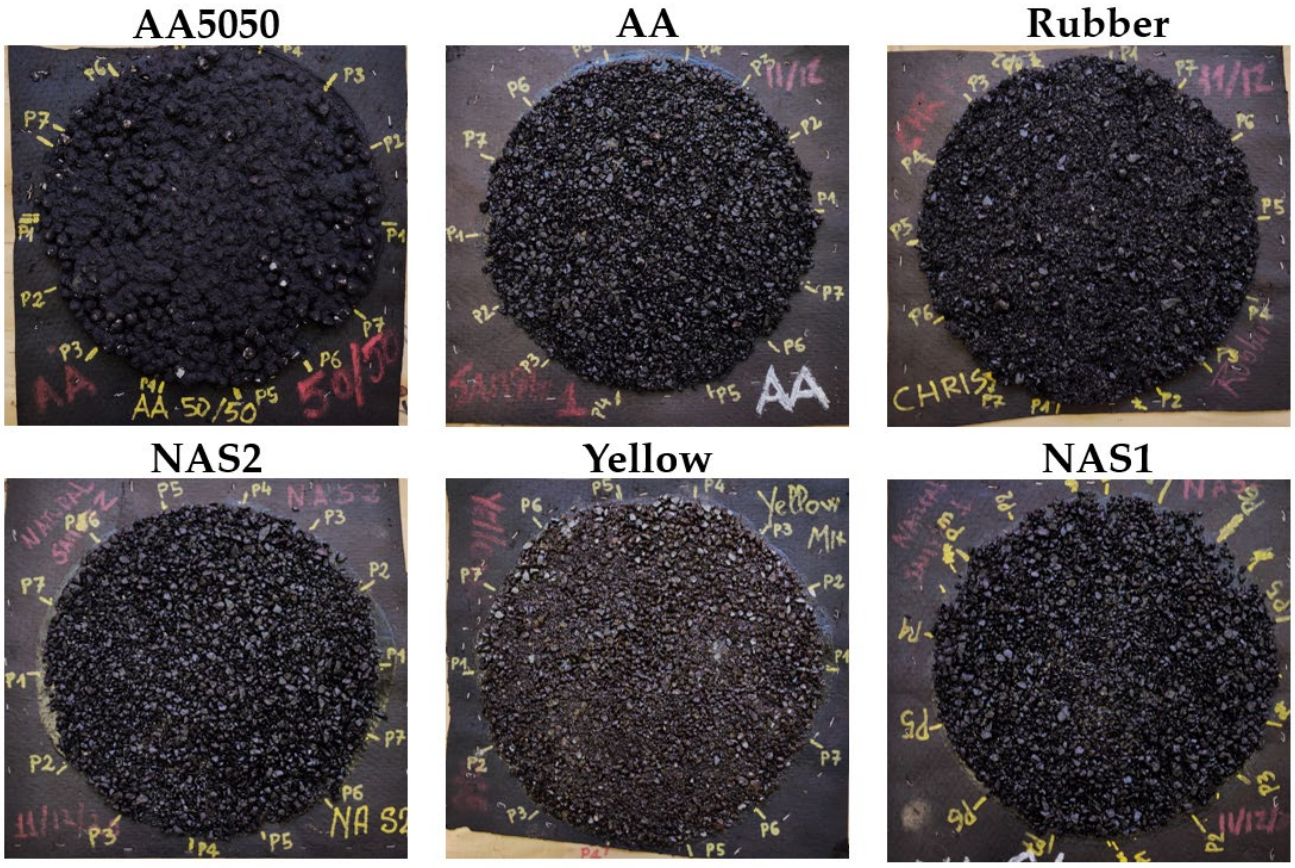

Figure 37. Asphaltic samples using natural aggregate (NAS1, NAS2), artificial engineered aggregate with natural aggregate (AA5050, AA), crumb rubber with natural aggregate (Rubber) and Resin sample with natural aggregate.

5.2.2. Methods

Microsurfacing samples produced with asphalt emulsion were made by following the ISSA mix design procedures [43], whereas the "Yellow" sample, which used resin emulsion, was made using the instructions of the producer.

Once the samples cured, a texture analysis was conducted by means of a contactless laser profilometer based on conoscopic holography [44]. According to the classification made by the standard ISO 13473-3 [19], this latter has the following characteristics:

a) Mobility: Stationary, slow;
b) Texture wavelength range: Range covered BD class 0.20 ÷ 50 mm;
c) Pavement contact: Contactless devices;
d) Principle of operation: laser profilometer;
e) Objective focal length: 100 mm;
f) Maximum vertical measuring range: 35 mm;
g) Vertical resolution for class 0.003 ÷ 0.03 mm: 0.012 mm;
h) Stand-off distance: 90 mm;
i) Minimum horizontal resolution Δx (sampling interval) BD for class 0.05 ÷ 1 mm: 0.01 mm;
j) Angle coverage: 170°.

The profilometer conducted seven diametral profiles spaced at a fixed angle, being each profile about 30 cm long (depending on the sample), as shown in Figure 38. This allowed to obtain a single joined linear profile with a total length of at least 2 meters for each sample, ensuring a good representativity of the sample's texture.

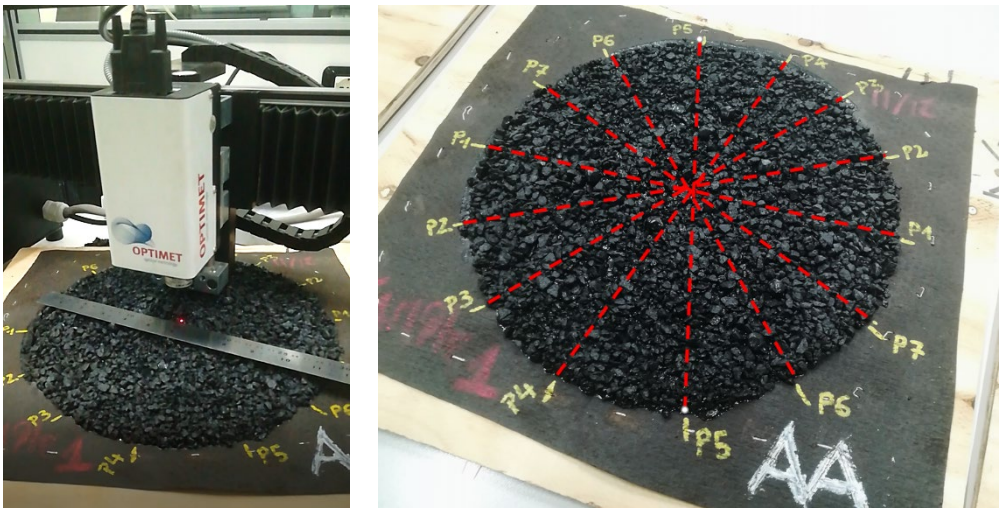

(a) **(b)**

Figure 38. Texture analysis by means of conoscopic holography laser profilometer. (a) Capturing of a profile; (b) Alignments identification on a sample

The texture data obtained from each sample as recorded from the laser profilometer were post-processed by means of the U-PaveTex software, developed for the University of Calabria within an Italian national project "USR342 - Urban safety, Sustainability, and Resilience: 3 paving solutions, 4 sets of modules, 2 platforms". The software analyses each profile and works out the roughness parameters, which will be discussed in the following section. Moreover, the software is able to combine the seven profiles for each sample providing the Texture level (LTX) as spectral intrinsic indicator. Instead, other texture aggregate intrinsic indicators, such as Skewness, Kurtosis and the Bearing Abbot Curve, were evaluated by processing data in Excel and using the Origin2021 software.

5.2.3. Roughness parameters

Surface texture can be assessed by means of intrinsic criteria, by which the surface geometry is described through the use of discrete functions like z(x,y), for a surface, or z(x), for a profile, or by means of extrinsic criteria, which analyzes the surface texture through the use of correlated parameters, such as friction or outflow [45].

For the present study, only intrinsic indicators were used. These latter may be divided into aggregate indicators, which look at the profile as a set of several wavelengths, and space-frequency or spectral indicators, for whom the profile is disaggregated by Fourier analysis as sum of several elementary components, each of them referred to a single wavelength "λ" [8,55,144]. The indicators' mathematical and graphical descriptions are presented in Table 16.

The most used aggregate intrinsic indicators to describe the pavement texture are the Mean Profile Depth (MPD) and the Estimated Texture Depth (ETD) [13,20,28,145,146]. The MPD and ETD were created to assess the pavement macrotexture, and they are based on the traditional sand patch method.

As reported in Table 16, MPD has two different representations. MPD_{iso} is the average value of the profile depth over a certain distance, the baseline, which assumes a value of 100 ± 0.5 mm [52]. MPD_{aipcr}, instead, is the average difference between the regression line of the profile and a line through the top of the highest peak within the sampling length, a baseline of 138 ± 0.5 mm [8].

The ETD is a parameter used to estimate the mean texture depth (MTD) starting from the MPD by using a transformation equation. Thanks to this equation, through the ETD it is possible to well-approximate the MTD measured with the sand patch method. The only difference between the indicators $ETD_{1995iso}$ and $ETD_{2019iso}$ is in their formulas [18,52].

The Average Roughness, Ra, is one of the most widely used parameters, which gives a gross measure of the surface roughness, and it represents the average height difference (taken in absolute value) in reference to the profile's average line. The parameter Ru, Height to the mean or Levelling Depth, is the height difference between the profile's average line and the maximum profile peak. It provides information on how the peaks diverge from the mean: a low value indicates that the profile is flatter in the part above the average value.

Table 16. Roughness/texture parameters.

Aggregate Intrinsic Indicators	Name	Formula	Graphical Explanation
MPDiso	Mean Profile Depth [52]	$MPD = \frac{1^{st}Peak + 2^{nd}Peak}{2} + - Average\ level$	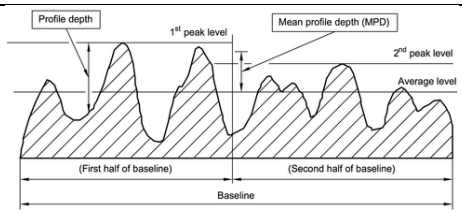
MPDaipcr	Mean Profile Depth [8]	-	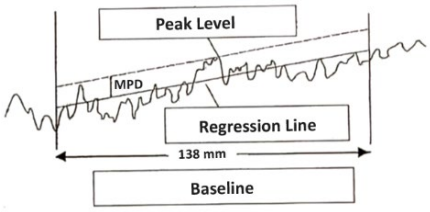
ETD1995iso	Estimated Texture Depth [18]	$ETD = 0.2 + 0.8 \cdot MPD$	-
ETD2019iso	Estimated Texture Depth [52]	$ETD = 1.1 \cdot MPD$	-
R_a	Average Roughness	$R_a = \frac{1}{L} \cdot \sum_{i=1}^{n} \lvert Z_i - Z_{mean} \rvert$	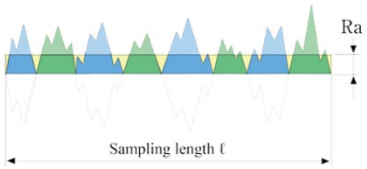
R_u	Height to the mean	$R_{max} = Z_{max} - Z_{mean}$	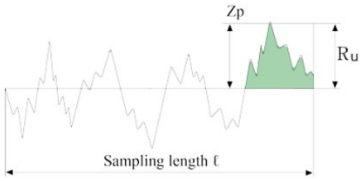
R_z	Average peak-to-valley height	$R_z = \frac{1}{5} \cdot \sum_{i=1}^{n} Z_{pi} - Z_{vi}$	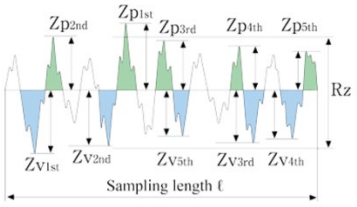

Rmax (Rt)	Maximum total height	$R_{max} = \max(Z_{pi}) + \max(Z_{vi})$	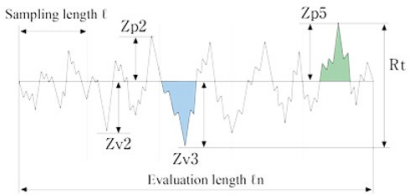
RMS (Rq)	Root Mean Square	$RMS = \sqrt{\frac{1}{n} \cdot \sum_{i=1}^{n} y_i^2}$	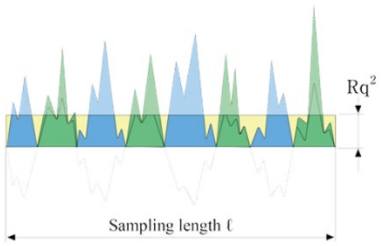

Spectral Intrinsic Indicators	Name	Formula	Graphical Explanation
$L_{TX,\lambda}$	Texture Level (for given wavelength λ)	$L_{TX,\lambda} = 10lg\left(2\left\|\frac{Z_k}{a_{ref}}\right\|^2\right)$ For $k = 0, \ldots, \left(\frac{1}{2}N - 1\right)$	-

The Average peak to valley height, Rz, represents the sum of the mean value of the five tallest peaks and the mean of the five deepest valleys of a profile within the sampling length. Rmax or Rt is called the Maximum total height, and it represents the sum of the maximum peak height Zp and the maximum valley depth Zv of a profile within the evaluation length, not sampling length.

The last parameter is the Root Mean Square (RMS or Rq) which is the deviation in the heights. Some studies have shown that there is an inverse proportion between RMS and friction, either dry or wet [33,53,54].

The Texture Level, indicated as $L_{TX,\lambda}$ and expressed in decibels (dB), is a logarithmic transformation of an amplitude representation of a surface profile curve Z(x), given a single texture wavelength λ. The texture wavelength describes the horizontal dimension of the amplitude variations of a surface profile and it is expressed in millimeters (mm) [55].

Also, it is possible with the provided profiles to calculate some statistical parameters such as the Skewness, Rsk, the Kurtosis, Rku, and the Bearing Abbot Curve, as presented in Table 17. The Skewness represents the degree of symmetry of the profile and it provides information on how the peaks and valleys are distributed in reference to the profile's average value. The Skewness is equal to 0 if the probability density curve of the profile's heights is symmetrical. If the number of peaks above the average value is relatively higher than that of valley, the Skewness assumes a negative value, whereas it will be positive if not. The Kurtosis is a good indicator of the probability density function's sharpness [56,57]. When the Kurtosis is equal to 3 (or 0 if normalized by subtracting 3), the distribution will have the same shape of a Gaussian distribution: than a value of Kurtosis much greater than 3 shows a sharp curve, whereas if it is much lower the curve becomes more rounder and flatter. Thus, when applied to the study of the surface texture, the Skewness and Kurtosis are both parameters that characterize the shape of the probability density distributions of the profile's heights [58].

Finally, the Probability Density Curve, also called the Bearing Abbott Curve or Abbot-Firestone (or just Abbot) Curve, is a parameter usually used in tribology in order to evaluate the functional behavior of surfaces in relative motion subjected to mechanical loading and it is a good indicator of the real area that will support the contact between the surfaces [59-61]. Although the Abbott curve is generally used in mechanical applications, it is possible to extend its use to evaluate the macrotexture of asphalt surfaces and so the road-tire contact, with the possibility of inferring on drainability and friction properties [2,62]. Mathematically, it represents the cumulative probability density function of the surface's profile heights, so that, given a certain elevation level, it is possible to have information on the percentage of matter that lies above or below that height. In this context, the following three parameters can be identified on the Abbot Curve:

- Rpk, which corresponds to the fraction of the profile with the highest peaks and might be linked to the part of the profile which will stick to the tire and polished under the traffic during the pavement service life;
- Rk, which is the contact area region and represents the core of the surface effectively subjected to the traffic loads;
- Rvk, which represents the percentage of the profile with the deepest valleys and perhaps related with the ability of the surface to evacuate or store water [63].

Table 17. Statistical roughness parameters.

Indicator	Name	Formula	Graphical Explanation
R_{sk}	Skewness	$R_{sk} = \frac{\sum_{i=1}^{n} \frac{1}{n}(z_i - \bar{z})^3}{\left(\sum_{i=1}^{n} \frac{1}{n}(z_i - \bar{z})\right)^{3/2}}$	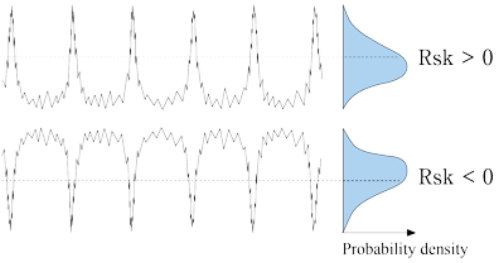
R_{ku}	Kurtosis	$R_{ku} = \frac{\sum_{i=1}^{n} \frac{1}{n}(z_i - \bar{z})^4}{\left(\sum_{i=1}^{n} \frac{1}{n}(z_i - \bar{z})^2\right)^2}$	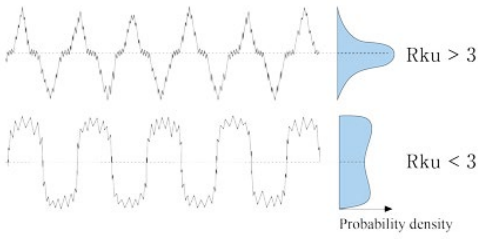
Probability Density Curve	Bearing curve (Abbot curve)	-	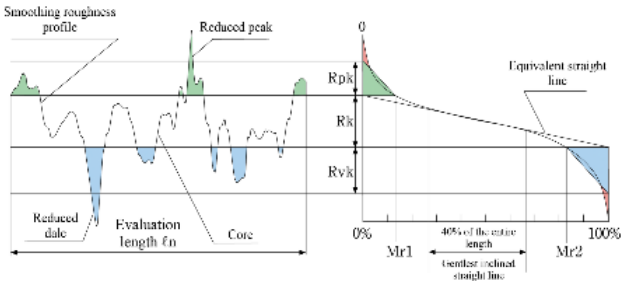

5.3. Results and Discussions

5.3.1. Texture profiles

The contactless laser collected seven profiles for each sample. One profile for each sample was selected as a representative profile, and it is presented in Figure 39.

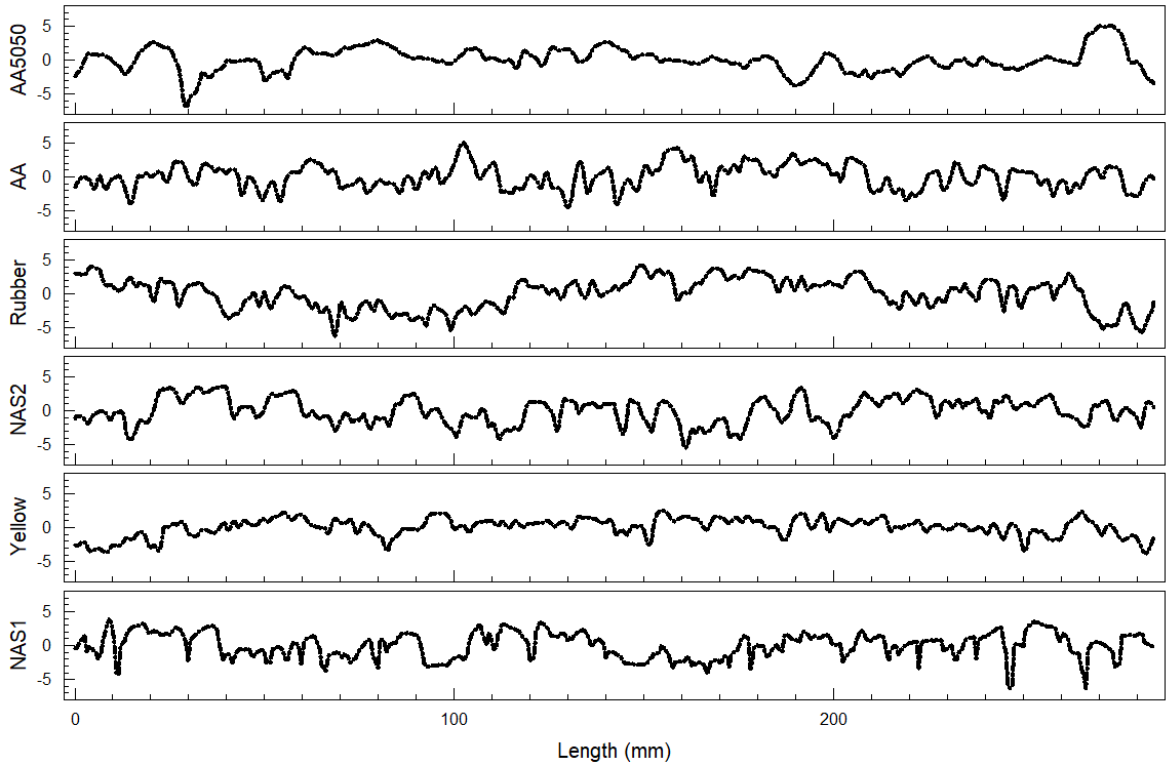

Figure 39. Representative profiles for each sample.

All profiles have the same length and are scaled at the same height. It is possible to note that some profiles appear to be smoother than others, mainly "AA5050" and "Yellow". However, only the profile by itself is not enough to assess and understand the pavement texture. It is necessary to assess the roughness through the parameters presented in Table 17.

5.3.2. Roughness Data Analysis

The texture of the pavement was collected and is presented in Table 18, summarizing an average of seven profiles to each of the indicators.

Table 18. Average roughness indicators for the whole captured profiles.

Indicator	AA5050 (avg mm)	AA (avg mm)	Rubber (avg mm)	NAS2 (avg mm)	Yellow (avg mm)	NAS1 (avg mm)
MPDiso	2.255	3.587	2.631	3.054	1.971	2.930
MPDaipcr	2.776	3.907	2.637	3.568	2.209	3.396
ETD1995iso	2.004	3.070	2.305	2.643	1.776	2.544
ETD2019iso	2.481	3.946	2.894	3.360	2.168	3.223
R_a	1.011	1.499	1.393	1.440	0.835	1.411
R_u	2.564	4.035	2.994	3.584	2.318	3.505
R_z	3.427	5.696	4.463	5.414	3.082	4.617
R_{max}	4.893	6.994	6.318	7.143	4.392	5.935
RMS	1.383	1.850	1.896	1.797	1.108	1.776

Samples “AA” and “AA5050” are the ones with the AEA, which have a nominal size of 10 mm, being the largest aggregates used. Sample “Rubber” has as a largest aggregate size of 14 mm. The “Yellow” has 6 mm aggregate size while the same granulometric curve are used for “NAS1” and “NAS2”, with 8 mm aggregate size.

It is noted that the lowest MPD is from the “Yellow” mix, followed by the “AA5050”, being the highest values of the “AA” and “NAS2”. It is clear that the smoother surfaces, indicated before in Figure 39, are indeed “Yellow” and “AA5050,” as shown by the Ra value close to 1, and the lowest RMS values. The “NAS1” and “NAS2” have quite similar values in all indicators, with the exception of Rmax. This can be due to a lack of homogeneity in the surface.

Finally, plotting the MPD by the indicators of roughness (Figure 40), even though each indicator has its own meaning and convey its particular information, they can be used interchangeably as a general indicator.

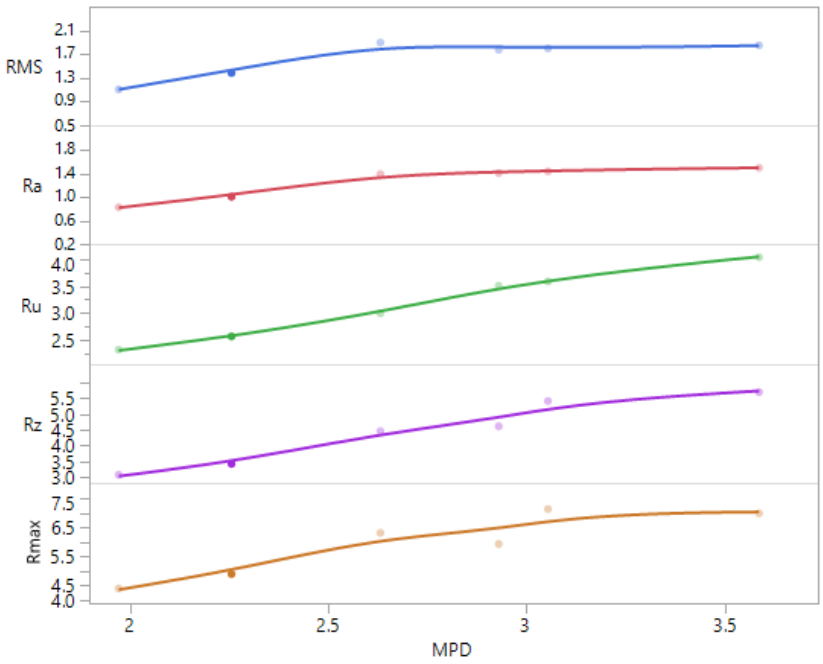

Figure 40. MPD by other height indicators.

5.3.3. Normality test

It is quite important to assess if the sample profiles are indeed Gaussian (normal) or not. This gives an indication of how the peaks and valleys are distributed. The Gaussian distribution has a very interesting property that the mean, mode and median are equal. In Figure 41(a), it is possible to see all samples probability distribution plotted together and (b) the boxplot of the same data.

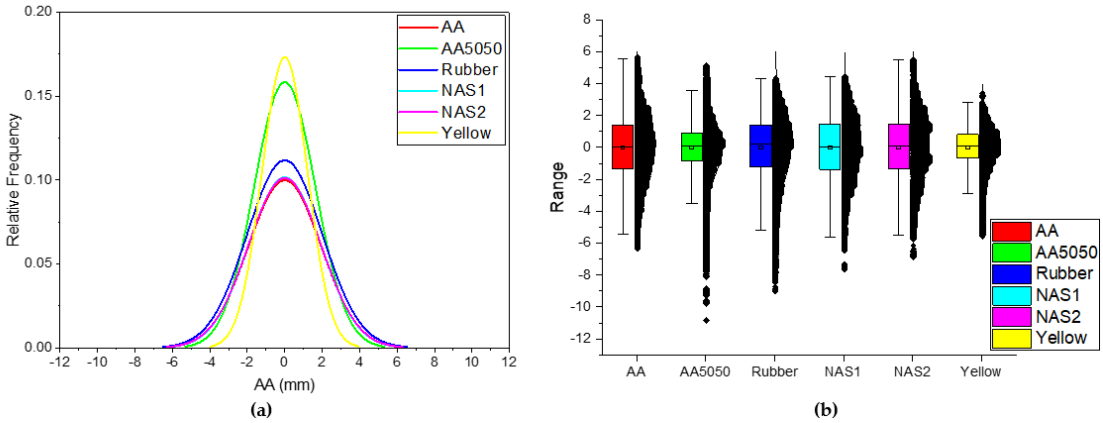

Figure 41. Plot probability density curves and Boxplot of the samples.

In Figure 41(b), the size of the tails in all data sets is showing that most samples have low kurtosis. Also, it is possible to note the median line in all box plots, are tilted to the positive range, and the mean in all samples is quite close to zero. Still, this is not an indication that the samples have a Gaussian distribution. For the purpose of assessing it a specific test is needed. Hence, all samples were tested to evaluate if they were Gaussian or not. To conduct this evaluation the Kolmogorov-Smirnov Goodness of Fit Test (K-S test) was applied using the Origin2021 software. The K-S test compares the data to a normal distribution and calculates the P-value and the data statistics. If the former is higher than the P-value, the data is not Gaussian (reject normal); if it is lower, then it is not possible to reject the normal hypothesis. The plotted distribution is shown in Figure 42, and the data are listed in Table 19.

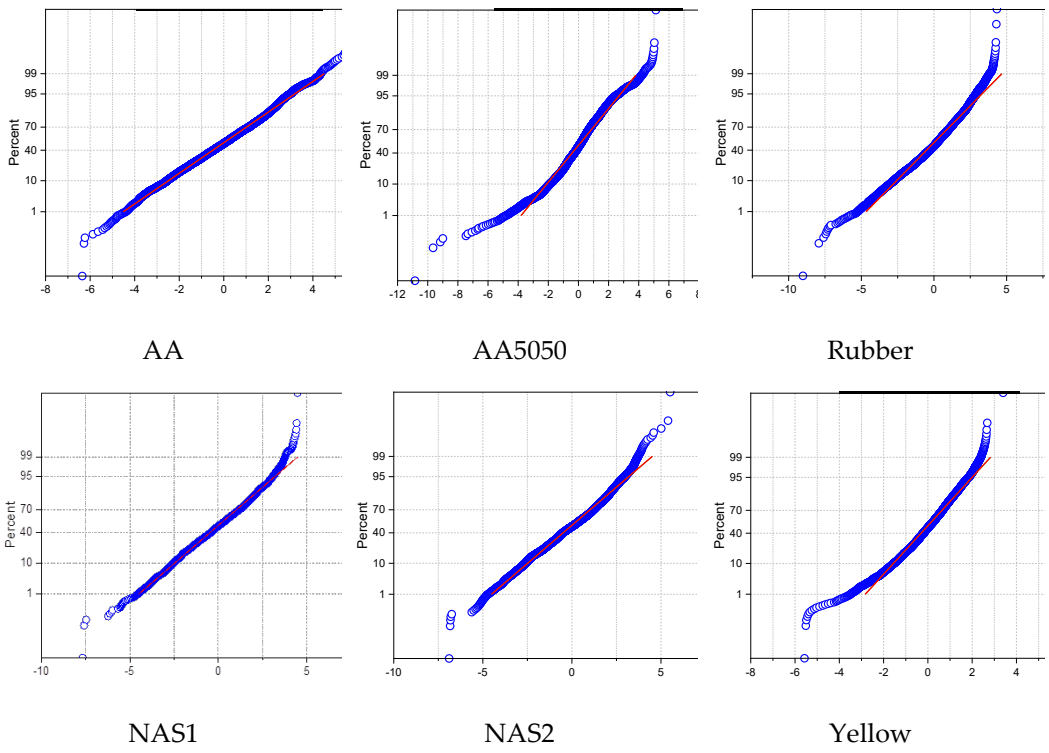

Figure 42. Probability distribution curves.

Table 19. K-S (modified) tests results and descriptive statistics

Sample	K-S Test			Descriptive Statistics			
	Statistics	**P-Value**	**Decision at level (5%)**	**Mean**	**Median**	**Rku**	**Rsk**
AA	0.05271	0.02158	Reject normal	-5.82 E^{-14}	0.05529	-0.24883	-0.11584
AA5050	0.01551	0.02130	Reject normal	-2.13 E^{-14}	0.06890	-2.62028	-0.50138
Rubber	0.04728	0.02140	Reject normal	-1.42 E^{-13}	0.21153	0.2621	-0.55149
NAS1	0.03569	0.02099	Reject normal	-1.21 E^{-13}	0.05504	-0.29347	-0.23178
Yellow	0.04174	≤0.01	Reject normal	7.92 E^{-14}	0.08778	1.2164	-0.68202
NAS2	0.02559	0.02130	Reject normal	-9.33 E^{-15}	0.01110	-0.34053	-0.2835

It is possible through the descriptive statistics in Table 19 to note some relevant differences, the first being that "AA5050" has the highest kurtosis, meaning that the heights are more distributed around the mean value and so it is close to a "flat" surface. This is true also for sample "Yellow", which shows a relatively high kurtosis. In addition, all samples have a negative skewness, which means that in all the profiles there is a greater concentration of valleys in respect to the average values.

With the help of a topological graphical representation, a well-stablished tool in tribology [147,148], it is possible to group and even rank the samples as their texture properties, as represented in Figure 43.

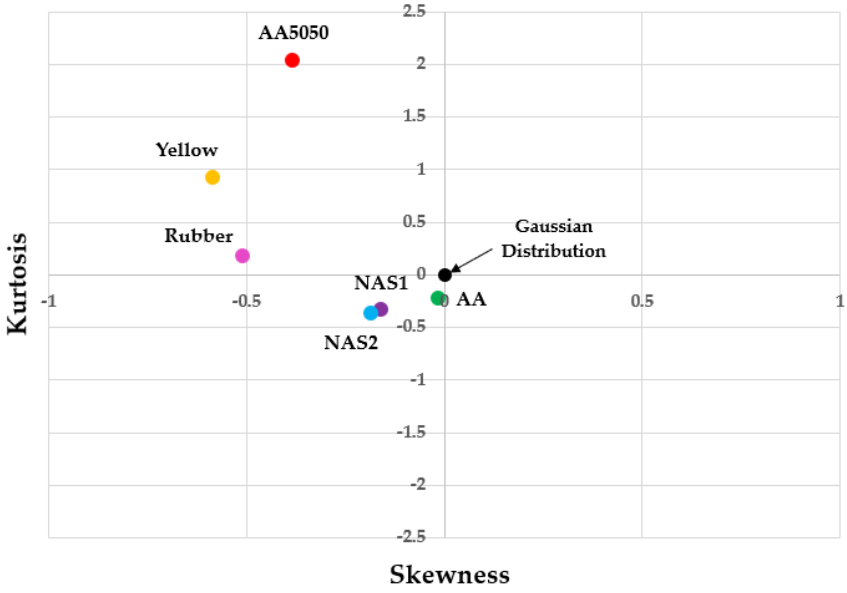

Figure 43. Topological graphical representation.

Sample "AA", which is close to a normal distribution, has nearly zero kurtosis , although still negative, and a negative skewness. Samples "NAS1" and "NAS2" show quite similar results, with a low negative kurtosis and skewness. However, their profiles cannot be approximated to a normal distribution. Samples "AA5050" and "Yellow" are similar in being both positive in kurtosis. However, they have quite different skewnesses. The "Yellow" sample has quite negative skewness but

a lower kurtosis, indicating that the data is highly concentrated in the center, with low tails in the distribution. Finally, “AA5050”, has a negative skewness and the highest kurtosis.

5.3.4. Abbott Curves

The last calculated parameters are presented in Figure 44, where the profile is plotted for each sample, followed by the histogram and the distribution, an eventually by the Bearing Abbot Curve.

The Mr1 and Mr2 points in the Abbott Curve represent respectively that height of the profile above or below which a certain portion of peaks or valleys is located. For the purpose, it was chosen the peak above which lies the 10% of the profile peaks and the valley beneath which the 20% of valleys is included (80% of the whole profile).

The inclination between Mr1 and Mr2 in the Abbot-Firestone Curve (Figure 44), is a good indicator of how the potential contact area of the sample is structured. This contact area can be related to friction, grip and also noise. An Abbot Curve with a steeper inclination has a less “flat” area, which can indicate that it has a high volume of peaks or valleys. These proportions, peaks and valleys are given by the Rpk (peaks) and Rvk (valleys), and Rk is the contact area region. This data is presented in Table 20.

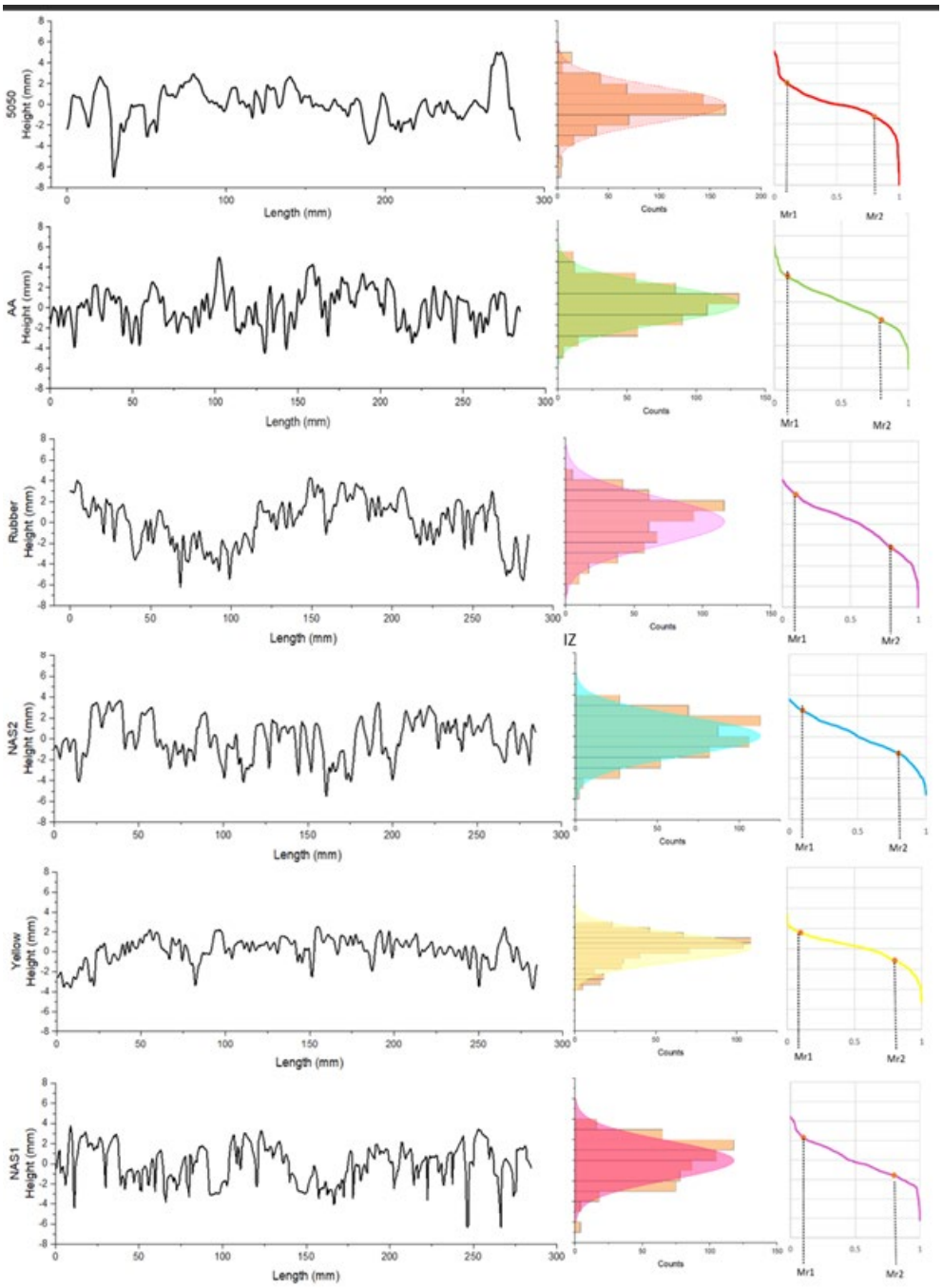

Figure 44. Profiles, histograms and probability density curve, and Abbot-Firestone curves.

Table 20. Abbot curve data and curve slope.

Sample	Mr1 (mm)	Mr2 (mm)	Slope(%)	R_{pk} (mm)	R_{vk} (mm)	R_k (mm)
AA5050	2.072	-1.356	4.897	2.996	5.580	3.428
AA	2.381	-1.574	5.649	3.226	4.908	3.954
Rubber	2.500	-1.639	5.913	1.892	3.268	7.098
NAS2	2.391	-1.568	5.655	2.834	5.489	3.959
Yellow	1.511	-0.996	3.581	1.289	4.572	2.507
NAS1	2.392	-1.582	5.678	2.233	6.053	3.974

It is possible to note that samples "AA5050" and "Yellow", previously cited as smoother according to the other indicators, have indeed a lower inclination, 4.897% and 3.581% respectively, then the other samples. Samples "AA", "NAS1" and "NAS2" show almost the same inclination and these results are consistent with those found in the topological representation.

5.3.5. Texture Level Spectrum

In Figure 10, it is possible to observe the Texture Level Spectrum of the different microsurfacing samples, which shows the texture level (LTX) for a certain class of wavelengths λ, from 0.063 mm to 20 mm. In particular, it is possible to observe the microtexture domain for wavelengths below 0.5 mm, whereas the macrotexture domain ranges from 0.5 mm to 50 mm [44,45].

For the analysis, microsurfacing samples were compared to an on-site application of an Open Graded (OG) mix and a Dense Graded (DG) mix. OG texture data were acquired at time of traffic opening, whereas the DG texture data were deliberately taken after conditioning by traffic. The OG mix used basalt with a maximum aggregate size between 15 and 20 mm, whereas the DG was a mixture made up of basalt and limestone with a 0/8 mm granulometric curve.

As for the OG spectra, it can be noted that at larger wavelengths the texture level is higher compared to the other mixtures, and this trend is also true in the microtexture domain. The DG spectra lies below all mixtures: it is clear that the traffic action

exposed the surface to raveling, which lead to loss of aggregates and to a reduction of the texture level in the macrotexture domain, and polishing, which explains the complete lack of microtexture. In conclusion, OG and DG spectra appear to include the microsurfacing's one, indicating that microsurfacing is a maintenance solution that can offer a texture level between them.

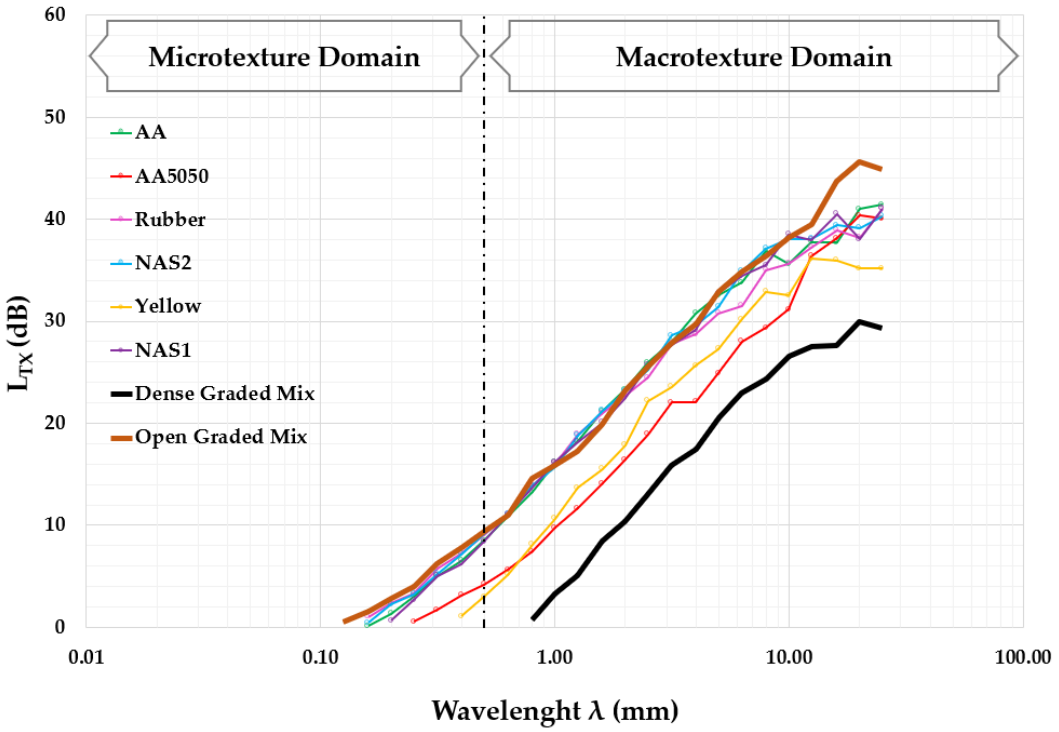

Figure 45. Texture Level Spectrum of the samples

As for the microsurfacing samples, it is clearly visible that all mixtures have similar results, except for "AA5050" and "Yellow", being these lower down in the spectra. This can be explained by comparing the results with the granulometric distribution of the samples. In fact, "AA5050" has a particle size obtained by combining 50% of a 0/6 mm granulometric curve passing sieve 2mm and 50% AEA of 10 mm size, whereas "Yellow" sample is made up with a 0/6 particle size distribution. Therefore, this explains the similar trend until the wavelength of 2 mm is reached. After this threshold the "Yellow" and "AA5050" mixes diverge, mainly because the gradation of the "AA5050" contains a gap 2 and 10 mm. Lastly, the "AA5050"

curve rises due to the presence of the AEA, whereas the "Yellow" one reaches a plateau.

The other mixtures' spectra follow the same trend, especially at shorter wavelengths. In fact, there are no major differences between the 0/8 mm granulometric distribution ("NAS1" and "NAS2") and the Australian curve ("AA"). Also, sample "AA" do not show particular differences despite the presence of AEA, because of the small percentage of them used in the mixture. The spectra of "Rubber" exhibits a lower texture level within the wavelengths of 4 and 10 mm. Finally, it should be noted that the small difference between the last discussed mixtures could be attributable to the way the mixtures were laid, and are not statistically relevant.

The microtexture in sample "Yellow" does not emerge, probably due to the use of resin that covers the roughness of the single aggregate. Sample "AA5050" shows a positive level of texture until the 0.25 mm wavelength, but microtexture is still more hidden than that of the other mixtures. This could be attributable to the shape and the surface finish of AEA, considering that they are cast in plastic molds.

These results might be related to the inclinations found in the Abbott Curves: actually, microtexture is obtained by the surface properties of the individual chippings or other small particles of the surface, which come in direct contact with the tire [19], and therefore the core of the surface. In fact, as previously noted, samples "Yellow" and "AA5050" have a smoother surface than the other samples.

5.4. Conclusions

The present paper aimed to assess and evaluate the texture of different microsurfacings samples. The proposed work consisted of testing: two benchmark mixtures that used traditional natural aggregates granulometry and asphalt emulsion; one mixture with the same aggregate but with a resin binder; a mixture with the asphalt emulsion as a binder and 60% crumb rubber and 40% natural

aggregate and finally the replacement of natural aggregate by artificial geopolymer aggregate, with two samples made with different granulometric curves.

In the light of the above it is possible to conclude the following:

- The texture parameters, traditional or statistical, are dependent on the type/size of aggregate and type of binder used;
- The result of kurtosis and skewness show a good correlation with the Abbot curve (bearing curve);
- The use of crumb rubber as an aggregate, even at a smaller nominal size, did not present relevant differences in terms of texture indicator when in comparison to the other mixtures;
- The use of AEA changed the mixtures substantially. This can be due to their size, 10 mm, or to their specific shape, more studies are needed on these aspects.
- Considering the "AA5050" that contains 50% AEA by mass, its texture indicators drastically changed;

According to the authors' experience:

- It would be necessary to replicate the tests with a more diverse sample scenario, using different binders and aggregates;
- It would be important to assess the texture parameters on a surface basis and not only on linear profiles;

Finally, the use of topology maps to describe and classify the surfaces according to Skewness and Kurtosis could provide interesting information as it is widely used in tribology to identify the polishing process in surfaces.

Chapter 6: Tire/road noise evaluation of microsurfacing paving solutions: A comparison between natural and artificial aggregates

Copetti Callai S, De Rose, M., Makoundou, C.Vaiana, B. Altreuther, R. Sangiorgi C. Tire/road noise evaluation of microsurfacing paving solutions: A comparison between natural and artificial aggregates (To be submitted to Building Acoustics (ISSN 1351-010X)).

Abstract: Noise pollution can cause a number of health to economic problems, from market price depreciation in housing and offices to high risk of cardiovascular diseases. Studies have shown that traffic noise is the most prevalent among the noise pollution sources. While in traffic noise, the aerodynamical noise is negligible as it is only relevant at higher speeds, and the powertrain noise is the main cause at very low speeds, leaving the tire/road noise the most relevant component. This paper aims to assess the noise properties of five different microsurfacing samples. Each sample had a combination of Natural Aggregate, Artificial Engineered Aggregate and Crumb Rubber. Two different binding agents were used, asphalt emulsion and resin. The texture of the samples was captured by a laser profilometer. This texture data served as input to the SPERoN® model. The model provided Lair and Lvib noise levels and frequencies. The study has shown that the type of binding agent is important to control the noise levels, as it changes the texture drastically. Also, the use of artificial aggregates can reduce the noise levels if the quantity of material is close to 50% by mass, as at lower levels, it did not improve the noise levels.

Keywords: Tire/road noise, SPERoN®, Noise model, Artificial aggregates, Geopolymer aggregates, Crumb rubber

6.1. Introduction

Noise pollution is related to several health problems such as cardiovascular disease [22,149,150], hypertension [151,152], sleep deprivation [153], depression and anxiety [149,153]. It is also associated with stress during pregnancy and child development [154,155]. Noise pollution is also related to economic factors [37,156,157], usually as a result of the cost of health problems, the burden of lost years to the economy, to more direct losses such as the cost of building noise barriers and the depreciation of houses caused by noise. The traffic noise is also an inequality indicator, as more socio-economically disadvantaged groups are more exposed to higher noise levels [150,158]. According to the European Environment Agency (EEA), in their 2020 report [150], the number of people exposed to road traffic noise exceeds that exposed to rail, aircraft and industrial noise, being estimated as 113 million people exposed to noise levels over 55dB.

The traffic noise, or road noise, is composed of aerodynamical noise, propulsion and tire/road noise [6]. The first one is only relevant at high speeds, as for the propulsion is it is regulated by the power train, and is quite relevant at very low speeds and in heavy vehicles, as for the tire/road noise it is the most relevant all around [6,9,43]. The auto motor industry has been studying and managing the aerodynamical and propulsion noise [159]. Even with electric cars, the noise problem will not disappear, as the most relevant noise component is not the power train but the tire/road noise. Thus, to control road noise pollution it is necessary to assess the tire/road noise component. In which the pavement characteristics, such as texture, voids and stiffness, are the major contributors.

The tire/road noise is prevalent between macro and megatexture, as presented in Figure 46. It is possible to use the pavement texture to reduce or even absorb part of the noise [9,23,57,72,76,94,160].

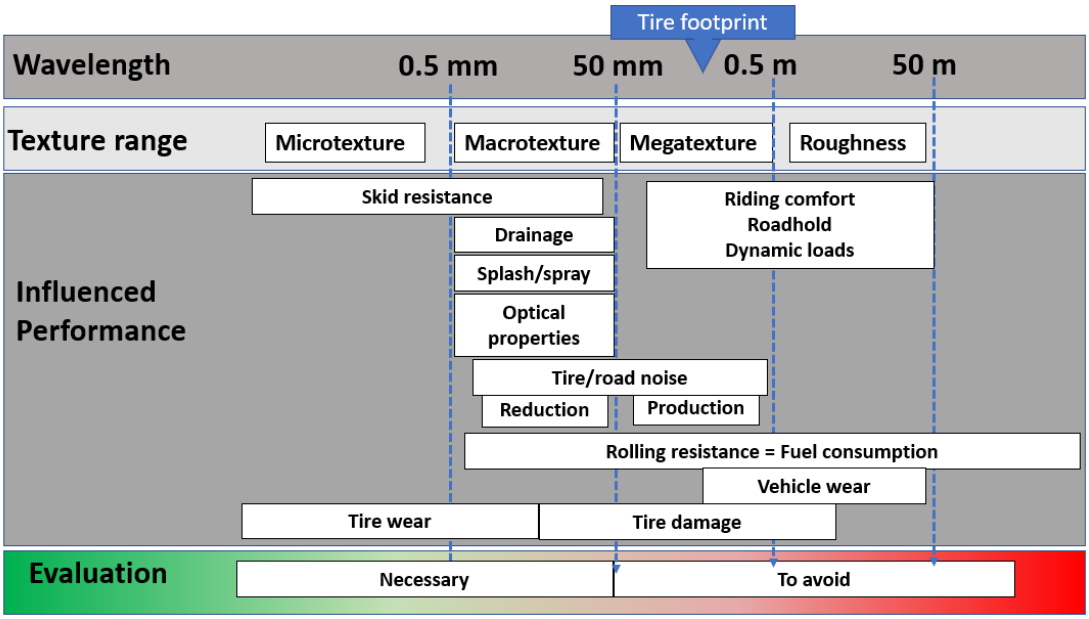

Figure 46. Pavement texture range and influence on tire/vehicle. Adapted from [161].

Different pavement solutions can be applied in order to reduce noise, most commonly are the open-graded[55], twin layers[64,67] and PERS[162,163]. However, these solutions have a high cost and are not as widely used as other traditional paving solutions. One of the traditional paving solutions has been also studied to improve the tire/road interaction regarding friction (skid resistance) and noise[55,73,142,164]; it is called microsurfacing. It is a functional solution, as its application has no structural behavior, but mainly acts to seal the cracks and restore the pavement skid resistance [73].

The noise generation and absorption mechanisms in the pavement are related to stiffness (relative to the tire), air voids (capacity to absorb noise waves), and texture. The last two elements are dependent of the aggregate size, origin and its granulometric curve. Mixtures such as open-graded ones, have a significant amount of air voids which contributes positively to the noise reduction, but it is possible to obtain similar results using microsurfacing. However it is needed to control precisely the aggregate shape, size and texture to promote a more silent pavement[165–167].

In order to comprehend the noise behavior, several studies have been conducted, both in situ and laboratory scale, as well as models were proposed[168–171]. For this research the SPERoN® (Statistical Physical Explanation of Rolling Noise), a noise framework model proposed and developed by M+P , Müller-BBM and Chalmers University, Division of Applied Acoustics, was selected. It has been used in several commercial instances and in different European projects such as SILVIA[22] and ITARI[172].

The present study will evaluate the noise behavior of five paving solutions, using natural and artificial aggregates (geopolymeric and rubber), as well as to compare two different binders, one asphaltic emulsion and a resin. In order to evaluate it, the samples were produced and tested in terms of texture properties using a laser profilometer, and the data collected served as an input for the noise model.

6.2. Materials and Methods

6.2.1 Research plan

The present work was designed to evaluate the behavior of a novel artificial aggregate developed in previous research [131]. Six samples were produced, and their texture indicators were measured and calculated using a laser profilometer.

Then, each profile was used as an input in the SPERoN® model to calculate the noise levels in terms of Noise Vibration Levels(Lvib) and Noise Airborne Levels (Lair). Both noise levels were calculated for six samples, four speeds and three different tires, with two airflow resistance levels, as presented schematically in Figure 47. Later all this data was analyzed to evaluate the proposed paving solutions.

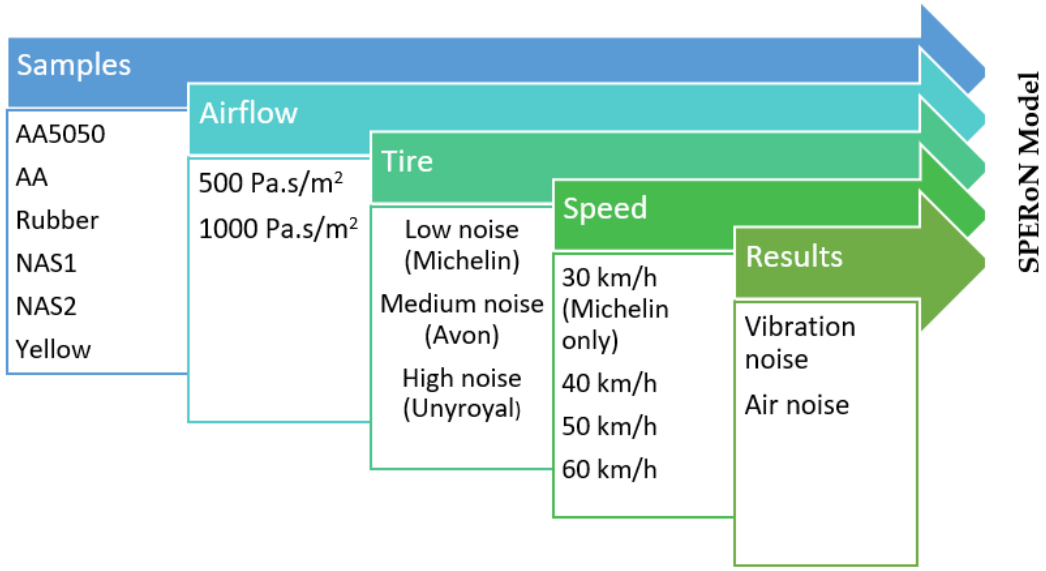

Figure 47. Schematic representation of the variables and workflow for the SPERoN® model.

6.2.2 Proposed Microsurfacing paving solutions.

The six samples produced in order to evaluate the noise levels, two samples used a mixture between Artificial Engineered Aggregate and natural aggregate, both of basaltic origin. One sample used a mixture of Crum Rubber as an artificial aggregate and natural aggregate. Another sample used resin as replacement to asphalt emulsion with natural aggregate. Finally, the last 2 samples worked as a benchmark, as they are a traditional microsurfacing solution, that used asphalt emulsion with natural aggregate. The mixtures are described below.

- AA5050 – 50% Artificial aggregate (geopolymer) and 50% natural aggregate.
- AA – 10% artificial aggregate (geopolymer), Australian granulometric curve (AP-R569-18).
- Rubber – 60% artificial aggregate (crumb rubber 0.8 – 4mm).
- NAS1 and NAS2 – 0/8 mm natural aggregate granulometric curve – Benchmark mixtures.

- Yellow – 0/8 mm natural aggregate – Resin.

All mixtures, except for "Yellow," used asphalt emulsion modified with latex; the "yellow" mix used a resin that is marketed as alternative to common bituminous emulsion. These samples were produced following the ISSA method (asphalt emulsion) and the instructions of the producer (resin emulsion).

A laser profilometer was used to extract the profiles of each sample. In Figure 48, it is possible to see the six samples produced as previously described, 5 with asphalt emulsion one with resin. It is shown the placement of each profile (seven in each sample), extracted in the dotted red line on the Figure 48.

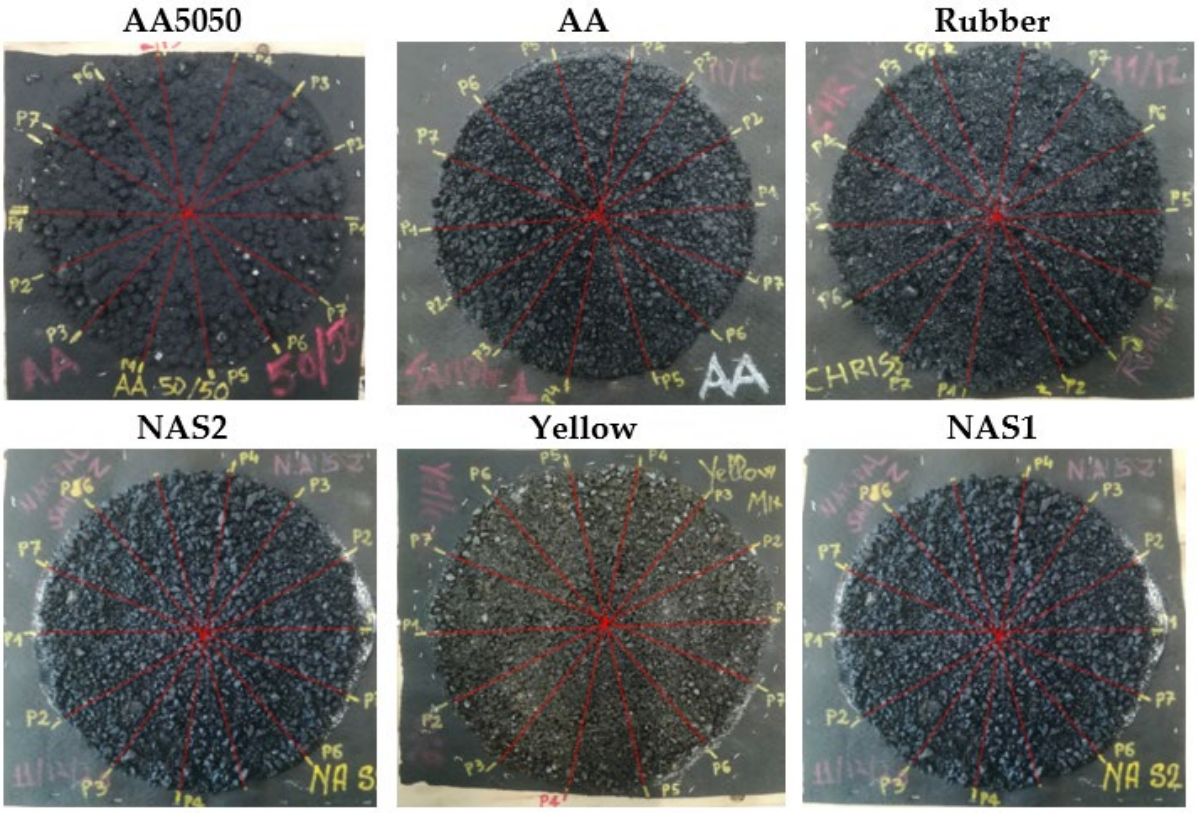

Figure 48. Surface samples with seven laser reading position for each sample.

The Artificial Engineered Aggregate is produced using an alkali-activation technique, presented in chapters 3 and 4. It consists of mixing the basalt powder and metakaolin with an alkali solution. This mortar is placed into 3D printed molds

and cured in the oven. The resulting artificial engineered aggregate has 10 mm diameter in a truncated octahedron shape, as shown in Figure 49.

Figure 49. Artificial Engineered Geopolymer Aggregate.

The aggregate mortar and itself were evaluated in previous studies, and its behavior regarding resistance to compression, water absorption and polishing resistance was acceptable [131,173].

6.2.3 Texture assessment

The most used parameters to describe the pavement texture are the Mean Profile Depth (MPD)[13,20,28,145,146]. The MPD was parameters created to assess the pavement macrotexture, and it were based on the traditional sand patch method [20]. Nonetheless, it is possible to use other parameters commonly used to describe texture, such as Roughness, skewness, Kurtosis, Root Mean Square and others[8,55,144,173]. The parameters' mathematical and graphical descriptions are presented in Table 21. The average roughness is one of the most widely used parameters, and it is the mean of the average height difference for the average surface. The last parameters are Ku (kurtosis) and (Sk) Skewness, and both are statistical parameters that help to describe the texture profile[174,175]. They were obtained from the profiles extracted by the laser profilometer, and posteriorly calculated in OriginPro 2021.

Table 21. Roughness/texture parameters.

Indicator	Name	Formula	Graphical Explanation
MPD	Mean Profile Depth	MPD=[(1st Peak-2nd Peak)/2]-average level	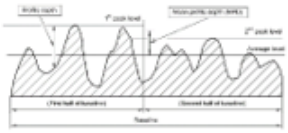
Ra	Average Roughness	$R_a = \frac{1}{n} \cdot \sum_{i=1}^{n} \lvert y_i \rvert$	
Rsk	Skewness	$Rsk = \frac{1}{Rq^3}\left[\frac{1}{l}\int_l^l Z^3(x)\,dx\right]$	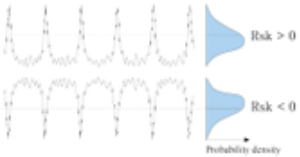
Rku	Kurtosis	$Rku = \frac{1}{Rq^4}\left[\frac{1}{l}\int_l^l Z^4(x)\,dx\right]$	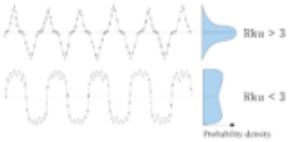

6.2.4 Noise evaluation using the SPERoN® model.

The SPERoN® is a hybrid modeling framework for tire/road noise prediction . Its constituted of physical parts for the prediction of the tire/road contact forces and of statistical parts such as a series of multivariate linear regression models to predict the noise spectrum resulting from tire vibrations, airflow-related mechanisms, tire friction, tire cavity noise and aerodynamic vehicle noise[172,176,177]. It's a hybrid approach combines a physical sub-model with a statistical sub-model. These models consider that the tire/road noise is composed of different noise generation mechanisms[172].Figure 50, has a schematic representation of the model.

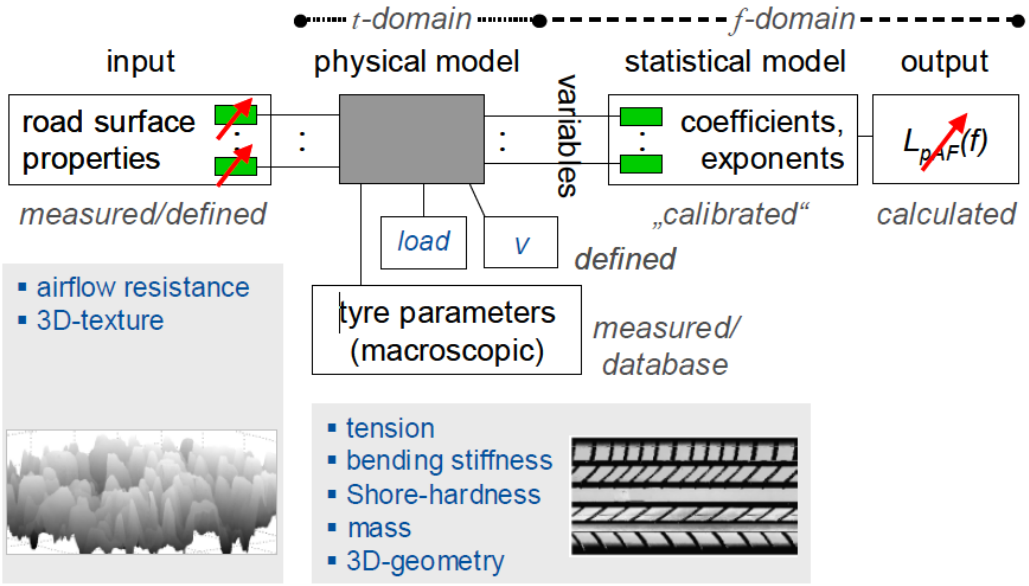

Figure 50. Schematic workflow of SPERoN® model. Adapted from[172].

The input data comes from the laser profilometer. However, the data collected in this research, because of constraints of the equipment and sample size, was collected in a radial pattern, which creates a repeated pattern in the intersection of the laser reading (close to the center of the sample). In this regard, it should be noted that the development of SPERoN® was originally not aimed at the calculation with artificially and periodically extended textures, as they result from texture measurements on laboratory test specimens. The intersection caused periodically similar values on the profile. These repeated elements can impact in the SPERoN® Model. This impact might falsify the calculation result in an unintelligible way. For this reason, the calculations can only give qualitative estimates of the extent to which changes on the surface influence the tire vibrations and the aerodynamics in tire-road contact. Consequently, in the case of the calculation from short profile elements, no accurate pass-by levels can be predicted. Thus, in this paper, the noise will be evaluated using the Lvib and Lair components available and at the frequency range of 400-2000 Hz.

6.3. Results

6.3.1 Texture parameters

The texture parameters of the samples are presented in Table 22, and it is possible to notice that the MPD and Ra for the Yellow and AA5050 are the lowest, which can be understood as them having lower peaks or lower number of peaks and valleys. The highest values are in the NAS2 and AA mixes.

Table 22. Texture indicators for each sample.

Sample	MPD (mm)	Ra (mm)	Rku (mm)	Rsk (mm)
AA5050	2.255	1.011	1.65766	-0.11832
AA	3.587	1.499	-0.2886	0.08429
Rubber	2.631	1.393	-0.5885	-0.37747
NAS2	3.054	1.440	-0.57394	-0.23811
Yellow	1.971	0.835	0.32476	-0.82706
NAS1	2.930	1.411	-0.29603	-0.38398

The kurtosis (Rku) and Skewness (Rsk) are good indicators of how the peaks and valleys are distributed in the profile of the texture. The lower the Rku, the highest amount of peaks, and the higher the number (i.e. AA5050), indicate that the surface is “flatter”. The Rsk indicates if the average line is higher or lower than the peak distribution, negative numbers mean that there is a higher amount of valleys than peaks and the reverse is also true.

6.3.2 Vibrational noise levels

The noise generated caused by the vibration in the tire/road noise was evaluated for each tire, airflow pressure and according to the speed and sample. In Figure 51 the vibration noise for the Michelin tire (low noise) is presented, Figure 52 for the AVON tire (medium noise) and Figure 53 for the Uniroyal tire (high noise).

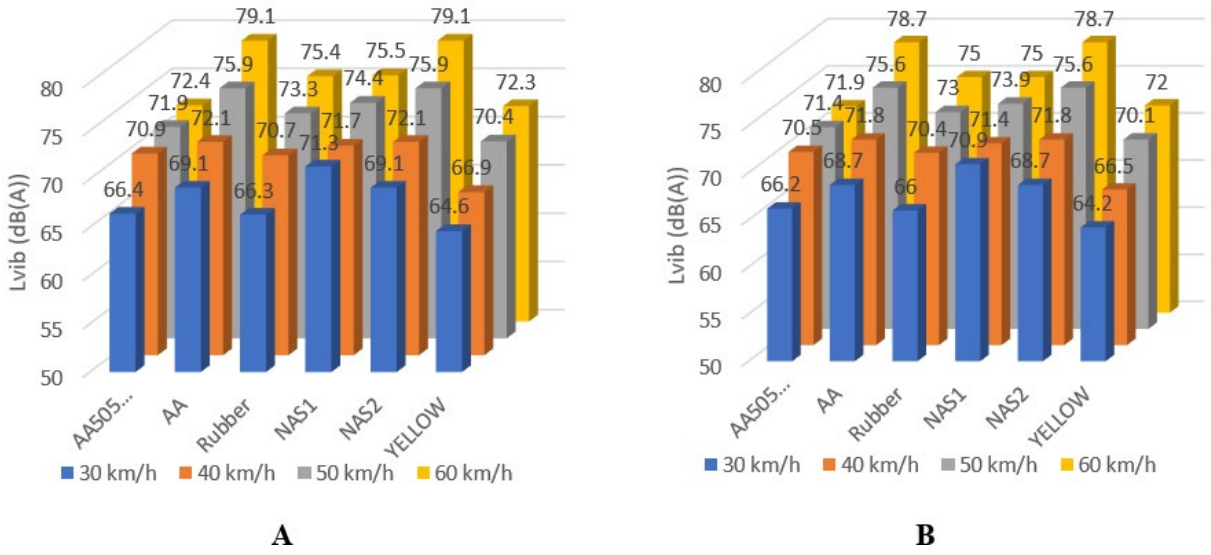

Figure 51. Lvib noise levels for Michelin tire, (A) Air Flow of 500 Pa.s/m^2 and (B) Air Flow of 1000 Pa.s/m^2.

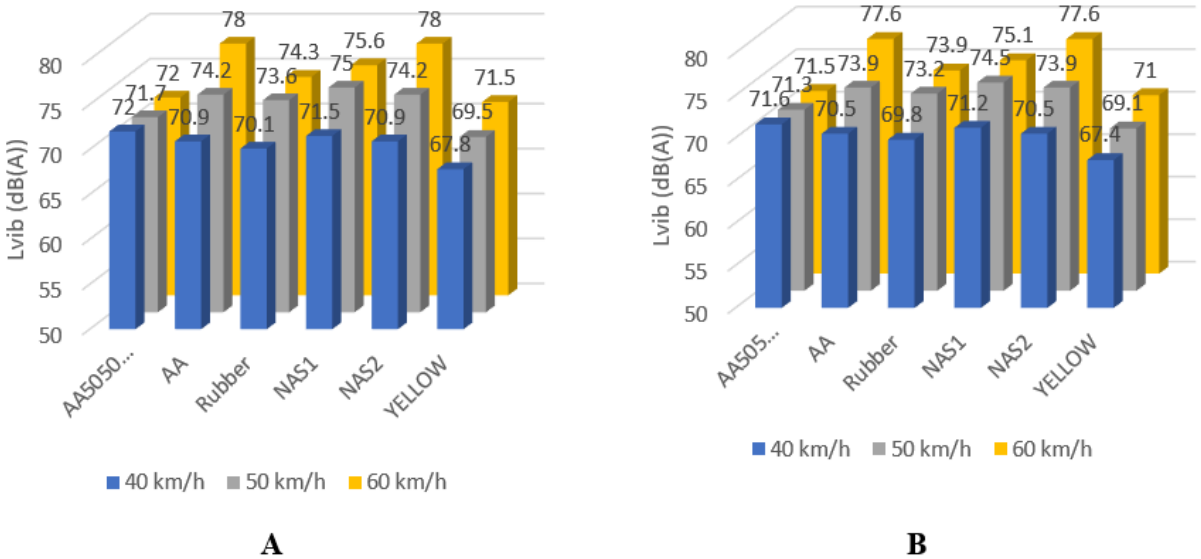

Figure 52. Lvib noise levels for Avon tire, (A) Air Flow of 500 Pa.s/m^2 and (B) Air Flow of 1000 Pa.s/m^2.

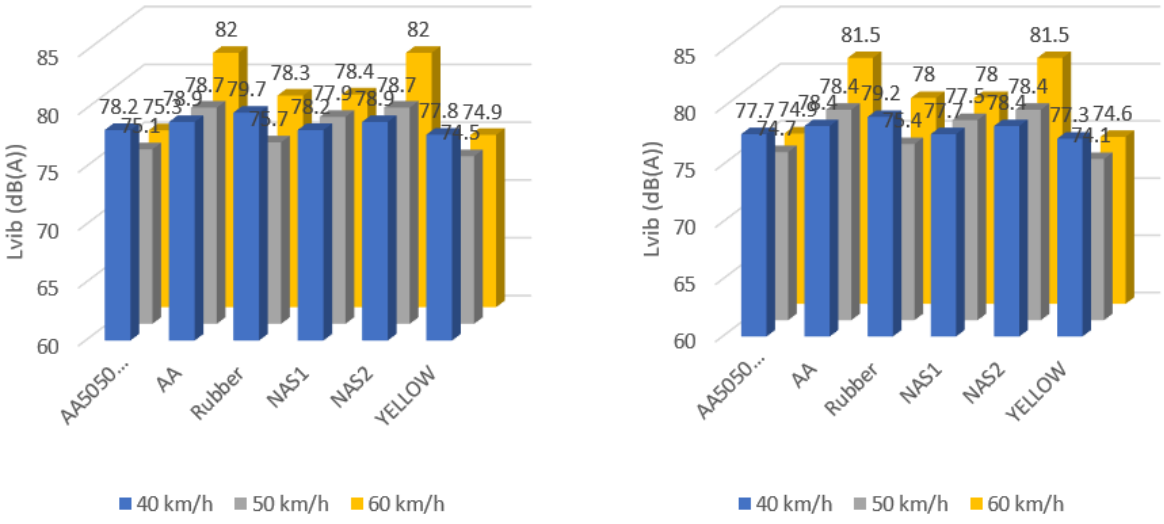

Figure 53. Lvib noise levels for Uniroyal tire, (A) Air Flow of 500 Pa.s/m² and (B) Air Flow of 1000 Pa.s/m²

It is noticeable in these figures that the Uniroyal tire has higher noise levels than the rest of the tires. Also, it is possible to note that for all tires and all airflow resistances, the AA sample has higher levels, followed by the NAS2. At the same time, the AA5050 and yellow mixes had the lowest overall indicators. Regarding the speed variation, in most cases the increase in the speed increased the noise, however the samples AA5050, Rubber and Yellow had lower noise level at 50km/h for the UNIROYAL tire, which might be due the texture pattern (between the tire pattern and pavement texture) and having a inflexion on the noise levels at this speed.

6.3.3 Air born noise levels

The noise generated attributable to the air displacement in the tire/road noise was evaluated for each tire, airflow pressure and according to the speed and sample. In Figure 54 is presented the air born noise for the Michelin tire (low noise), Figure 55, for the Avon tire (medium noise) and Figure 56 for the Uniroyal tire (high noise).

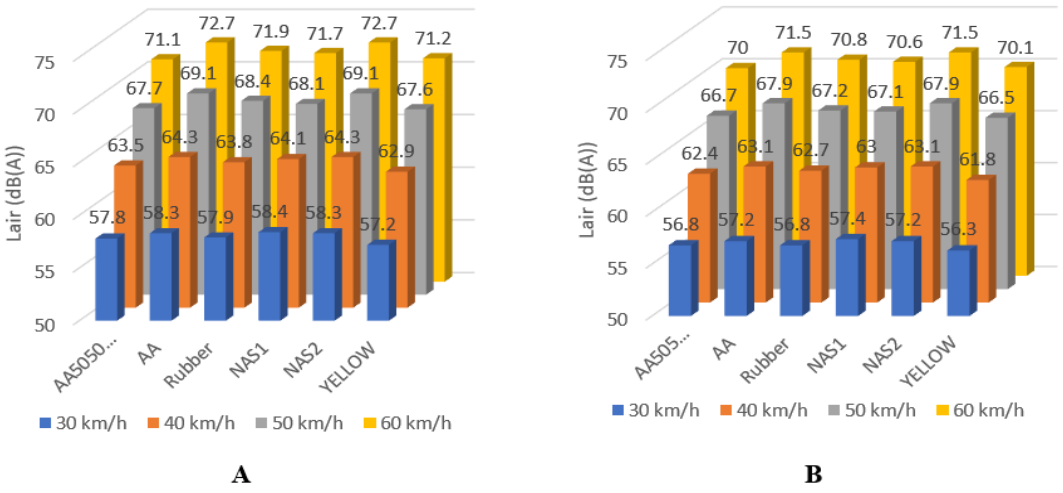

Figure 54. Lair noise levels for Michelin tire, (A) Air Flow of 500 Pa.s/m2 and (B) Air Flow of 1000 Pa.s/m2.

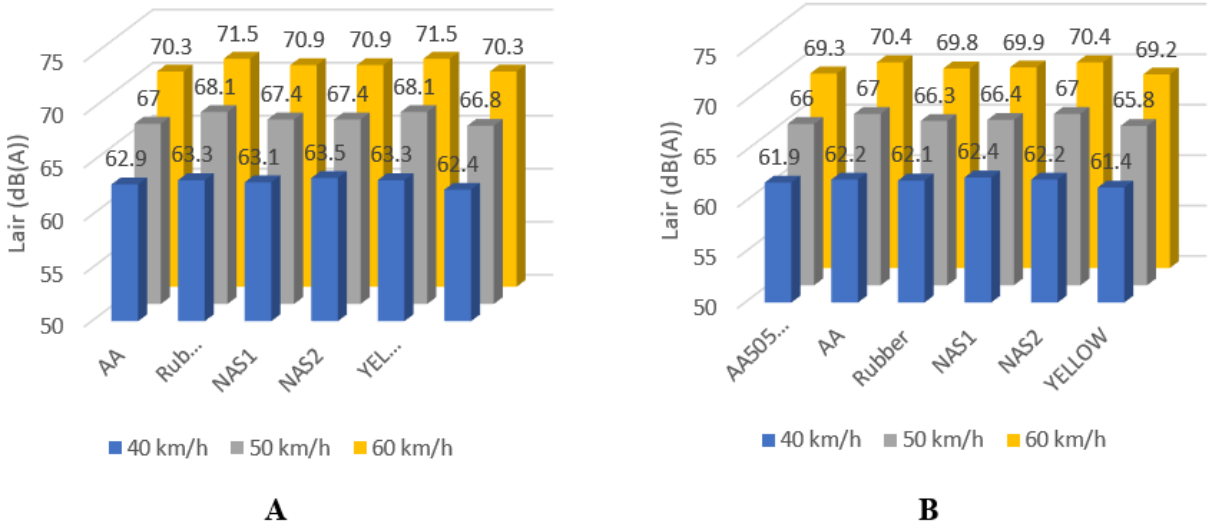

Figure 55. Lair noise levels for Avon tire, (A) Air Flow of 500 Pa.s/m2 and (B) Air Flow of 1000 Pa.s/m2.

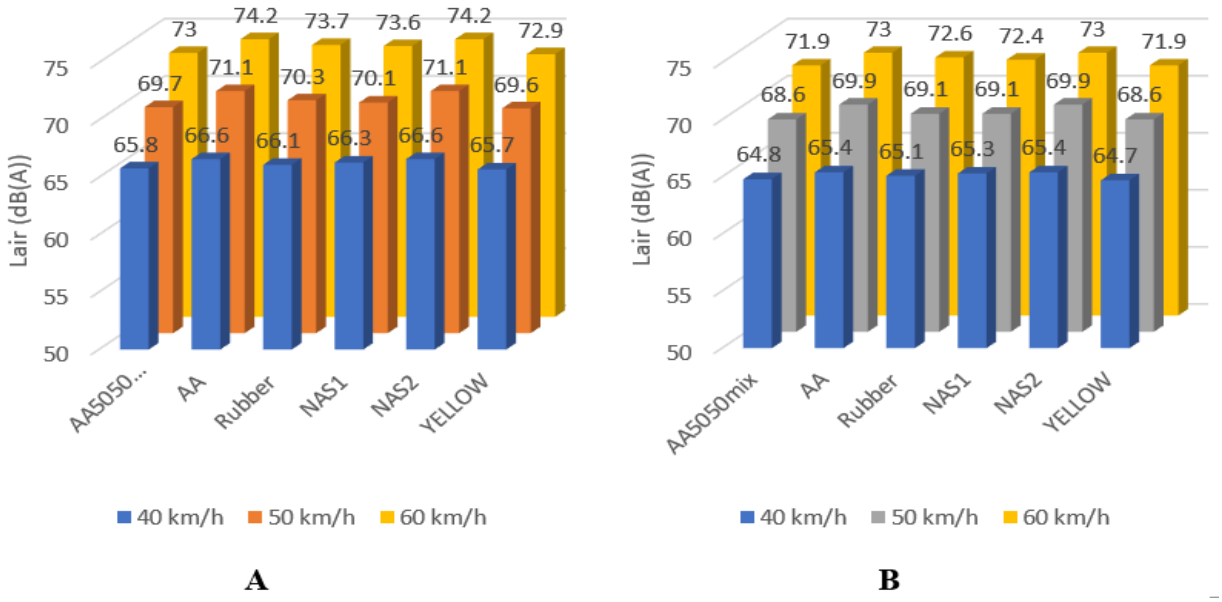

Figure 56. Lair noise levels for Uniroyal tire, (A) Air Flow of 500 Pa.s/m2 and (B) Air Flow of 1000 Pa.s/m2.

Air noise (Lair) has overall lower values than the Lvib, which was expected as the vibration component usually has higher values. The lowest values, independently of speed, airflow resistance and tire type, are in the samples Yellow and AA5050. In contrast, the higher is in the NAS2 and AA samples. This might be explained due the texture levels and kurtosis and skewness of this samples. For the air born noise the inflexion noted on the noise vibrational levels for UNIROYAL tire, are non-existing.

This denotes that, nevertheless, both noise sources are dependent on the same pavement texture properties thus the noise levels being similar progression, it has some important differences as the mechanisms which produce the noise are not the same.

6.3.4 Noise levels per texture indicators

In order to have a better understanding on the noise levels it is necessary to evaluate the noise level regarding several texture indicators, such as MPD, Ra, Skewness

and Kurtosis, as they are extremely representative indicators of how the texture is distributed.

The first evaluated parameters were the Mean Profile Depth and Ra, by the Lvib according to the speed and tire type. In Figure 57 it is possible to see that the noise levels increase due to the speed and tire type. Also, the higher is the MPD/Ra number, the higher is the noise level, which is on par with the literature [24,67,178,179].

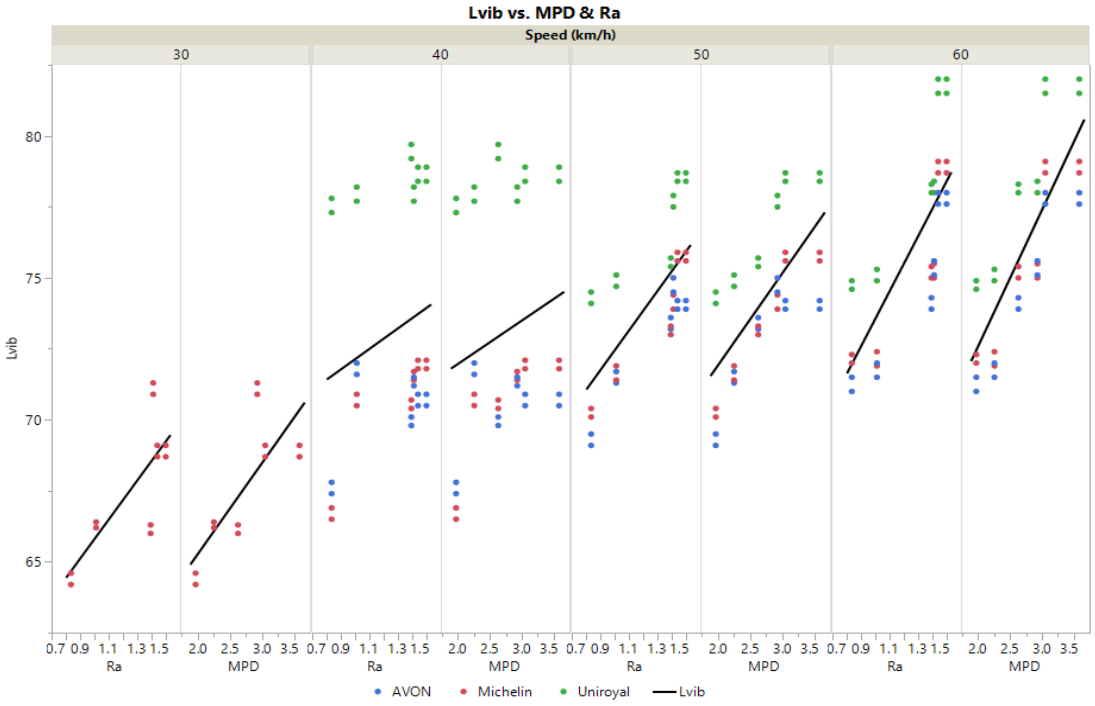

Figure 57. Lvib vs MPD/Ra by speed and tire type.

The same data is presented in Figure 58, but with respect to Lair. It is observed that while the noise levels are lower than Lvib, the pattern of higher noise by speed and by tire type does not change. It is important to notice that the inclination of the tire lines is less steep than for the Lvib, which might indicate that the Lair is less susceptible to texture changes.

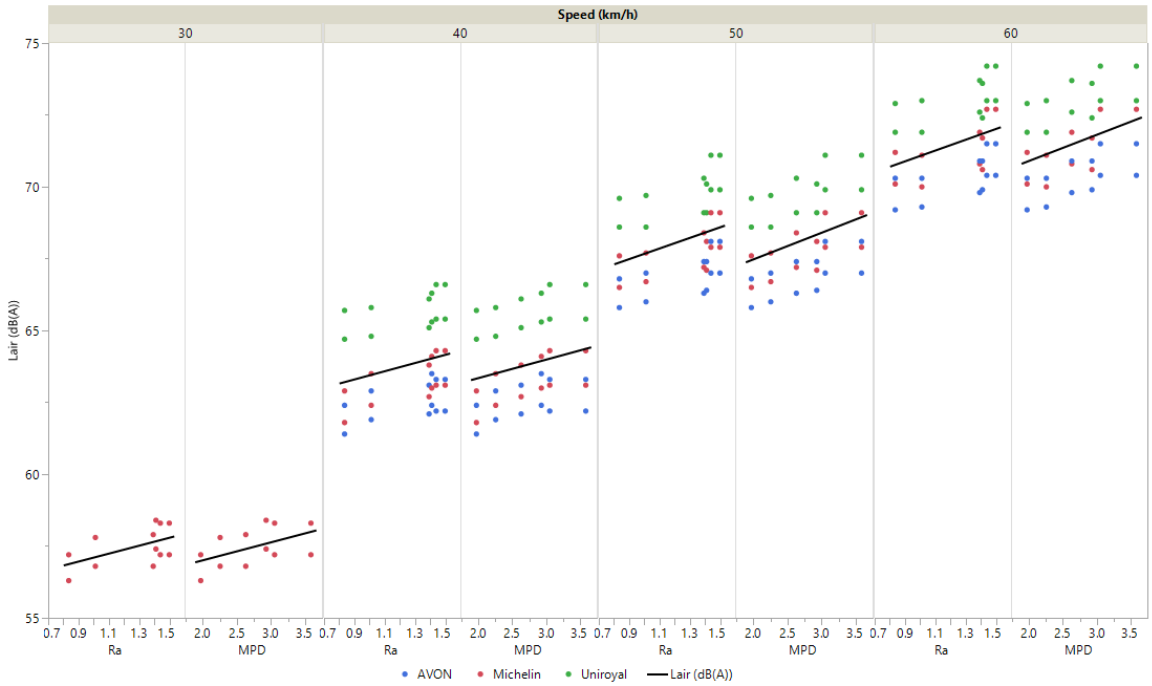

Figure 58. Lair vs MPD/Ra by speed and tire type.

As both Ra and MPD have quite similar behavior, even though the data distribution is not the same, it is necessary to assess other parameters, such as skewness in the deviation of the data distribution regarding the average and kurtosis of the relation of peaks distribution in the pavement. This Figure 59 presents the Lvib vs the skewness and kurtosis, and Figure 60 is the same for Lair.

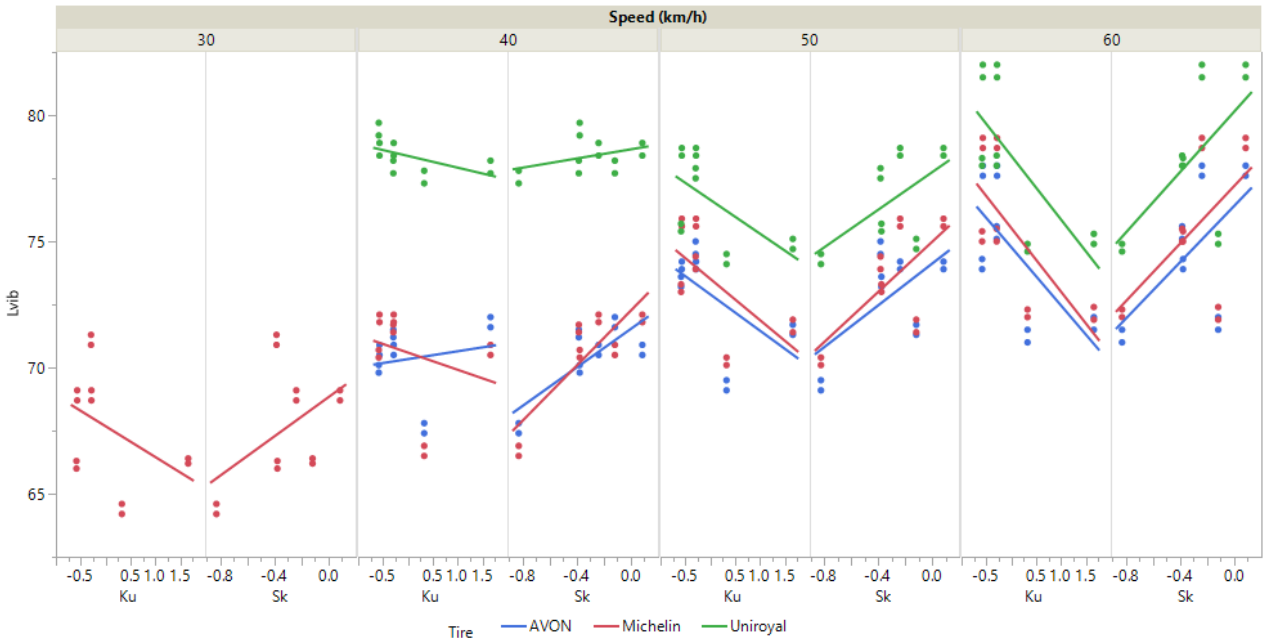

Figure 59. Lvib noise levels by the skewness and kurtosis.

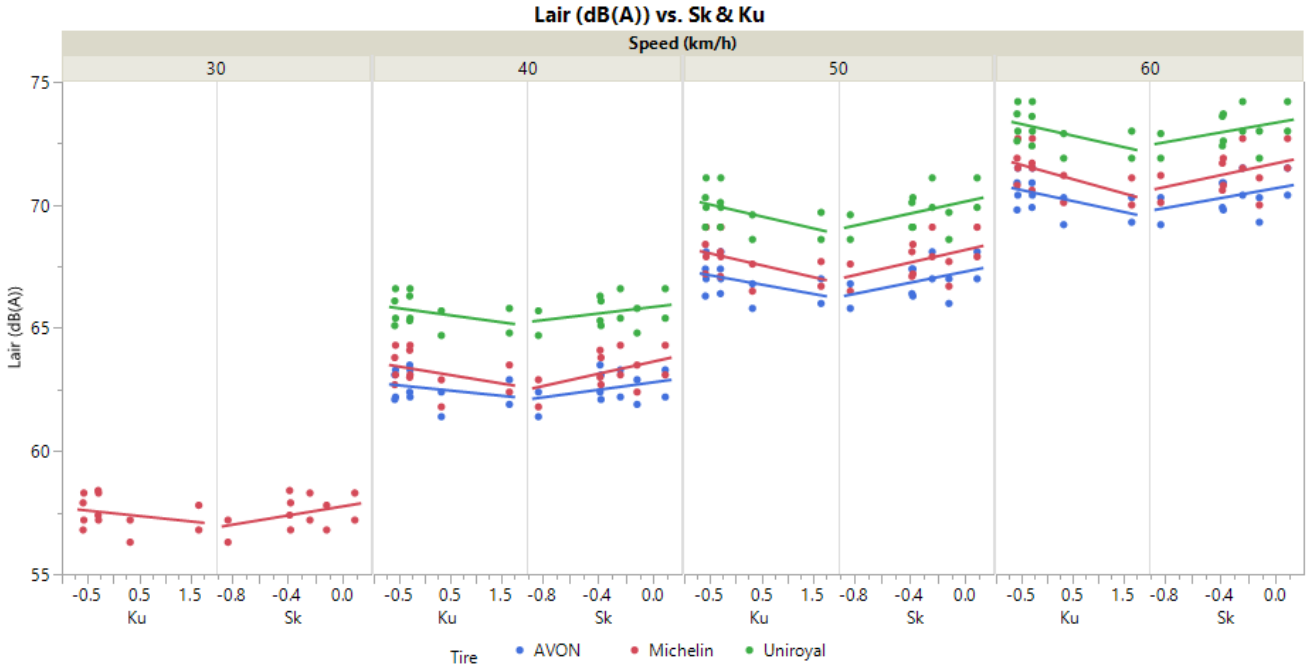

Figure 60. Lair noise levels by the skewness and kurtosis.

In both figures it is possible to observe that the noise levels increase as the skewness is higher and decrease as the kurtosis increases. This happens because the higher the kurtosis the texture has more plateaus, which excite less the tire/pavement

contact. The lower skewness (or negative) it is due the fact that the texture has more valley than peaks. The higher amount of valley allows the noise waves to “enter” the pavement and the lower amount of peaks produce less indentations which produces less noise.

6.3.5 Noise per frequency

Another way to analyze the data, thus gathering more information, is regarding the frequency of the noise levels. The simulation is done with SPERoN® capture the frequencies of 400 to 2000 Hz, which are quite relevant as they are close to the human speech and hearing sensibility.

In Figure 61 it is presented noise levels by the frequency range by the Lvib levels regarding the speed, type of tire and air resistance levels. The same arrangement is resented on Figure 62, but for Lair.

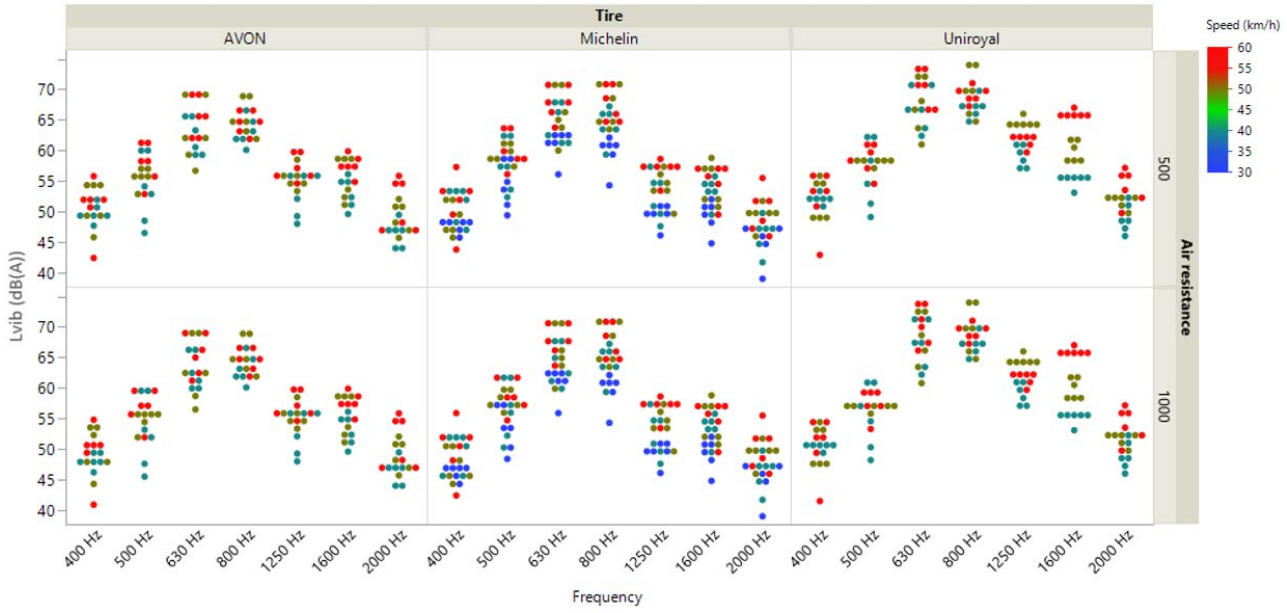

Figure 61. Lvib by frequency, categorized by tire, speed and air resistance.

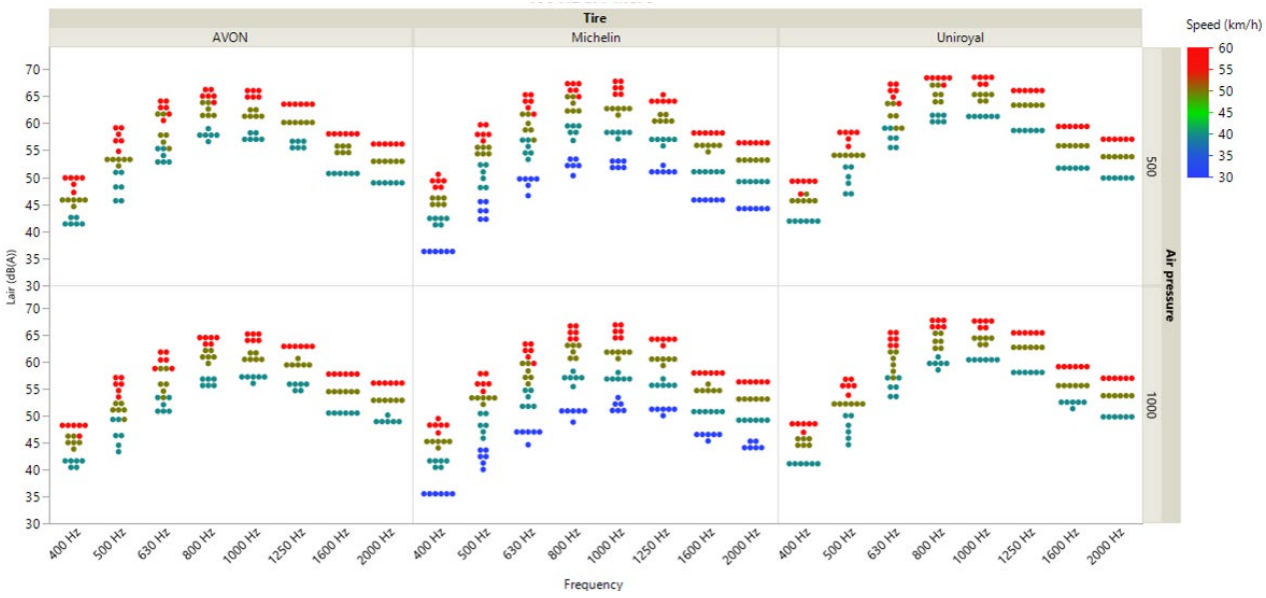

Figure 62. Lair by frequency, categorized by tire, speed and air resistance.

In these two figures, it is possible to note that the noise levels are higher between 800-1250 Hz, independently of the tire type and air pressure. It is noticeable that the speed is the most relevant variable presented here. It is also observed that in the tire difference by frequency band is not so clear when comparing to the Lvib and Lair total noise levels. The peak in dB(A) between 800-1250 Hz, can be explained by the tire tread excitement due the surface texture of the pavement.

Finally, the last data presented are the noise levels by frequency, categorized by speed and surface type. Figure 63 shows the data for Lvib, and it is possible to note that the Yellow and AA5050 mixes also have lower levels in most frequencies, at any speed, than the other samples. While both NAS and AA again have higher levels in most frequencies.

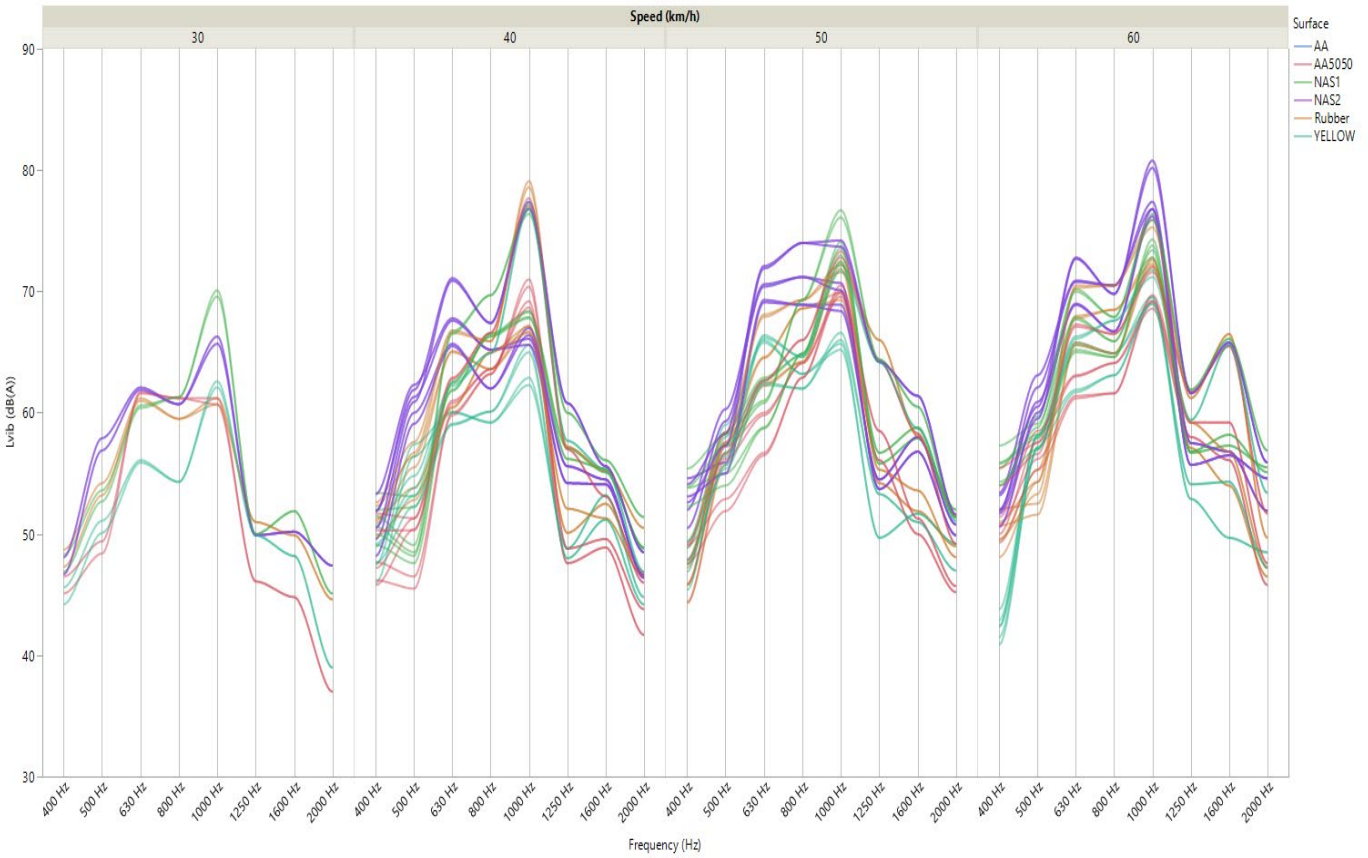

Figure 63.Frequency vs Lvib, by speed and samples.

It is noted that at 1000 Hz and at 40 km/h, the Rubber and AA5050 present a peak exclusively on this part, this might be due the fact that these two surfaces are the only ones with positive kurtosis. The Rubber behavior shows that is not falling too behind in low noise levels when compared to AA5050 and Yellow.

As for the Lair by the frequency, categorized by speed and surface type, it is presented in Figure 64. It is possible to see that at higher frequencies, the difference is negligible. At medium and low frequencies, the NAS2, NAS1 and AA have higher noise levels independently of the frequency.

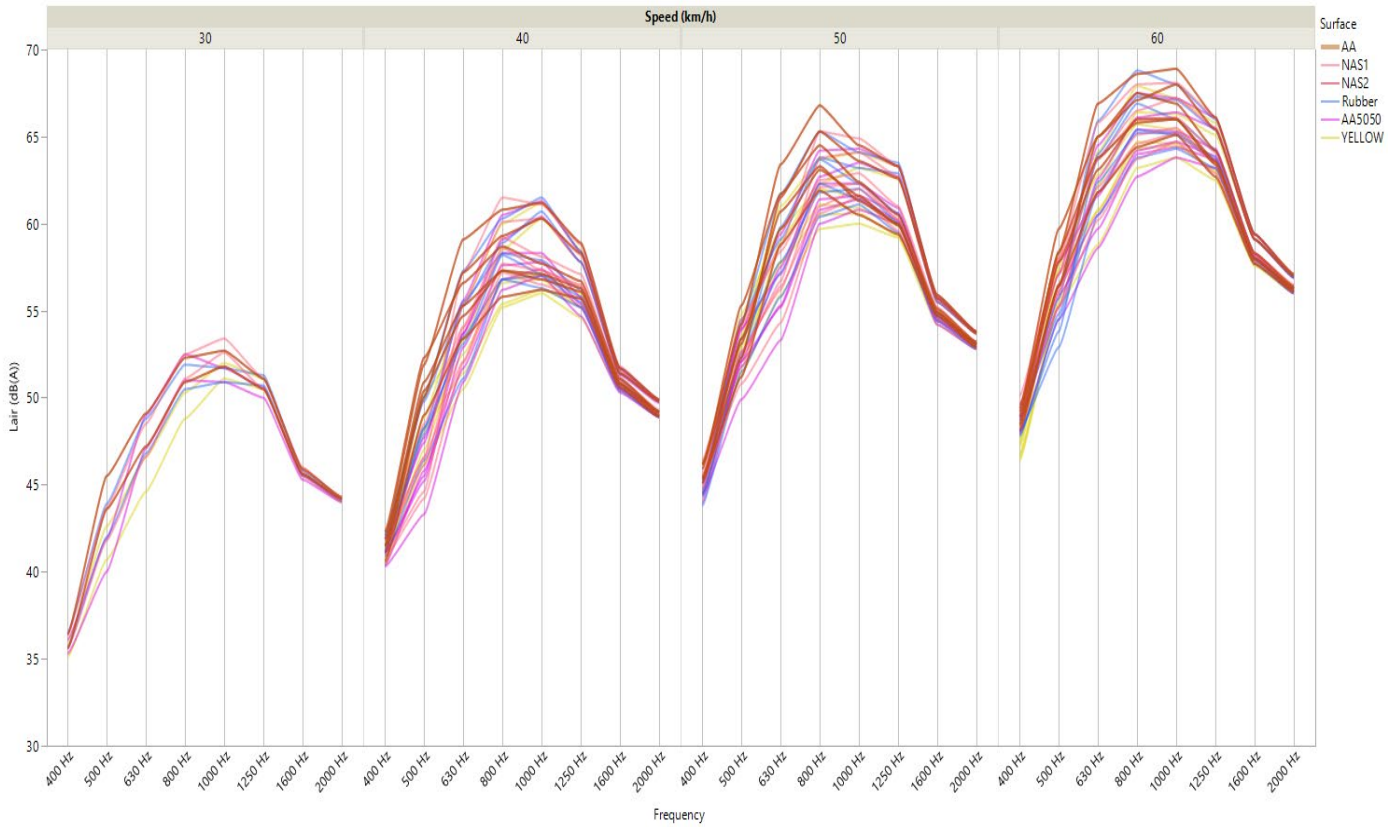

Figure 64. Frequency vs Lair, by speed and samples.

The rubber has mid-range level noise in all frequencies independently of the speed. However, the Yellow and AA5050 have lower levels of noise, the yellow mix at lower speed has the lowest noise levels, while AA5050 has at lower noise levels at medium frequencies at mid and higher speeds.

It is possible to note in both figures, that the noise levels are dependable in the speed. However, when analyzing the data using the skewness and kurtosis texture parameters is possible to see that for Lvib (Figure 65) the lower the skewness lower is the noise except for high kurtosis (A5050).

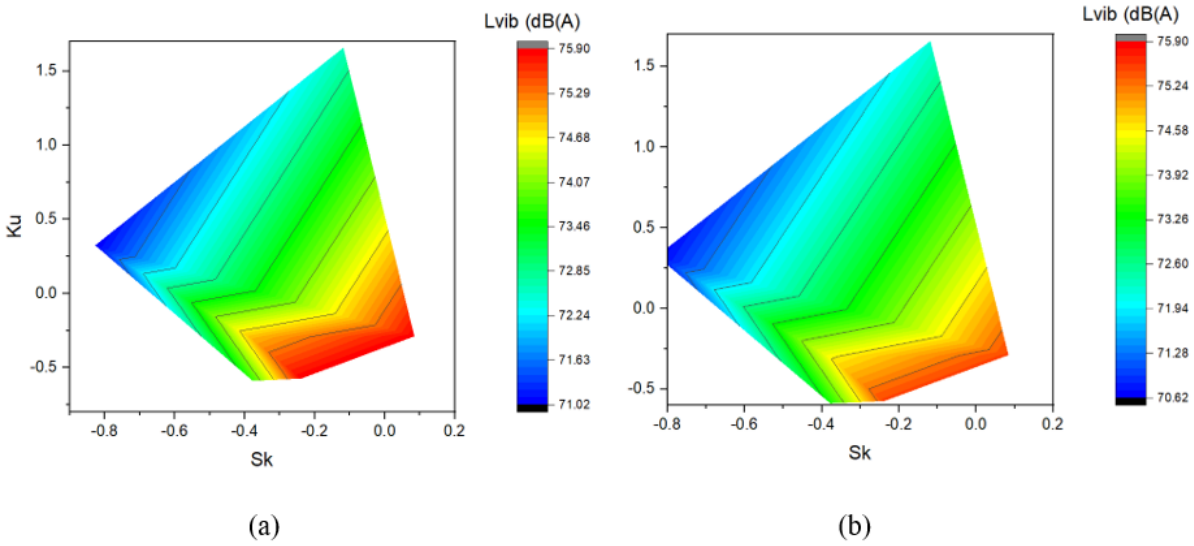

Figure 65. Kurtosis by skewness texture parameters by Lvib noise levels for (a)500 Pa.s/m^2 and (b) 1000 Pa.s/m^2.

That is corroborated when checking the same skewness value (between) -0.2 and 0, the noise level increases by from 72 dB(A) – AA5050 to 75 dB(A) AA.

For the Lair noise levels Figure 66 the total range is narrower than for Lvib, but the same here applies. High kurtosis (AA5050) compensates for the higher skewness, and still have a lower noise level then most samples. Nonetheless, the noise also decreases on par with the decrease in the skewness, being the lowest value the sample “yellow”.

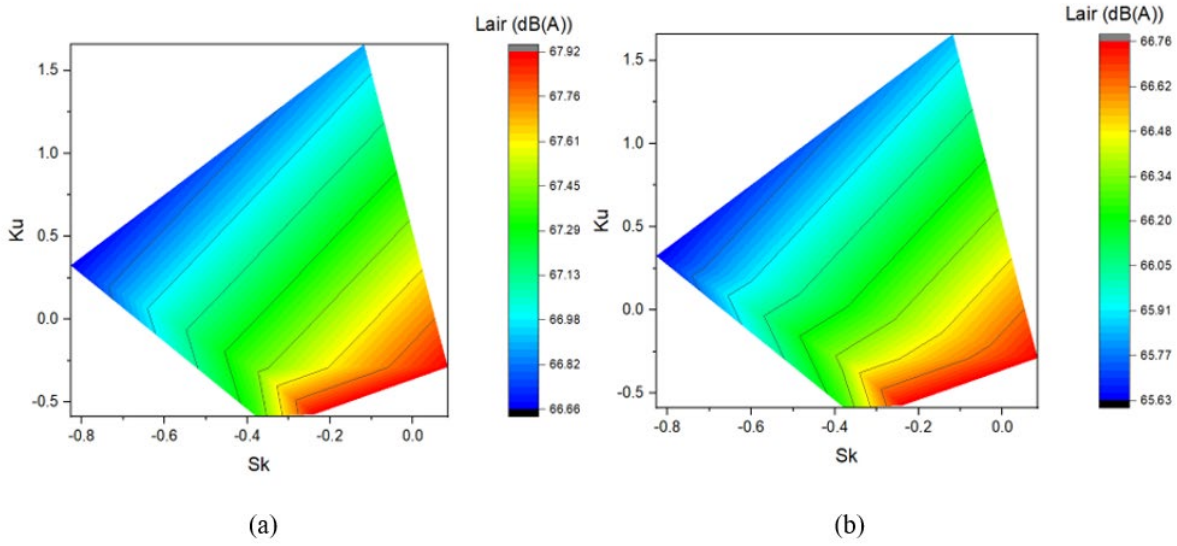

Figure 66. Kurtosis by skewness texture parameters by Lair noise levels for (a)500 Pa.s/m^2 and (b) 1000 Pa.s/m^2.

That is substantiated, again, for samples AA5050 and AA, where the noise difference is around 1dB(A).

Although both samples had artificial engineered aggregates the amount of material in each is fairly different, from less than 10% for AA, up to 50% on AA5050. This could mean that there is a minimal amount of Artificial Engineered Aggregate that must be added in order to reduce the noise. This happens because the higher amount of Artificial Engineered Aggregate changes considerably the kurtosis without substantially changing the skewness.

6.4. Conclusions

The use of different aggregates and binders to produce acoustic asphalt layers is not new, it has been studied and implemented for several years as shown in the literature review. However, the present work aimed to apply a different approach, not only by using a traditional paving solution that generally is applied to increase friction but proposing a novel artificial aggregate solution to be incorporated in the wearing course mixtures. The SPERoN® model confirmed that:

- The speed and tire type play a very important role in the tire/road noise.
- The use of different aggregates, natural vs artificial, can contribute to noise reduction.
    - It is possible to assert that the shape and size of the aggregates play an important role, as the artificial aggregates sample (Rubber and AA5050), behaved quite differently from the natural samples or even from the AA mix.
- The use of different binding agents, asphalt emulsion vs resin, seems to play an important role in the noise levels. This might be due the way each binder involves the aggregates.

Also is possible to conclude that:

- The crumb rubber aggregate sample has a midlevel noise behavior, and this is probably because the model does not compute the modulus of the pavement materials. If this was taken into consideration it could improve the results as 60% crumb rubber mixes have shown promising results regarding impact reduction[180,181]. The low stiffness has a direct impact on the noise levels as reduces the tread impact of the tire.
- Resin binder had significantly better results than the asphalt binder solutions with the same granulometric curve.

- The artificial aggregate solution had mixed behaviors. The AA mix with 10% Artificial aggregate had the worst results, equivalent to the NAS2.
- In the other hand the mix with 50% of Artificial Engineered Aggregate (AA5050), it had good results.
    - This indicates that the use of artificial aggregates in low quantities has negligible effectiveness in noise reduction, and it appears that the lower possible amount is 50%, to improve the noise reduction capabilities.
    - This change could also help in the frictional parameters, as those are more dependable in the skewness, therefore is possible to have a lower noise surface without compromising the friction.
- This can be an indicator that the Artificial Geopolymer Aggregate can be used as an aggregate in microsurfacing also designed to reduce the road noise.

It is important to carry on with this study, using different percentages of artificial geopolymeric aggregate in substitution of the natural aggregate. A trail site would provide more insights as to the complexity of real scale paving, and laboratory one is quite different.

Chapter 7: Conclusions

7.1 Retrospective

The present thesis aimed to develop Artificial Engineered Aggregates that could be used in high friction and acoustics surfaces, thus contributing to road safety (skid resistance) and noise reduction. Several steps were necessary to develop Artificial Engineered Aggregates for high friction and acoustic surfaces for pavements. Each one of those was presented in the chapters that compose this thesis. Each chapter is a self-contained paper, and each one has its specific objectives and conclusions. Nevertheless, a clear line of work is seen when combining the papers, starting from a literature review of the best practices for low noise and high friction surfaces are defined. Followed up by research papers that evaluated several aspects and steps of the production and use of Artificial Engineered Aggregates. The final two papers assessed the use of the Artificial Engineered Aggregate in microsurfacing mixes, evaluating several texture indicators using a laser profilometer and conducting a noise simulation using the SPERoN® software.

7.1.1 Chapters conclusions

As a self-contained paper, each chapter had its conclusions that, as described before, are relevant as they demonstrate how the objective was achieved.

Chapter 2 – Presented an extensive literature review on the acoustical and safety aspects of road pavements. It presented several paving solutions that could mitigate the noise or reduce accident risks. The use of Artificial Engineered Aggregates can be an asset to the production of High Friction Acoustic Surfaces for Pavement. Artificial aggregates can be engineered to a desired shape, size and texture, so they can be designed to target specific aspects, such as friction and noise. When it comes to using natural aggregates in high friction/low noise surfaces, it is necessary to select the most appropriate aggregates, as not all natural aggregates are suitable for this use.

Chapter 3 – Focused on the mix design and production of a geopolymer mortar using DOE as a tool to select the best mix design. The work showed that the DOE is a relevant tool for selecting the most appropriate mix design. With it was possible to draw a model that guided the production of artificial aggregates. The quality of the Metakaolin is paramount to a high-quality final product. The workability of the mortar is a good indicator of the feasibility of aggregate production.

Chapter 4 – Was dedicated to producing and evaluating the Artificial Engineered Aggregates using 3D printed molds. This work demonstrated that producing aggregates using 3D printed molds is promising but laborious. The mechanical tests recorded promising results in some aspects and failed in others. The MK quality is of the utmost importance, and directly related to the overall characteristics. The use of the MK2 improved the material and better results are expected in future tests. An industrial upscaling should be developed.

Chapter 5 - This chapter investigated the texture parameters of microsurfacing pavement solutions using different binding agents and different aggregates. The work showed that both aggregate type and binder could influence the final texture of the paving solution. Using a resin binder in place of the asphalt emulsion completely changed the texture characteristics, especially considering that both used the same granulometric curve. The use of crumb rubber to replace natural aggregates is promising, as the texture changes were quite interesting. Artificial Engineered Aggregate can drastically change the pavement texture as the thesis shows. Nevertheless, the best results were obtained regarding noise when a higher quantity of artificial aggregate was used.

Chapter 6 – The final research paper evaluated the microsurfacing samples concerning the potential noise generation. It is shown that the use of non-natural aggregates can contribute to noise reduction, as crumb rubber had average results and AA5050 had very promising ones. As for the crumb rubber, even though it had interesting results, the most relevant quality of the rubber is its modulus, which cannot be simulated in the SPERoN® software. The use of an alternative binder

contributed to the noise reduction. Finally, 50% artificial aggregate reduced the overall noise levels and in most frequencies. t is possible to consider that this change happens especially due the change on the kurtosis that this material provided.

7.1.2 Final considerations

The thesis posed the following objectives addressed in the previously mentioned papers. The objectives are:

- Develop a geopolymer mortar with acceptable strength characteristics with the minimum curing time and temperature.

This objective was assessed in Chapter 3. A complete Design of Experiments was done to obtain a regression equation that could optimize the mix design and obtain a mortar with high resistance to compression while cured at medium temperature and short period.

- Produce satisfactory Artificial Engineered Aggregates using 3D printed molds.

The production of the aggregates using the 3D printed molds was presented in Chapters 3 and 4, which showed that it was feasible to produce the artificial aggregates. It is important to note that the production is quite laborious and not fast; thus, it is necessary to develop this part further.

- Artificial Engineered Aggregates should have suitable mechanical properties.

The mechanical properties were presented in Chapter 4, where it is shown that the change in the Metakaolin plays a significant role in improving seral properties. The resistance to abrasion obtained through PSV, is relatively high for both Artificial Engineered Aggregates. However, the results improve with the change in the MK and the inclusion of a second curing process. The results for the micro-Deval are a good indication that the aggregate produced with the MK2 will perform better in Los Angeles.

- Produce microsurfacing solutions using artificial aggregate to replace natural aggregate partially.

The production of microsurfacing mixtures was done in Chapters 5 and 6. There were four mixes with asphalt emulsion, 100% Natural Aggregate, 50% Artificial Engineered Aggregate, 10% Artificial Engineered Aggregate, Crum rubber. One mix was produced using 100% Natural Aggregate but with resin as a binding agent.

- Evaluate the surface characteristics of the samples using this aggregate and compare them to other solutions.

In Chapter 5, the microsurfacing samples were examined using the laser profilometer, collecting profiles for all samples. The data was curated, and the samples had several texture indicators calculated. Thus was possible to categorize and understand how the Artificial Engineered Aggregate changes the surface texture.

- Evaluate the noise characteristics of the samples using this aggregate and compare them to other solutions.

Finally, in Chapter 6, with the texture data obtained and presented in Chapter 5, it was possible to conduct noise simulations using the SPERoN® model. It is possible to see that the use of different binding agents contributed to different noise levels. Artificial Engineered Aggregates can help reduce the noise levels if they are used in the 50% proportion. At a lower proportion (10%) it achieved higher noise levels.

This thesis discusses using a novel aggregate and its behavior regarding pavement texture and noise. The use of artificial aggregates is interesting not only in the environmental aspects. It is clear that with the appropriate design, it is possible to achieve a high-quality material that has the specific characteristics to reduce noise and increase friction, while preserving good mechanical and physical properties.

3D printing techniques to create the desired shape and size, are of tremendous value. As 3D printing prototyping allows the fast production of mold samples with

different characteristics, a Minimal Viable Product can be obtained after testing. With the 3D printed molds, it is possible to provide the mortar a shape quite different from the natural aggregates, enhancing the best qualities from the natural aggregate (such as texture), and ensuring reproducibility to select the size shape and desired texture. In the future, it might be possible even to embed a sensor, allowing it to collect information about the pavement.

The Artificial Engineered Aggregate has its properties due to its shape/size (obtained by the 3D molds) and the use of a geopolymerization technique. This geopolymerization can produce strong and durable materials. Its mix design allows producing workable materials, which are mandatory if the mortar should be inserted into molds. This technique is greener than its traditional counterpart (cement Portland), however, it will be only environmentally friendly if the curing process could be done at low temperatures. Finally, it is not necessary to use either metakaolin or basalt power. Other precursors can be implemented, and in alternative to the basalt powder, several other waste powders can be used, and the literature has shown it.

The selected shape and size showed encouraging results when used in the asphalt mixes. The behavior of using only 50% artificial aggregate was quite relevant in both noise and texture aspects. The replacement of only 10% into the Australian mix, did not show promising results regarding noise, in the texture aspect, however, it created a highly positive and rough texture that could be an asset in accident risk zones.

7.1.3 Future work

Even though the present study shows exciting and promising results, other aspects and new trials are needed. It is a novel material with a shape that was never used, it is necessary to conduct experiments on a larger scale, even, if possible, with a trail site. The author suggests evaluating the use of different waste powders to find the most economically viable, as it will only be accepted by the market if it is

competitive. The future works can be divided into aggregate and microsurfacing solutions.

The first studies that should be conducted are to reproduce the tests and material in this thesis, evaluate the chemical and environmental impacts and assess the risk of leaching. Increase the production of Artificial Engineered Aggregates to run more physical tests, like micro-Deval and Los Angeles, altering the curing times to improve the geopolymerization of the material. Reproduce the process with different 3D molds materials to select the most reliable one to produce the aggregates.

Replace the basalt power with different waste powders, as different regions have different waste materials. Studies conducted in the same laboratory evaluated the use of waste silt [3,79,132], as a geopolymer material, with quite interesting results. It is possible that the use of different waste powders could provide different physical/chemical characteristics, which need to be evaluated. With different Artificial Engineered Aggregate (size, material), it would be possible to create a wide range of applications; therefore, it is suggested to recreate the tests conducted here, using the same aggregate, with different precursors, in order to evaluate if similar results can be obtained without changing the AEA shape.

To the thesis, all production was hand-made. It was laborious and not time efficient. Thus, it is necessary to conduct a manufacturing study, evaluate the manufacturing improve the quality and speed up the process to be closer to a market application.

Regarding the microsurfacing mixes, it is essential to reconduct the experiments made in this thesis on a real scale. It would be interesting to collect 3D data from the pavement surface. Real-scale friction and noise tests could enrich the results and confirm the simulation data.

It is important to conduct a mix design of the microsurfacing regarding the granulometric curve (natural/Artificial) in order to obtain the optimum amount of Artificial Engineered Aggregates in the mixtures. With would be possible to be

closer to a real site application, where the material would be subjected to real traffic and weather, hence providing valuable information, such as durability and noise and real friction data.

Finally, an essential step that must be taken, and the author advises in this direction, it is needed to conduct the Social Life Cycle Assessment to provide valuable information on how cost-efficient this material is. The author believes that the use of Artificial Engineered Aggregates is a topic that must be researched, applying different shapes, source materials and applications.

References

1. Plati, C.; Pomoni, M.; Georgouli, K. Quantification of skid resistance seasonal variation in asphalt pavements. *J. Traffic Transp. Eng. (English Ed.* **2019**, doi:10.1016/j.jtte.2018.07.003.
2. Afonso, M.L.; Dinis-Almeida, M.; Fael, C.S. Characterization of the Skid Resistance and Mean Texture Depth in a Permeable Asphalt Pavement. *IOP Conf. Ser. Mater. Sci. Eng.* **2019**, *471*, doi:10.1088/1757-899X/471/2/022029.
3. Solouki, A.; Viscomi, G.; Lamperti, R.; Tataranni, P. Quarry waste as precursors in geopolymers for civil engineering applications: A decade in review. *Materials (Basel).* **2020**, *13*, 1–29, doi:10.3390/ma13143146.
4. Chen, W.; Jin, R.; Xu, Y.; Wanatowski, D.; Li, B.; Yan, L.; Pan, Z.; Yang, Y. Adopting recycled aggregates as sustainable construction materials: A review of the scientific literature. *Constr. Build. Mater.* **2019**, *218*, 483–496, doi:https://doi.org/10.1016/j.conbuildmat.2019.05.130.
5. Provis, J.L., Rees, C.. *Geopolymers: Structures, Processing, Properties and Industrial Applications*; Woodhead, 2009;
6. Haider, M.; Descornet, G.; Sandberg, U.; Pratico, F.G. Road Traffic Noise Emission: Recent Develpments and Future... *4th Int. SIIV Congr.* **2007**.
7. Frei, P.; Mohler, E.; Röösli, M. Effect of nocturnal road traffic noise exposure and annoyance on objective and subjective sleep quality. *Int. J. Hyg. Environ. Health* **2014**, *217*, 188–195, doi:10.1016/j.ijheh.2013.04.003.
8. Ongel, A.; Harvey, J. Pavement characteristics affecting the frequency content of tire/pavement noise. *Noise Control Eng. J.* **2010**, *58*, 563–571, doi:10.3397/1.3514588.
9. Sandberg, Ulf; Ejsmont, J.A. *Tyre/road noise reference book*; First Edit.; INFORMEX Ejsmont & Sandberg Handelsbolag, 2002; ISBN 91-613-2610-9.
10. Rado, Z.; Kane, M. An initial attempt to develop an empirical relation between texture and pavement friction using the HHT approach. *Wear* **2014**, *309*, 233–246, doi:10.1016/j.wear.2013.11.015.
11. Kogbara, R.B.; Masad, E.A.; Kassem, E.; Scarpas, A.; Anupam, K. A state-of-the-art review of parameters influencing measurement and modeling of skid resistance of asphalt pavements. *Constr. Build. Mater.* **2016**, *114*, 602–617, doi:10.1016/j.conbuildmat.2016.04.002.
12. Tsubota, T.; Fernando, C.; Yoshii, T.; Shirayanagi, H. Effect of Road Pavement Types and Ages on Traffic Accident Risks. *Transp. Res. Procedia* **2018**, *34*, 211–218, doi:10.1016/j.trpro.2018.11.034.
13. Puzzo, L.; Loprencipe, G.; Tozzo, C.; D'Andrea, A. Three-dimensional survey method of pavement texture using photographic equipment. *Meas. J. Int. Meas. Confed.* **2017**, *111*, 146–157, doi:10.1016/j.measurement.2017.07.040.
14. Klüppel, M.; Heinrich, G. Rubber friction on self-affine road tracks. *Rubber Chem. Technol.* **2000**, *73*, 578–606, doi:10.5254/1.3547607.
15. Edmondson, V.; Woodward, J.; Lim, M.; Kane, M.; Martin, J.; Shyha, I. Improved non-contact 3D field and processing techniques to achieve macrotexture characterisation of pavements. *Constr. Build. Mater.* **2019**, *227*, 116693, doi:10.1016/j.conbuildmat.2019.116693.
16. Swinburn, T.K.; Hammer, M.S.; Neitzel, R.L. Valuing Quiet: An Economic

Assessment of U.S. Environmental Noise as a Cardiovascular Health Hazard. *Am. J. Prev. Med.* **2015**, *49*, 345–353, doi:10.1016/j.amepre.2015.02.016.

17. Pardillo Mayora, J.M.; Jurado Piña, R. An assessment of the skid resistance effect on traffic safety under wet-pavement conditions. *Accid. Anal. Prev.* **2009**, *41*, 881–886, doi:10.1016/j.aap.2009.05.004.
18. Woodward,WD; Woodside, A. Early and mid life SMA skid resistance. *Safer Road Conf.* 1–10.
19. ISO Characterization of pavement texture by use of surface profiles -- Part 3: Specification and classification of profilometers. *ISO 13473-3* **2002**, *3*.
20. Praticò, F.G.; Vaiana, R. A study on the relationship between mean texture depth and mean profile depth of asphalt pavements. *Constr. Build. Mater.* **2015**, *101*, 72–79, doi:10.1016/j.conbuildmat.2015.10.021.
21. Rezaei, A.; Masad, E.; Chowdhury, A. Development of a Model for Asphalt Pavement Skid Resistance Based on Aggregate Characteristics and Gradation. *J. Transp. Eng.* **2012**, *137*, 863–873, doi:10.1061/(ASCE)TE.1943-5436.0000280.
22. Nilsson Roger, Phil Abbott, Bent Andersen, Fabienne Anfosso-Ledee, W.; Bartolomaeus, Hans Bendtsen, Gijsjan van Blokland, and G.D. *Silvia-sustainable road surface for traffic noise control. Technical report, Brussel*; 2006; ISBN 9789090204048.
23. Vieira, T.; Sandberg, U.; Erlingsson, S. Negative texture, positive for the environment: effects of horizontal grinding of asphalt pavements. *Road Mater. Pavement Des.* **2019**, *0*, 1–22, doi:10.1080/14680629.2019.1610476.
24. Knabben, R.M.; Trichês, G.; Gerges, S.N.Y.; Vergara, E.F. Evaluation of sound absorption capacity of asphalt mixtures. *Appl. Acoust.* **2016**, *114*, 266–274, doi:10.1016/j.apacoust.2016.08.008.
25. Del Pizzo, A.; Teti, L.; Moro, A.; Bianco, F.; Fredianelli, L.; Licitra, G. Influence of texture on tyre road noise spectra in rubberized pavements. *Appl. Acoust.* **2020**, *159*, 107080, doi:10.1016/j.apacoust.2019.107080.
26. Davies, B, R.; Cenek D, P.; Henderson J, R. The effect of skid resistance and texture on crash risk. *Int. Surf. Frict. Conf. 2005, Christchurch, New Zeal.* **2005**, 17P (SESSION 6).
27. Andriejauskas, T.; Vorobjovas, V.; Mielonas, V. Evaluation of skid resistance characteristics and measurement methods. *9th Int. Conf. Environ. Eng. ICEE 2014* **2014**, doi:10.3846/enviro.2014.141.
28. Wambold, J.C.; Henry, J.J. International PIARC experiment to compare and harmonize texture and skid resistance measurements. *Nord. Road Transp. Res.* **1995**, doi:10.1364/OE.14.008263.
29. World Health Organization (WHO) *A Road Safety Technical Package*; 2017; ISBN 9789241511704.
30. Ivan, J.N.; Ravishanker, N.; Jackson, E.; Aronov, B.; Guo, S. A Statistical Analysis of the Effect of Wet-Pavement Friction on Highway Traffic Safety. *J. Transp. Saf. Secur.* **2012**, *4*, 116–136, doi:10.1080/19439962.2011.620218.
31. Fwa, T.F. Skid resistance determination for pavement management and wet-weather road safety. *Int. J. Transp. Sci. Technol.* **2017**, *6*, 217–227, doi:10.1016/j.ijtst.2017.08.001.
32. Singh, D.; Patel, H.; Habal, A.; Das, A.K.; Kapgate, B.P.; Rajkumar, K. Evolution of coefficient of friction between tire and pavement under wet conditions using

surface free energy technique. *Constr. Build. Mater.* **2019**, doi:10.1016/j.conbuildmat.2019.01.122.

33. Ueckermann, A.; Wang, D.; Oeser, M.; Steinauer, B. Calculation of skid resistance from texture measurements. *J. Traffic Transp. Eng. (English Ed.* **2015**, *2*, 3–16, doi:10.1016/j.jtte.2015.01.001.
34. Hall, J.W.; Smith, K.L.; Titus-Glover, L.; Wambold, J.C.; Yager, T.J.; Rado, Z. *Guide for Pavement Friction*; Transportation Research Board: Washington, D.C., 2009;
35. Kane, M.; Rado, Z.; Timmons, A. Exploring the texture-friction relationship: From texture empirical decomposition to pavement friction. *Int. J. Pavement Eng.* **2015**, *16*, 919–928, doi:10.1080/10298436.2014.972956.
36. Gabriel, P.; Thomas, A.G.; Busfield, J.J.C. Influence of interface geometry on rubber friction. *Wear* **2010**, *268*, 747–750, doi:10.1016/j.wear.2009.11.019.
37. European Comission *REPORT FROM THE COMMISSION TO THE EUROPEAN PARLIAMENT AND THE COUNCIL On the Implementation of the Environmental Noise Directive in accordance with Article 11 of Directive 2002/49/EC*; Brussels, 2017; Vol. 151;.
38. Dzhambov, A.M.; Lercher, P. Road Traffic Noise Exposure and Birth Outcomes: An Updated Systematic Review and Meta-Analysis. *Int. J. Environ. Res. Public Health* **2019**, *16*, doi:10.3390/ijerph16142522.
39. Dzhambov, A.M.; Lercher, P. Road traffic noise exposure and depression/anxiety: An updated systematic review and meta-analysis. *Int. J. Environ. Res. Public Health* 2019, *16*.
40. Simões, M.R.L.; Souza, C.; Alcantara, M.A. de; Assunção, A.Á. Precarious working conditions and health of metropolitan bus drivers and conductors in Minas Gerais, Brazil. *Am. J. Ind. Med.* **2019**, *62*, 996–1006, doi:10.1002/ajim.23041.
41. WHO Burden of disease from Burden of disease from. **2011**, 126.
42. Imagine-project Available online: http://www.imagine-project.org/ (accessed on Dec 20, 2020).
43. Ramussen, R.O.; Bernhard, R.J.; Sandberg, U.; Mun, E.P. The little book of quieter pavements. *Security* **2007**, 1–33.
44. Vázquez, V.F.; Terán, F.; Viñuela, U.; Paje, S.E. Study of a road test track with and without crumb rubber. Solutions for noise pollution. *Environ. Eng. Manag. J.* **2014**, *13*, 2487–2495, doi:10.30638/eemj.2014.278.
45. Vázquez, V.F.; Luong, J.; Bueno, M.; Terán, F.; Paje, S.E. Assessment of an action against environmental noise: Acoustic durability of a pavement surface with crumb rubber. *Sci. Total Environ.* **2016**, *542*, 223–230, doi:10.1016/j.scitotenv.2015.10.102.
46. Praticò, F. On the dependence of acoustic performance on pavement characteristics. *Transp. Res. Part D Transp. Environ.* **2014**, *29*, 79–87, doi:10.1016/j.trd.2014.04.004.
47. Umnova, O.; Attenborough, K.; Shin, H.C.; Cummings, A. Deduction of tortuosity and porosity from acoustic reflection and transmission measurements on thick samples of rigid-porous materials. *Appl. Acoust.* **2005**, *66*, 607–624, doi:10.1016/j.apacoust.2004.02.005.
48. Kim, H.K.; Lee, H.K. Acoustic absorption modeling of porous concrete considering the gradation and shape of aggregates and void ratio. *J. Sound Vib.* **2010**, *329*, 866–879, doi:10.1016/j.jsv.2009.10.013.
49. Siebert, D. How wear affects road surface texture and its impact on tire/road noise

texture, NTNU Norwegian University of Science and Technology, 2017.
50. International Organization for Standardization Acoustics - Measurement of the influence of road surfaces on traffic noise - Part 2: The close-proximity method. *Iso/Dis 11819-2* 2014.
51. ASTM ASTM E1960-07(2015)-Standard Practice for Calculating International Friction Index of a Pavement Surface 2015.
52. Li, W.; Han, S.; Huang, Q. Performance of noise reduction and skid resistance of durable granular ultra-thin layer asphalt pavement. *Materials (Basel).* **2020**, *13*, doi:10.3390/MA13194260.
53. Alvarez, A.E.; Martin, A.E.; Estakhri, C.K.; Button, J.W.; Glover, C.J.; Jung, S.H. *Synthesis of Current Practice on the Design, Construction, and Maintenance of Porous Friction Courses Report No. FHWA/TxDOT Report 0-5262-1:*; 2006; Vol. 7;.
54. Wu, H.; Yu, J.; Song, W.; Zou, J.; Song, Q.; Zhou, L. A critical state-of-the-art review of durability and functionality of open-graded friction course mixtures. *Constr. Build. Mater.* **2020**, *237*, 117759, doi:10.1016/j.conbuildmat.2019.117759.
55. Aybike Ongel, John T. Harvey, Erwin Kohler, Qing Lu, and B.D.S. *Investigation of Noise, Durability, Permeability, and Friction Performance Trends for Asphalt Pavement Surface Types: First- and Second-Year Results*; Sacramento, California, 2008;
56. Woodward, D.; Millar, P.; Lantieri, C.; Sangiorgi, C.; Vignali, V. The wear of Stone Mastic Asphalt due to slow speed high stress simulated laboratory trafficking. *Constr. Build. Mater.* **2016**, *110*, 270–277, doi:10.1016/j.conbuildmat.2016.02.031.
57. Tonin, R. Quiet Road Pavements: Design and Measurement—State of the Art. *Acoust. Aust.* **2016**, *44*, 235–247, doi:10.1007/s40857-016-0066-3.
58. Praticò, F.; Mark, S. *Quiet Pavement Technologies. PIARC - 2013R10EN*; France, 2013;
59. Wu, Y.; Parker, F.; Kandhal, P.S. Aggregate toughness/abrasion resistance and durability/soundness tests related to asphalt concrete performance in pavements. *Transp. Res. Rec.* 1998, 85–93.
60. Wasilewska, M.; Gardziejczyk, W.; Gierasimiuk, P. Evaluation of Skid Resistance Using CTM, DFT and SRT-3 Devices. *Transp. Res. Procedia* **2016**, *14*, 3050–3059, doi:10.1016/j.trpro.2016.05.449.
61. Ejsmont, J.; Świeczko-Żurek, B.; Owczarzak, W.; Sommer, S.; Ronowski, G. Tire / Road Noise On Poroelastic Road Surfaces -. *EuroNoise 2018* **2018**, 2719–2724.
62. Meiarashi, S. Porous Elastic Road Surface as Urban Highway Noise Measure. *Transp. Res. Rec.* **2004**, *1880*, 151–157, doi:10.3141/1880-18.
63. PERSUADE Available online: http://persuade.fehrl.org (accessed on Jan 22, 2021).
64. Morgan, P.A.; Stait, R.E.; Reeves, S.; Clifton, M. The feasibility of using twin-layer porous asphalt surfaces on England's strategic road network. **2007**, *PPR433*, 106.
65. Bernhard, R.; Wayson, R. An introduction to tire/pavement noise of asphalt pavement. *Inst. Safe, Quiet …* **2005**, 26.
66. Tang, G.Q.; Li, M.L.; Ji, T.J.; Liu, Z. Current Status of Research on Two-Layer Porous Asphalt. *Appl. Mech. Mater.* **2014**, *716–717*, 443–447, doi:10.4028/www.scientific.net/amm.716-717.443.
67. Kragh, J.; Bendtsen, H. Performance of New Twin-Lay Drainage Asphalt Laid in Denmark. **2000**, 2–7.
68. Liu, M.; Huang, X.; Xue, G. Effects of double layer porous asphalt pavement of urban streets on noise reduction. *Int. J. Sustain. Built Environ.* **2016**, *5*, 183–196,

doi:10.1016/j.ijsbe.2016.02.001.
69. Woodward, D.; Friel, S. Predicting the wear of high friction surfacing aggregate. *Coatings* **2017**, *7*, doi:10.3390/coatings7050071.
70. Robati, M.; Carter, A.; Perraton, D. Evaluation of Test Methods and Selection of Aggregate Grading for Type Iii Application of Micro-Surfacing. *Int. J. Pavemnet Eng. Asph. Technol.* **2014**, *14*, 11–35, doi:10.2478/ijpeat-2013-0001.
71. Karyawan, I.D.A.; Ahyudanari, E.; Ekaputri, J.J. Potential Use of Fly Ash Base-Geopolymeras Aggregate Substitution in Asphalt Concrete Mixtures. *Int. J. Eng. Technol.* **2017**, *9*, 3744–3752, doi:10.21817/ijet/2017/v9i5/170905005.
72. Sangiorgi, C.; Bitelli, G.; Lantieri, C.; Irali, F.; Girardi, F. A Study on Texture and Acoustic Properties of Cold Laid Microsurfacings. *Procedia - Soc. Behav. Sci.* **2012**, *53*, 223–234, doi:10.1016/j.sbspro.2012.09.875.
73. Grilli, A.; Graziani, A.; Carter, A.; Sangiorgi, C.; Pivoto Specht, L.; Copetti Callai, S. Slurry surfacing: a review of definitions, descriptions and current practices. *RILEM Tech. Lett.* **2019**, *4*, 103–109, doi:10.21809/rilemtechlett.2019.91.
74. Heitzman, M.; Turner, P.; Greer, M. *High Friction Surface Treatment Alternative Aggregates Study*; Auburn, 2015;
75. CEDR (Conférence Européenne des Directeurs des Routes) *State of the art in managing road traffic noise: noise-reducing pavements noise-reducing*; 2017; ISBN 9791093321271.
76. McIntosh, J.; Wong, F.; Macha, P.; Buret, M. Long term acoustic performance of different asphalt configurations. *Acoust. 2019, Sound Decis. Mov. Forw. with Acoust. - Proc. Annu. Conf. Aust. Acoust. Soc.* **2020**, 1–10.
77. Losa, M.; Leandri, P.; Bacci, R. Mechanical and Performance-Related Properties of Asphalt Mixes Containing Expanded Clay Aggregate. *Transp. Res. Rec.* **2008**, *2051*, 23–30, doi:10.3141/2051-04.
78. Tataranni, P.; Sangiorgi, C. Synthetic aggregates for the production of innovative low impact porous layers for urban pavements. *Infrastructures* **2019**, *4*, doi:10.3390/infrastructures4030048.
79. Solouki, A.; Viscomi, G.; Tataranni, P. Preliminary Evaluation of Cement Mortars Containing Waste Silt Optimized with the Design of Experiments Method. **2021**.
80. Gunasekara, C.; Setunge, S.; Law, D.W.; Willis, N.; Burt, T. Engineering properties of geopolymer aggregate concrete. *J. Mater. Civ. Eng.* **2018**, *30*, 1–11, doi:10.1061/(ASCE)MT.1943-5533.0002501.
81. Birgin, H.B.; D'alessandro, A.; Laflamme, S.; Ubertini, F. Hybrid carbon microfibers-graphite fillers for piezoresistive cementitious composites. *Sensors (Switzerland)* **2021**, *21*, 1–13, doi:10.3390/s21020518.
82. Birgin, H.B.; D'alessandro, A.; Laflamme, S.; Ubertini, F. Smart graphite–cement composite for roadway-integrated weigh-in-motion sensing. *Sensors (Switzerland)* **2020**, *20*, 1–17, doi:10.3390/s20164518.
83. Zaumanis, M.; Arraigada, M.; Wyss, S.A.; Zeyer, K.; Cavalli, M.C.; Poulikakos, L.D. Performance-based design of 100% recycled hot-mix asphalt and validation using traffic load simulator. *J. Clean. Prod.* **2019**, *237*, 117679, doi:10.1016/j.jclepro.2019.117679.
84. Lizárraga, J.M.; Ramírez, A.; Díaz, P.; Marcobal, J.R.; Gallego, J. Short-term performance appraisal of half-warm mix asphalt mixtures containing high (70%)

and total RAP contents (100%): From laboratory mix design to its full-scale implementation. *Constr. Build. Mater.* **2018**, *170*, 433–445, doi:10.1016/j.conbuildmat.2018.03.051.

85. Sangiorgi, C.; Tataranni, P.; Simone, A.; Vignali, V.; Lantieri, C.; Dondi, G. A laboratory and filed evaluation of Cold Recycled Mixture for base layer entirely made with Reclaimed Asphalt Pavement. *Constr. Build. Mater.* **2017**, *138*, 232–239, doi:10.1016/j.conbuildmat.2017.02.004.
86. Sangiorgi, C.; Tataranni, P.; Lantieri, C.; Mazzotta, F. Application of Mining Waste Powder as filler in Hot Mix Asphalt. *MATEC Web Conf.* **2019**, *274*, 04002, doi:10.1051/matecconf/201927404002.
87. Barbuta, M.; Bucur, R.D.; Cimpeanu, S.M.; Paraschiv, G.; Bucur, D. Wastes in Building Materials Industry. *Agroecology* **2015**, 2014–2020, doi:10.5772/59933.
88. Sui, Y.; Ou, C.; Liu, S.; Zhang, J.; Tian, Q. Study on properties of waste concrete powder by thermal treatment and application in mortar. *Appl. Sci.* **2020**, *10*, doi:10.3390/app10030998.
89. Franco de Carvalho, J.M.; Melo, T.V. de; Fontes, W.C.; Batista, J.O. dos S.; Brigolini, G.J.; Peixoto, R.A.F. More eco-efficient concrete: An approach on optimization in the production and use of waste-based supplementary cementing materials. *Constr. Build. Mater.* **2019**, *206*, 397–409, doi:10.1016/j.conbuildmat.2019.02.054.
90. Paiva, H.; Yliniemi, J.; Illikainen, M.; Rocha, F.; Ferreira, V.M. Mine tailings geopolymers as awaste management solution for a more sustainable habitat. *Sustain.* **2019**, *11*, doi:10.3390/su11040995.
91. Mohajerani, A.; Suter, D.; Jeffrey-Bailey, T.; Song, T.; Arulrajah, A.; Horpibulsuk, S.; Law, D. Recycling waste materials in geopolymer concrete. *Clean Technol. Environ. Policy* **2019**, *21*, 493–515, doi:10.1007/s10098-018-01660-2.
92. Mabroum, S.; Moukannaa, S.; El Machi, A.; Taha, Y.; Benzaazoua, M.; Hakkou, R. Mine wastes based geopolymers: A critical review. *Clean. Eng. Technol.* **2020**, *1*, 100014, doi:10.1016/j.clet.2020.100014.
93. Borges, J.K.; Pacheco, F.; Tutikian, B.; de Oliveira, M.F. An experimental study on the use of waste aggregate for acoustic attenuation: EVA and rice husk composites for impact noise reduction. *Constr. Build. Mater.* **2018**, *161*, 501–508, doi:10.1016/j.conbuildmat.2017.11.078.
94. Copetti Callai, S.; Sangiorgi, C. A review on acoustic and skid resistance solutions for road pavements. *Infrastructures*.
95. Manaf, M.B.H.A.; Abdul Razak, R.; Muhamad, K.; Abdul Rahim, M.; Ahmad, M.M.; Hao, T.P. A study on the potential of geopolymer artificial aggregate as substitute for granite and limestone aggregate. *IOP Conf. Ser. Earth Environ. Sci.* **2020**, *476*, doi:10.1088/1755-1315/476/1/012034.
96. George, G.K.; Revathi, P. Production and Utilisation of Artificial Coarse Aggregate in Concrete - A Review. *IOP Conf. Ser. Mater. Sci. Eng.* **2020**, *936*, doi:10.1088/1757-899X/936/1/012035.
97. Cerveira, A.; Correia, E.; Cristelo, N.; Miranda, T.; Castro, F.; Fernández-Jiménez, A. Statistical Analysis of the Influence of Several Factors on Compressive Strength of Alkali Activated Fly Ash. *Procedia Struct. Integr.* **2017**, *5*, 1116–1122, doi:10.1016/j.prostr.2017.07.099.
98. Davidovits, J. *Geopolymer Chemistry and Application*; 4th ed.; Institut Geopolymere:

Saint-Quentin, France, 2015;
99. Liu, Z.; Cai, C.S.; Liu, F.; Fan, F. Feasibility Study of Loess Stabilization with Fly Ash–Based Geopolymer. *J. Mater. Civ. Eng.* **2016**, *28*, 04016003, doi:10.1061/(asce)mt.1943-5533.0001490.
100. Jiao, X.; Zhang, Y.; Chen, T.; Bao, S.; Liu, T.; Huang, J. Geopolymerisation of a silica-rich tailing. *Miner. Eng.* **2011**, *24*, 1710–1712, doi:10.1016/j.mineng.2011.09.008.
101. Siddique, R.; Klaus, J. Influence of metakaolin on the properties of mortar and concrete: A review. *Appl. Clay Sci.* **2009**, *43*, 392–400, doi:10.1016/j.clay.2008.11.007.
102. Aboulayt, A.; Riahi, M.; Ouazzani Touhami, M.; Hannache, H.; Gomina, M.; Moussa, R. Properties of metakaolin based geopolymer incorporating calcium carbonate. *Adv. Powder Technol.* **2017**, *28*, 2393–2401, doi:10.1016/j.apt.2017.06.022.
103. Medri, V.; Papa, E.; Lizion, J.; Landi, E. Metakaolin-based geopolymer beads: Production methods and characterization. *J. Clean. Prod.* **2020**, *244*, 118844, doi:10.1016/j.jclepro.2019.118844.
104. Longhi, M.A.; Rodríguez, E.D.; Walkley, B.; Zhang, Z.; Kirchheim, A.P. Metakaolin-based geopolymers: Relation between formulation, physicochemical properties and efflorescence formation. *Compos. Part B Eng.* **2020**, *182*, doi:10.1016/j.compositesb.2019.107671.
105. Romagnoli, M.; Leonelli, C.; Kamse, E.; Lassinantti Gualtieri, M. Rheology of geopolymer by DOE approach. *Constr. Build. Mater.* **2012**, *36*, 251–258, doi:10.1016/j.conbuildmat.2012.04.122.
106. BSI Standards Publication Grout for prestressing tendons Part 3 : Test methods. **2012**.
107. EN 1015-11 BSI Standards Publication Methods of test for mortar for masonry. **2019**.
108. Langer, W. 9 - Sustainability of aggregates in construction. In *Sustainability of Construction Materials (Second Edition)*; Khatib, J.M., Ed.; Woodhead Publishing Series in Civil and Structural Engineering; Woodhead Publishing, 2016; pp. 181–207 ISBN 978-0-08-100995-6.
109. The Freedonia Group Global Demand for Construction Aggregates to Exceed 48 Billion Metric Tons in 2015 Available online: https://www.freedoniagroup.com/World-Construction-Aggregates.html.
110. Akhtar, A.; Sarmah, A.K. Construction and demolition waste generation and properties of recycled aggregate concrete: A global perspective. *J. Clean. Prod.* **2018**, *186*, 262–281, doi:https://doi.org/10.1016/j.jclepro.2018.03.085.
111. Zabalza Bribián, I.; Valero Capilla, A.; Aranda Usón, A. Life cycle assessment of building materials: Comparative analysis of energy and environmental impacts and evaluation of the eco-efficiency improvement potential. *Build. Environ.* **2011**, *46*, 1133–1140, doi:10.1016/j.buildenv.2010.12.002.
112. Standard, B. BS EN 13242:2015 - Aggregates for unbound and hydraulically bound materials for use in civil engineering work and road construction 2015, *44*.
113. Bai, G.; Zhu, C.; Liu, C.; Liu, B. An evaluation of the recycled aggregate characteristics and the recycled aggregate concrete mechanical properties. *Constr. Build. Mater.* **2020**, *240*, 117978, doi:https://doi.org/10.1016/j.conbuildmat.2019.117978.
114. Aslam, M.S.; Huang, B.; Cui, L. Review of construction and demolition waste management in China and USA. *J. Environ. Manage.* **2020**, *264*, 110445,

doi:https://doi.org/10.1016/j.jenvman.2020.110445.
115. Behera, M.; Bhattacharyya, S.K.; Minocha, A.K.; Deoliya, R.; Maiti, S. Recycled aggregate from C&D waste & its use in concrete – A breakthrough towards sustainability in construction sector: A review. *Constr. Build. Mater. 68*.
116. Ren, P.; Ling, T.-C.; Mo, K.H. Recent advances in artificial aggregate production. *J. Clean. Prod.* **2021**, *291*, 125215, doi:https://doi.org/10.1016/j.jclepro.2020.125215.
117. Colangelo, F.; Messina, F.; Cioffi, R. Recycling of MSWI fly ash by means of cementitious double step cold bonding pelletization: Technological assessment for the production of lightweight artificial aggregates. *J. Hazard. Mater.* **2015**, *299*, 181–191, doi:https://doi.org/10.1016/j.jhazmat.2015.06.018.
118. Tajra, F.; Abd Elrahman, M.; Lehmann, C.; Stephan, D. Properties of lightweight concrete made with core-shell structured lightweight aggregate. *Constr. Build. Mater.* **2019**, *205*, 39–51, doi:https://doi.org/10.1016/j.conbuildmat.2019.01.194.
119. Tajra, F.; Elrahman, M.A.; Stephan, D. The production and properties of cold-bonded aggregate and its applications in concrete: A review. *Constr. Build. Mater.* **2019**, *225*, 29–43, doi:https://doi.org/10.1016/j.conbuildmat.2019.07.219.
120. Balapour, M.; Zhao, W.; Garboczi, E.J.; Oo, N.Y.; Spatari, S.; Hsuan, Y.G.; Billen, P.; Farnam, Y. Potential use of lightweight aggregate (LWA) produced from bottom coal ash for internal curing of concrete systems. *Cem. Concr. Compos.* **2020**, *105*, 103428, doi:https://doi.org/10.1016/j.cemconcomp.2019.103428.
121. Qaidi, S.M.A.; Dinkha, Y.Z.; Haido, J.H.; Ali, M.H.; Tayeh, B.A. Engineering properties of sustainable green concrete incorporating eco-friendly aggregate of crumb rubber: A review. *J. Clean. Prod.* **2021**, *324*, 129251, doi:https://doi.org/10.1016/j.jclepro.2021.129251.
122. Saikia, N.; de Brito, J. Use of plastic waste as aggregate in cement mortar and concrete preparation: A review. *Constr. Build. Mater.* **2012**, *34*, 385–401, doi:https://doi.org/10.1016/j.conbuildmat.2012.02.066.
123. Liu, Y.; Shi, C.; Zhang, Z.; Li, N. An overview on the reuse of waste glasses in alkali-activated materials. *Resour. Conserv. Recycl.* **2019**, *144*, 297–309, doi:https://doi.org/10.1016/j.resconrec.2019.02.007.
124. Valášková, M.; Blahůšková, V.; Vlček, J. Effects of Kaolin Additives in Fly Ash on Sintering and Properties of Mullite Ceramics. *Minerals* **2021**, *11*, doi:10.3390/min11080887.
125. Yue, M.; Yue, Q.Y.; Qi, Y.F. Effect of Sintering Temperature on the Properties of Sludge Ceramics and Fly-Ash Ceramics. In Proceedings of the Advances in Composites; Trans Tech Publications Ltd, 2011; Vol. 150, pp. 1068–1072.
126. Tang, P.; Xuan, D.; Poon, C.S.; Tsang, D.C.W. Valorization of concrete slurry waste (CSW) and fine incineration bottom ash (IBA) into cold bonded lightweight aggregates (CBLAs): Feasibility and influence of binder types. *J. Hazard. Mater.* **2019**, *368*, 689–697, doi:https://doi.org/10.1016/j.jhazmat.2019.01.112.
127. Khale, D.; Chaudhary, R. Mechanism of geopolymerization and factors influencing its development: a review. *J. Mater. Sci.* **2007**, *42*, 729–746, doi:10.1007/s10853-006-0401-4.
128. Morone, M.; Costa, G.; Georgakopoulos, E.; Manovic, V.; Stendardo, S.; Baciocchi, R. Granulation–Carbonation Treatment of Alkali Activated Steel Slag for Secondary Aggregates Production. *Waste and Biomass Valorization* **2017**, *8*, 1381–1391,

doi:10.1007/s12649-016-9781-0.
129. Bui, L.A.; Hwang, C.; Chen, C.; Lin, K.; Hsieh, M. Manufacture and performance of cold bonded lightweight aggregate using alkaline activators for high performance concrete. *Constr. Build. Mater.* **2012**, *35*, 1056–1062, doi:https://doi.org/10.1016/j.conbuildmat.2012.04.032.
130. Ismaiel Saraya, M.E.-S.; El-Fadaly, E. Preliminary Study of Alkali Activation of Basalt: Effect of NaOH Concentration on Geopolymerization of Basalt. *J. Mater. Sci. Chem. Eng.* **2017**, *05*, 58–76, doi:10.4236/msce.2017.511006.
131. Callai, S.C.; Tataranni, P.; Sangiorgi, C. Preliminary evaluation of geopolymer mix design applying the design of experiments method. *Infrastructures* **2021**, *6*, doi:10.3390/infrastructures6030035.
132. Moro, D.; Fabbri, R.; Romano, J.; Ulian, G.; Calafato, A.; Solouki, A.; Sangiorgi, C.; Valdrè, G. Thermal, X-ray Diffraction and Oedometric Analyses of Silt-Waste/NaOH-Activated Metakaolin Geopolymer Composite. *J. Compos. Sci.* **2021**, *5*, 269, doi:10.3390/jcs5100269.
133. Rill, E.; Lowry, D.R.; Kriven, W.M. Properties of basalt fiber reinforced geopolymer composites. *Ceram. Eng. Sci. Proc.* **2010**, *31*, 57–67, doi:10.1002/9780470944103.ch6.
134. Tataranni, P.; Besemer, G.M.; Bortolotti, V.; Sangiorgi, C. Preliminary research on the physical and mechanical properties of alternative lightweight aggregates produced by alkali-activation ofwaste powders. *Materials (Basel).* **2018**, *10*, doi:10.3390/ma11071255.
135. Artoni, R.; Cazacliu, B.; Hamard, E.; Cothenet, A.; Parhanos, R.S. Resistance to fragmentation of recycled concrete aggregates. *Mater. Struct. Constr.* **2017**, *50*, doi:10.1617/s11527-016-0900-y.
136. Dunford, A. Published Project Report PPR603. Establishing a new supply of UK PSV control stone Including results of supplementary experiments. **2013**, 20.
137. Zhou, X.; Kastiukas, G.; Lantieri, C.; Tataranni, P.; Vaiana, R.; Sangiorgi, C. Mechanical and thermal performance of macro-encapsulated phase change materials for pavement application. *Materials (Basel).* **2018**, *11*, 1–18, doi:10.3390/ma11081398.
138. Vaiana, R.; Balzano, F.; Iuele, T.; Gallelli, V. Microtexture performance of EAF slags used as aggregate in asphalt mixes: A comparative study with surface properties of natural stones. *Appl. Sci.* **2019**, *9*, doi:10.3390/app9153197.
139. Czinder, B.; Vásárhelyi, B.; Török, Á. Long-term abrasion of rocks assessed by micro-Deval tests and estimation of the abrasion process of rock types based on strength parameters. *Eng. Geol.* **2021**, *282*, doi:10.1016/j.enggeo.2021.105996.
140. Korkanç, M.; Tuğrul, A. Evaluation of selected basalts from Nĭde, Turkey, as source of concrete aggregate. *Eng. Geol.* **2004**, *75*, 291–307, doi:10.1016/j.enggeo.2004.06.015.
141. Li, S.; Xiong, R.; Dong, X.; Sheng, Y.; Guan, B.; Zong, Y.; Xie, C.; Zhai, J.; Li, C. Effect of chemical composition of calcined bauxite aggregates on mechanical and physical properties for high friction surface course. *Constr. Build. Mater.* **2021**, *302*, 124390, doi:10.1016/j.conbuildmat.2021.124390.
142. Li, S.; Xiong, R.; Yu, D.; Zhao, G.; Cong, P.; Jiang, Y. Friction Surface Treatment Selection: Aggregate Properties, Surface Characteristics, Alternative Treatments, and Safety Effects. **2017**, 54, doi:10.5703/1288284316509.
143. Li, S.; Xiong, R.; Yu, D.; Zhao, G.; Cong, P.; Jiang, Y. *Friction Surface Treatment*

Selection: Aggregate Properties, Surface Characteristics, Alternative Treatments, and Safety Effects; 2017; ISBN 9781622604784.

144. Aavik, A.; Kaal, T.; Jentson, M. Use of Pavement Surface Texture Characteristics Measurement Results in Estonia. *Ercc.Ee* **2013**, 1–10.
145. Meegoda, J.N.; Gao, S.; Liu, S.; Gephart, N.C. Pavement texture from high-speed laser for pavement management system. *Int. J. Pavement Eng.* **2013**, *14*, 697–705, doi:10.1080/10298436.2012.655246.
146. Vaitkus, A.; Andriejauskas, T.; Šernas, O.; Čygas, D.; Laurinavičius, A. Definition of concrete and composite precast concrete pavements texture. *Transport* **2019**, *34*, 404–414, doi:10.3846/transport.2019.10411.
147. Kovács, Z.F.; Viharos, Z.J.; Kodácsy, J. Determination of the working gap and optimal machining parameters for magnetic assisted ball burnishing. *Meas. J. Int. Meas. Confed.* **2018**, *118*, 172–180, doi:10.1016/j.measurement.2018.01.033.
148. Krolczyk, G.M.; Krolczyk, J.B.; Maruda, R.W.; Legutko, S.; Tomaszewski, M. Metrological changes in surface morphology of high-strength steels in manufacturing processes. *Meas. J. Int. Meas. Confed.* **2016**, *88*, 176–185, doi:10.1016/j.measurement.2016.03.055.
149. Münzel, T.; Sørensen, M.; Daiber, A. Transportation noise pollution and cardiovascular disease. *Nat. Rev. Cardiol.* **2021**, *18*, 619–636, doi:10.1038/s41569-021-00532-5.
150. European Environment Agency *Environmental noise in Europe - 2020*; 2020; ISBN 978-92-9480-209-5.
151. Peterson, E.A.; Augenstein, J.S.; Tanis, D.C.; Augenstein, D.G. Noise Raises Blood Pressure Without Impairing Auditory Sensitivity. *Science (80-.).* **1981**, *211*, 1450–1452, doi:10.1126/science.7466404.
152. Pyko, A.; Lind, T.; Mitkovskaya, N.; Ögren, M.; Östenson, C.G.; Wallas, A.; Pershagen, G.; Eriksson, C. Transportation noise and incidence of hypertension. *Int. J. Hyg. Environ. Health* **2018**, *221*, 1133–1141, doi:10.1016/j.ijheh.2018.06.005.
153. Beutel, M.E.; Brähler, E.; Ernst, M.; Klein, E.; Reiner, I.; Wiltink, J.; Michal, M.; Wild, P.S.; Schulz, A.; Münzel, T.; et al. Noise annoyance predicts symptoms of depression, anxiety and sleep disturbance 5 years later. Findings from the Gutenberg Health Study. *Eur. J. Public Health* **2020**, *30*, 487–492, doi:10.1093/eurpub/ckaa015.
154. Zhang, Y.; Tayarani, M.; Wang, S.; Liu, Y.; Sharma, M.; Joly, R.; RoyChoudhury, A.; Hermann, A.; Gao, O.H.; Pathak, J. Identifying urban built environment factors in pregnancy care and maternal mental health outcomes. *BMC Pregnancy Childbirth* **2021**, *21*, 1–11, doi:10.1186/s12884-021-04056-1.
155. Christensen, J.S.; Hjortebjerg, D.; Raaschou-Nielsen, O.; Ketzel, M.; Sørensen, T.I.A.; Sørensen, M. Pregnancy and childhood exposure to residential traffic noise and overweight at 7 years of age. *Environ. Int.* **2016**, *94*, 170–176, doi:10.1016/j.envint.2016.05.016.
156. Pignier, N. The impact of traffic noise on economy and environment: a short literature study: Performed within the scope of the ECO2 project Noise propagation from sustainable. *Cent. ECO2 Veh. Des. KTH Aeronaut. Veh. Eng. Stock. Sweden* **2015**, 1–17.
157. Boer, L.C. (Eelco) den; Schroten, A. (Arno) Traffic noise reduction in Europe Health

effects , social costs and. **2007**, 1–64.
158. Dreger, S.; Schüle, S.A.; Hilz, L.K.; Bolte, G. Social inequalities in environmental noise exposure: A review of evidence in the WHO european region. *Int. J. Environ. Res. Public Health* **2019**, *16*, doi:10.3390/ijerph16061011.
159. Poulikakos, L.D.; Athari, S.; Mikhailenko, P.; Kakar, M.R.; Bueno, M.; Piao, Z.; Pieren, R.; Heutschi, K. Effect of waste materials on acoustical properties of semi-dense asphalt mixtures. *Transp. Res. Part D Transp. Environ.* **2022**, *102*, 103154, doi:https://doi.org/10.1016/j.trd.2021.103154.
160. Goubert, L.; Bendtsen, H.; Bergiers, A.; Kalman, B.; Kokot, D. The Poroelastic Road Surface (PERS): Is the 10 dB Reducing Pavement within Reach? *Mater. Infrastructures 1* **2016**, 253–268, doi:10.1002/9781119318583.ch19.
161. Praticò, F.G.; Vaiana, R. Permeable friction courses: Area-based vs. Line-based surface performance and indicators. *42nd Int. Congr. Expo. Noise Control Eng. 2013, INTER-NOISE 2013 Noise Control Qual. Life* **2013**, *1*, 117–126.
162. Goubert, L. A new test track with the ultra noise reducing Poro-elastic Road Surface (PERS) in Gent, Belgium. *INTER-NOISE 2019 MADRID - 48th Int. Congr. Exhib. Noise Control Eng.* **2019**.
163. Meiarashi, S.; Ohishi, F. INTER-NOISE 2006. **2006**.
164. Praticò, F.G.; Vaiana, R.; Iuele, T. Macrotexture modeling and experimental validation for pavement surface treatments. *Constr. Build. Mater.* **2015**, *95*, 658–666, doi:10.1016/j.conbuildmat.2015.07.061.
165. Bennert, T.; Hanson, D.; Maher, A.; Vitillo, N. Influence of Pavement Surface Type on Tire/Pavement Generated Noise. *J. Test. Eval.* **2005**, doi:10.1520/JTE12641.
166. Bhargava, N.; Siddagangaiah, A.K.; Ryntathiang, T.L. State of the art review on design and performance of microsurfacing. *Road Mater. Pavement Des.* **2020**, *21*, 2091–2125, doi:10.1080/14680629.2019.1607771.
167. Nowoświat, A.; Sorociak, W.; Żuchowski, R. The impact of the application of thin emulsion mat microsurfacing on the level of noise in the environment. *Constr. Build. Mater.* **2020**, *263*, doi:10.1016/j.conbuildmat.2020.120626.
168. Del Pizzo, L.G.; Bianco, F.; Moro, A.; Schiaffino, G.; Licitra, G. Relationship between tyre cavity noise and road surface characteristics on low-noise pavements. *Transp. Res. Part D Transp. Environ.* **2021**, *98*, 102971, doi:https://doi.org/10.1016/j.trd.2021.102971.
169. Li, F.; Xue, W.; Rong, Y.; Du, C.; Tang, J.; Zhao, Y. A probability distribution prediction method for expressway traffic noise. *Transp. Res. Part D Transp. Environ.* **2022**, *103*, 103175, doi:https://doi.org/10.1016/j.trd.2022.103175.
170. Garg, N.; Maji, S. A critical review of principal traffic noise models: Strategies and implications. *Environ. Impact Assess. Rev.* **2014**, *46*, 68–81, doi:https://doi.org/10.1016/j.eiar.2014.02.001.
171. Rahmani, S.; Mousavi, S.M.; Kamali, M.J. Modeling of road-traffic noise with the use of genetic algorithm. *Appl. Soft Comput.* **2011**, *11*, 1008–1013, doi:https://doi.org/10.1016/j.asoc.2010.01.022.
172. Beckenbauer, T.; Klein, P.; Hamet, J.F.; Kropp, W. Tyre/road noise prediction: A comparison between the SPERoN and HyRoNE models - Part 1. *Proc. - Eur. Conf. Noise Control* **2008**, 2933–2938.
173. Sergio Copetti Callai; Piergiorgio Tataranni; Manuel de Rose; Annalisa Natali

Murri; Rosolino Vaiana;Cesare Sangiorgi Artificial aggregates from Alkali-Activated basalt powder: a preliminary evaluation. *not Publ.*

174. Zhan, W.; Huang, P. Modeling tangential contact based on non-Gaussian rough surfaces. *Proc. Inst. Mech. Eng. Part J J. Eng. Tribol.* **2019**, *233*, 51–60, doi:10.1177/1350650118758742.
175. Tayebi, N.; Polycarpou, A.A. Modeling the effect of skewness and kurtosis on the static friction coefficient of rough surfaces. *Tribol. Int.* **2004**, *37*, 491–505, doi:10.1016/j.triboint.2003.11.010.
176. Dascotte, E. The 32nd International Congress and Exposition on Noise Control Engineering Jeju International Convention Center, Seogwipo, Korea, August 25-28, 2003. *Noise Control Eng.* **2003**, 506–513.
177. Hoffmann, A. Perception of rolling noise. **2015**, 74 pp.
178. Specht, L.P.; Callai, S.C.; Khatchatourian, O.A.; Kohler, R. Noise evaluation using the SPBI (Statistical Pass-By Index) for different pavements. *Rev. Esc. Minas* **2009**, *62*.
179. Praticò, F.G.; Vaiana, R.; Iuele, T. Acoustic absorption and surface texture: An experimental investigation. *42nd Int. Congr. Expo. Noise Control Eng. 2013, INTER-NOISE 2013 Noise Control Qual. Life* **2013**, *4*, 2901–2909, doi:10.13140/RG.2.1.2478.9520.
180. Makoundou, C.; Johansson, K.; Wallqvist, V.; Sangiorgi, C. Functionalization of crumb rubber surface for the incorporation into asphalt layers of reduced stiffness: An overview of existing treatment approaches. *Recycling* **2021**, *6*, 1–22, doi:10.3390/recycling6010019.
181. Makoundou, C.; Sangiorgi, C.; Johansson, K.; Wallqvist, V. Development of functional rubber-based impact-absorbing pavements for cyclist and pedestrian injury reduction. *Sustain.* **2021**, *13*, doi:10.3390/su132011283.